UNIVERSITÉ LAVAL

Analysis of earth dam-flexible canyon interaction by 3D hybrid FEM-SBFEM

Thèse

Alireza Yaseri

Doctorat en génie civil
Philosophiæ doctor (Ph. D.)

Québec, Canada

Résumé

La géométrie et la flexibilité d'un canyon sont les paramètres qui affectent grandement la valeur des périodes naturelles dans les barrages en terre. Le canyon entourant des barrages peut être considéré comme un domaine illimité. Pour prendre en compte ces deux effets, le canyon a été modélisé par SBFEM et le barrage en terre, à géométrie limitée, par FEM. La technique hybride SBFEM-FEM pour l'analyse tridimensionnelle dynamique de l'interaction sol-barrage a été validée avec les résultats disponibles dans la littérature. Comme la matrice de rigidité dynamique du domaine non borné est complexe et dépendante de la fréquence, la méthode classique de superposition de modes n'est pas simple pour le système d'interaction sol-structure. Ainsi, pour obtenir la fréquence propre fondamentale, le barrage a été excité en direction amont-aval. Les périodes naturelles du barrage de terre pour des canyons de formes géométriques et de coefficient de impédance différents ont été obtenues. Ils se sont avérés avoir des effets significatifs sur la période naturelle. Les résultats ont été comparés aux données enregistrées réelles. Il a été constaté que les graphiques proposés dans cette étude peuvent être utilisés par des concepteurs de barrages pour l'estimation des périodes naturelles des barrages en terre dans des canyons de formes et de propriétés matérielles différentes. Plusieurs fonctions d'amplification correspondant à différentes conditions de canyon ont été obtenues en appliquant un déplacement uniforme à la limite du canyon. Une étude approfondie a été réalisée pour examiner les effets de la géométrie et de la flexibilité du canyon sur la réponse en régime permanent du barrage. Ces deux effets ont influencé de manière importante les fonctions d'amplification. Alors que la flexibilité du canyon affecte de manière significative la valeur de la fonction d'amplification maximale, cette valeur ne change pas pour les barrages en terre dans lesquels les canyons ont des formes différentes et la même longueur. De plus, la réponse latérale du barrage de terre dans le domaine temporel a été calculée pour analyser les effets susmentionnés lors d'un tremblement de terre réel. Les fonctions d'amplification proposées ont été utilisées pour comparer les spectres de réponse enregistrés du barrage d'El Infiernillo lors des tremblements de terre de 1966 avec la fonction d'amplification calculée. Un accord raisonnable a été observé entre eux. La méthode linéaire équivalente (EQL) a été implémentée dans le FEM. La technique FEMSBFEM a été étendue pour prendre en compte l'effet du comportement non linéaire des barrages en terre. Il a été observé que le comportement non linéaire affecte grandement la fréquence naturelle, la fonction d'amplification et l'accélération de crête maximale du barrage de terre situé dans les canyons. Les effets de la géométrie et de la flexibilité du canyon sur le comportement non linéaire ont été examinés, et on a vu qu'en augmentant la flexibilité du canyon, l'effet de la non-linéarité était diminué. Le barrage d'El Infiernillo a été modélisé par FEM-SBFEM non linéaire 3D, et une comparaison de la fonction d'amplification de crête obtenue par la méthode proposée avec les données enregistrées montre la précision du FEM-SBFEM non linéaire.

Abstract

The canyon surrounding a dam can be assumed as an unbounded domain, and the geometry and flexibility of a canyon are parameters that greatly affect the values of natural periods in earth dams. In this thesis, in order to take into account these two effects, canyons are modeled by SBFEM, and earth dams, which have limited geometries, are modeled by FEM. The hybrid FEM-SBFEM technique used for the dynamic three-dimensional analysis of soil-earth dam interactions is validated with results available in the literature. Because the dynamic-stiffness matrix of the unbounded domain is complex and frequency-dependent, the classical mode-superposition method is not straightforward for a soil-structure interaction system, and thus, to obtain their fundamental natural frequencies, the modeled dams were excited in the upstream-downstream direction. The natural periods of earth dams in canyons with different geometries shapes and impedance ratios are obtained, and are found to have significant effects on the dams' natural periods. The results are compared with actual recorded data, and it is found that the graphs put forward in this study may be used by practical engineers for the estimation of natural periods of earth dams in canyons with different shapes and material properties. Several amplification functions corresponding to different canyon conditions are obtained by applying a uniform displacement at the canyons' boundaries. A comprehensive study is performed to examine the effects of canyon geometry and flexibility on the steady-state responses of the dams, and it is found that these two effects significantly influence the amplification functions. While the flexibility of the canyon does affect the maximum amplification function value, this value does not change for earth dams in canyons that have different shapes but the same length. In addition, the lateral responses of earth dams in the time domain are computed in order to analyze the aforementioned effects under an actual earthquake. The proposed amplification functions are used to compare the recorded response spectra of the El Infiernillo dam under the two 1966 earthquakes with the calculated amplification function, and a reasonable agreement is observed between them. The equivalent linear method (EQL) is implemented into the FEM, and the FEM-SBFEM technique is extended in order to take into consideration the effect of earth dams' nonlinear behavior. It is observed that such nonlinear behavior greatly affects the natural frequency, the amplification function, and peak crest acceleration of earth dams located in canyons. The effects of canyon geometry and flexibility on the nonlinear behavior are examined, and it is found that by increasing canyon flexibility, the effect of nonlinearity is decreased. The El Infiernillo dam is modeled by the 3D nonlinear FEM-SBFEM, and comparison of the crest amplification function obtained by the proposed method with the recorded data shows the accuracy of the nonlinear FEM-SBFEM

Table des matières

Résumé ii
Abstract iii
Table des matières iv
List of figures vii
List of tables x
Acknowledgements xii
Foreword xiii
Introduction 1
Chapter 1 A review of earth dam-canyon interaction 5
1.1 Unbounded domain 5
1.1.1 Non-reflecting boundary conditions 6
1.1.2 Infinite Elements 7
1.1.3 Perfectly matched layer technique 7
1.1.4 Thin layer method 9
1.1.5 Exact non-reflecting boundary conditions (ENRBCs) 9
1.1.6 Boundary element method (BEM) 10
1.1.7 The scaled boundary finite-element method (SBFEM) 11
1.2 Amplification function 16
1.2.1 Natural frequency 22
1.3 Nonlinear behavior of earth dams 26
1.4 Conclusion 28
Chapter 2 Analysis of Earth Dam-Flexible Canyon Interaction with 3D Coupled FEM-SBFEM 30
2.1 Résumé 30
2.2 Abstract 30
2.3 Introduction 32
2.4 Methodology 34
2.4.1 SBFEM equation 34
2.5 Numerical examples 38
2.5.1 The rigid square massless plate on an isotropic homogeneous elastic half space 38
2.5.2 Earth dam foundation under an horizontal excitation 39
2.6 Conclusion 51

2.7 Appendix 52
2.8 Acknowledgements 53
Chapter 3 Computation of Amplification Functions of Earth Dam-Flexible Canyon Systems by the Hybrid FEM-SBFEM Technique 55
3.1 Résumé 55
3.2 Abstract 55
3.3 Introduction 57
3.4 Formulation 59
3.4.1 FEM formulation 60
3.4.2 SBFEM formulation 60
3.4.3 Coupled FEM-SBFEM formulation 61
3.4.4 Amplification Function 62
3.5 Verification 62
3.6 Numerical Examples 65
3.6.1 Results and discussions 66
3.7 Application of the calculated amplification functions 70
3.7.1 The El Infiernillo dam 71
3.8 Conclusion 73
3.9 Acknowledgments 74
Chapter 4 Shear Strain Dependent Amplification Function of Earth Dam-Flexible Canyon system by the Hybrid FEM-SBFEM Technique 75
4.1 . Résumé 75
4.2 Abstract 75
4.3 Introduction 76
4.4 Formulation 77
4.4.1 FEM formulation 78
4.4.2 SBFEM formulation 78
4.4.3 Coupled FEM-SBFEM formulation 79
4.4.4 Amplification function 80
4.4.5 Equivalent linear analysis 80
4.5 Numerical examples and discussion 83
4.6 The results and discussion 85
4.6.1 The El Infiernillo dam 93
4.7 Conclusion 95

4.8 Acknowledgments 97
Conclusion 98

List of figures

Figure 0-1. Earth dam: foundation layer (FEM), and elastic half-space (SBFEM) 2
Figure 1-1. Model for seismic analysis of surface structures and free field [7]..... 6
Figure 1-2. (a) Homogeneous isotropic, (b) a PML model [20] 8
Figure 1-3. Dynamic stiffness coefficients of elastic semi-infinite layer on fixed base computed using a PML model, as well as a viscous dashpot boundary model: L = d/2, LP = d, nb = np = 15, nd = 15, f1(x1)= 10(x1 – L)/LP [20] 8
Figure 1-4. Schematic model discretized in TLM 9
Figure 1-5. Finite element mesh using absorbing boundaries [35] 11
Figure 1-6. Vertical displacement at point A due to a vertical impulse load with different methods [35] 11
Figure 1-7. SBFE mesh for modeling the bounded half-space domains in the dynamic analysis of underground train-induced vibrations [51]..... 13
Figure 1-8. 3D FE extended mesh used for dynamic analysis of underground train-induced vibrations [51] ... 13
Figure 10 Scaled boundary coordinates: (a) scaling center O, radial coordinate ξ and boundary dis- cretization in circumferential coordinates η and for 3D modeling; (b) representation of the unbounded domain in 2D problems. 14
Figure 1-10. A linear elastic soil deposit [54] 17
Figure 1-11. Amplification function of an elastic undamped soil layer [54]..... 17
Figure 1-12. The AF of the damped soil on rigid bedrock [54] 18
Figure 1-13. Elastic soil layer on elastic bedrock [54] 18
Figure 1-14. Effect of impedance ratio on the AF [54] 19
Figure 1-15. a) Dam Cross-Section; b) Perspective View of Dam Geometry [56] 20
Figure 1-16. The mid-crest amplification function of an earth dam located in a rectangular canyon under incident excitation with different angles [56]..... 20
Figure 1-17. Three-dimensional view of darn in a rigid semi-cylindrical canyon [57]. 20
Figure 1-18. a) Steady-state response to harmonic base excitation for 2D and 3D models; b) effect of canyon shape on the mid-crest amplification function [57] 21
Figure 1-19. Effect of impedance ratio on the amplification function. 21
Figure 1-20. 2D dam on an elastic foundation [34] 22
Figure 1-21. The horizontal crest amplification function for a 2D earth dam on an elastic foundation 22
Figure 1-22. Model proposed by Ambraseys [59] 23
Figure 1-23. Natural frequencies of earth dams with different canyon shapes 24
Figure 1-24. Ratio of 3D natural frequencies to 2D natural frequencies of an earth dam located in a rectangular and triangular canyon [64] 25
Figure 1-25. Effect of canyon geometry on the fundamental natural period, T1 of a dam [65] 26
Figure 1-26. Time history of shear strain γyz at a point 40 m the crest of linear and nonlinear models of dam [67]..... 27
Figure 1-27. Strain-compatible soil properties [71] 28
Figure 2-1. Schematic view of a symmetric soil-structure interaction system 34
Figure 2-2. Scaled boundary coordinates: (a) scaling center O, radial coordinate ξ and boundary discretization in circumferential coordinates η and ζ for 3D modeling; (b) representation of the unbounded domain in 2D problems 35
Figure 2-3. Algorithm for coupled FEM-SBFEM solution 37

Figure 2-4. FEM-SBFEM mesh for a rigid square massless plate resting on an isotropic homogeneous elastic half-space 38
Figure 2-5. Vertical compliance of a rigid square massless plate resting on an isotropic homogeneous elastic half-space; (a) real part; (b) imaginary part..... 39
Figure 2-6. a) The geometry of the earth dam model; b) The location of earth dam in the canyon 40
Figure 2-7. Different canyons geometries: (a) Rectangular Canyon; (b) Wide trapezoidal canyon; (c) Narrow trapezoidal canyon; (d) Triangular canyon..... 40
Figure 2-8. General algorithm of the study 42
Figure 2-9. Displacement amplitude at the crest of dam in a rectangular canyon with L/H=2.5 and α =0.4..... 42
Figure 2-10. Effect of rectangular canyon geometry on the fundamental period 43
Figure 2-11. Deformation plot due to the excitation in direction of upstream-downstream(y direction) for the earth dam in the rectangular canyon with L/H=5 44
Figure 2-12. Comparison between natural frequencies of 2D and 3D models for the rectangular canyon with L/H=5 44
Figure 2-13. a) Real and b) imaginary parts of first mode shape of earth dam located in a rectangular canyon 45
Figure 2-14. Effect of wide trapezoidal canyon geometry on the fundamental period 46
Figure 2-15. a) Real and b)imaginary parts of first mode shape of earth dam located in a wide trapezoidal canyon 46
Figure 2-16. Effect of narrow trapezoidal canyon geometry on the fundamental period..... 47
Figure 2-17 a) Real and b) imaginary parts of first mode shape of earth dam located in a narrow trapezoidal canyon. 47
Figure 2-18. Effect of triangular canyon geometry on the fundamental period 48
Figure 2-19. a) Real and b) imaginary parts of first mode shape of earth dam located in a triangular canyon. 48
Figure 2-20. The effect of canyon geometry on natural periods of earth dams with $L/H = 5$ for: a) $\alpha = 0.6$ and b) $\alpha = 0$..... 49
Figure 2-21. Comparison of natural periods for different values of α and L/H=5..... 49
Figure 2-22. Transverse and longitudinal cross sections of Cogswell Dam [96]..... 50
Figure 2-23. Comparison of obtained natural period by FEM-SBFEM and recorded natural periods under the Sierra Madre earthquake 51
Figure 3-1. Symmetric earth dam-canyon interaction system..... 60
Figure 3-2. Diagram of AF application 62
Figure 3-3. (a) Vertical compliance; (b) Horizontal compliance; and (c) Rocking compliance of a rigid square massless plate resting on an isotropic homogeneous elastic half-space [114]..... 64
Figure 3-4. Amplification value for the first natural frequency 65
Figure 3-5. Displacement contours in upstream-downstream direction under harmonic canyon excitation for: a) the canyon mesh; b) the assembled earth dam-canyon mesh 66
Figure 3-6. Amplification function of the earth dam in a rectangular canyon with different values α, L/H and β66
Figure 3-7. Amplification function of an earth dam in a wide trapezoidal canyon with different α, L/H and β ... 67
Figure 3-8. Amplification function of an earth dam in a narrow trapezoidal canyon with different α, L/H, and β68
Figure 3-9. Amplification function of an earth dam in a triangular canyon with different values α, L/H and β... 69
Figure 3-10. Comparison of the effect of canyon geometry on the first amplitude for an earth dam located in a canyon with L/H=2.5 and β=10% 70

Figure 3-11. Different steps to obtain the crest response due to an earthquake: a) The S90W El-Centro earthquake (1940) horizontal ground motion; b) Fourier amplitude spectrum of the earthquake; c) The transfer function obtained by FEM-SBFEM for α=0.1 and L/H=5; d) product of the amplification function (c) and the Fourier series of the input motion (b); e) time history of the crest under the earthquake obtained by inverting the Fourier series from (d) 72
Figure 3-12. El Infiernillo dam: (a) maximum cross section; (b) geological profile [117] 73
Figure 3-13. Response Spectra of El Infiernillo rockfill dam due to two earthquakes during the year 1966 73
Figure 4-1. a symmetric earth dam-canyon interaction system 78
Figure 4-2. The different steps of the nonlinear FEM-SBFEM methodology 82
Figure 4-3. Strain-Compatible Soil Properties [71] 83
Figure 4-4. (a) Vertical compliance; (b) Horizontal compliance and; (c) Rocking compliance of a rigid square 84
Figure 4-5. a) the effective shear strain, b) G/Gmax ratio for the earth dam located in the rectangular canyon with L/H=2.5 85
Figure 4-6. Nonlinear and linear amplification functions of earth dams in triangular canyons with different values of α and L/H 87
Figure 4-7. Nonlinear and linear amplification functions of the earth dams in trapezoidal canyons with different values of α and L/H 88
Figure 4-8. Nonlinear and linear amplification functions of the earth dams in rectangular canyons with different values of α and L/H 89
Figure 4-9. a) The S90W El-Centro earthquake horizontal ground motion (1940); b) The input motion in the frequency domain; c) The calculated crest amplification functions by the linear and nonlinear FEM-SBFEM for the earth dam, with β=10%, located in a rectangular canyon with L/H=5 and α=0.5; d) Multiplying the crest amplifications (c) and the input Fourier amplitude (b); e) The crest response in the time domain 92
Figure 4-10. Crest acceleration time history, obtained by linear and nonlinear FEM-SBFEM under the El Centro earthquake, for the earth dam with L/H=5 located in a rectangular canyon with different values of the impedance ratio (α), ... 92
Figure 4-11. a) Plan view of the El Infiernillo Dam; b) Cross-section of the El Infiernillo Dam 94
Figure 4-12. a) 3D CAD model of El Infiernillo; b) 3DFEM model of El Infiernillo 95
Figure 4-13. a) The AF of the earth dam-canyon system with α=0.3 and β=8% by nonlinear FEM-SBFEM, and the response spectra of the 1975 earthquake 95

List of tables

Table 1-1. An [59] 23
Table 2-1. Comparison of obtained natural frequencies for 3D canyons with L/H=5 and 2D results 45
Table 2-2. β parameter for different values of impedance ratio and L/H for different canyon shapes 53
Table 3-1. Material Properties of the El Infiernillo dam 71
Table 4-1. The linear and nonlinear natural frequency and AF_{max} calculated by FEM-SBFEM 90
Table 4-2. Comparison of the crest acceleration obtained by linear and nonlinear FEM-SBFEM 93
Table 4-3. Material properties 94

Dedicated to the students of Taleghani Technical High School of Shazand

Acknowledgements

First, I am extremely grateful to my supervisor, Professor Jean-Marie Konrad, for his continuous support, patience, and trust during my Ph.D. studies. His invaluable knowledge and experience in different engineering subjects helped me to find relationships between complex mathematical equations and engineering problems. I would also like to thank all the members of our group, especially Mr. Luc Boisvert for his administrative aid.

My appreciation also goes out to my family for their spiritual support throughout my life, and to my friends for all their support during my studies.

Foreword

This doctoral thesis is written in an article-based format comprising three scientific papers. The papers constitute Chapters 2-4, followed by the conclusion in Chapter 5. Chapter 1 presents the literature review. The papers have been either published or accepted for publication in scientific journals, or have been submitted for publication. The list of papers is as follows:

Chapter 2:

A. Yaseri and J. Konrad, "Estimation of Natural periods of Earth Dam-Flexible canyon systems with 3D coupled FEM-SBFEM," Computer and Geotechnics., vol. 123, no. March, p. 103546, 2020. doi: 10.1016/j.compgeo.2020.103546. (Submitted 1 November 2019; Submitted in revised form 16 February 2020; Accepted 13 March 2020).

Chapter 3:

A. Yaseri and J. Konrad, "Computation of Amplification Functions of Earth Dam-Flexible Canyon Systems by the Hybrid FEM-SBFEM Technique" Earthquake Engineering and Structural Dynamics. (Submitted 14 December 2020; Submitted in revised form 8 February 2021; Accepted in 3 May 2021)

Chapter 4:

A. Yaseri and J. Konrad, "Nonlinear Earth Dam-Flexible Canyon Interaction by the Hybrid FEMSBFEM Technique" Engineering Geology. (under review)

Introduction

Dams are built for different purposes, such as hydropower, water supply, flood control, sediment control, etc. Earth dams constitute 75% of all of the dams in the world, and they are subjected to a wide variety of natural hazards; e.g., landslides, earthquakes, flooding, etc. Earthquakes are the most significant natural disasters regarding dam stability and safety. Though many studies have been done to investigate the behavior of earth dams under earthquake loading, more in-depth study is still required to further understand of the seismic behavior of earth dams.

There exist over 10,000 dams in Canada, with more than 8000 dams and dikes in Quebec, and around 72% of these structures are earth-filled or rock-filled. The majority of dams are located in the western and eastern parts of the country, which are considered to be the areas with the most significant seismic activities in Canada. Dams have experienced Richter magnitude 7.2 and 6 earthquakes in just the last century in British Columbia (1949) and Saguenay, Québec (1988), respectively.

Statement of problems

The seismic response of an earth dam to earthquake loading is affected by interactions between the dam and the soil (or rock) surrounding the dam. The geometry and material of the canyon play a key role in determining the characteristics of an earth dam's seismic response. A geometrically limited earth dam has dynamic interactions with the surrounding soil or rock, which has an unlimited geometry. In the literature, this effect is known as earth dam-foundation interaction, canyon-earth dam interaction, etc. In the present work, the term unbounded- earth dam will be used to refer to this effect.

Some parts of the soil adjacent to an earth dam exhibit nonlinear behavior. This region and the earth dam's dimensions are finite and make a bounded domain. Many approaches are capable of doing a nonlinear dynamic analysis of a bounded domain, with the finite element method (FEM) being the most popular. Although FEM is well suited for modeling the complex geometry and nonlinear behavior of materials, it is not possible to model an unbounded domain by FEM, as an unbounded domain must be terminated by an artificial boundary. To compensate for this weakness, different techniques have been utilized, and the scaled boundary finite element method (SBFEM) has received increasing attention as an appropriate approach for modeling unbounded domains for different soil-structure interaction problems. The nonlinear interaction of an earth dam and unbounded soil occurs at the boundary (Figure 1) by using the coupled FEM-SBFEM. This is divided into two parts: bounded and unbounded domains, which are modeled by the FEM and SBFEM, respectively.

As the SBFEM can successfully model even unbounded domains with complex geometries, boundary 1 can be chosen at the nearest possible distance to the dam body (Figure 2). This computational-efficient model is capable of doing a 3D nonlinear analysis considering all three effects.

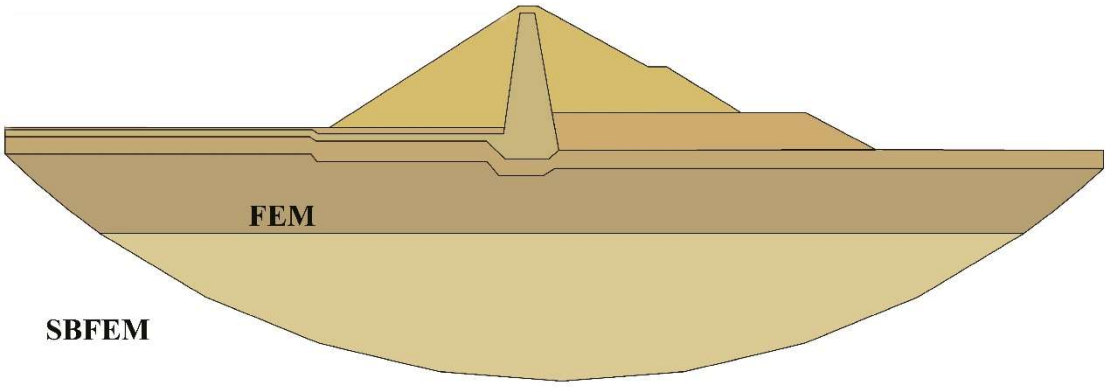

Figure 0-1. Earth dam: foundation layer (FEM), and elastic half-space (SBFEM)

The 3D FEM-SBFEM equation is derived in order to conduct a comprehensive study of the effects of the flexibility and geometry of canyons on the seismic responses of earth dams. Therefore, the objectives of this thesis are as follows:

(1) Introducing the 3D FEM-SBFEM hybrid technique as an appropriate tool for the dynamic analysis of earth dam-canyon interaction systems in the frequency domain

(2) Examining the effects of the flexibility and geometry of canyons on natural periods

(3) Proposing new graphs for the estimation of natural periods in canyons with different shapes and material properties

(4) Developing the FEM-SBFEM technique to calculate the amplification function of earth dam-flexible canyon systems

(5) Studying the flexibility and geometry effects of canyons on the seismic responses of dam crests

(6) Suggesting several amplification functions relevant to different canyon conditions that can be straightforwardly used to obtain earth dam time and frequency domain responses considering the effect of canyon flexibility and geometry

(7) Developing the FEM-SBFEM technique to consider the effect of nonlinearity

(8) Examining nonlinear behavior effects on the natural frequency, amplification function, and peak crest acceleration of earth dams located in canyons with different material and geometry conditions

Scope of research

In Chapter 1, the importance of the effects of unbounded-dam interaction, canyon-dam interaction, and nonlinearity are discussed, and state-of-the-art knowledge is presented. Although a lot of work has been done to consider these effects separately, there is limited work taking into account all three effects simultaneously, and this is especially true for earth dams.

Chapter 2 presents a paper published in the journal “Computers and Geotechnics”. The FEM-SBFEM hybrid technique is introduced in order to estimate the natural periods of earth dams, incorporating the effects of a canyon’s 3D geometry and flexibility. The canyon was modeled by SBFEM and the earth dam, which has limited geometry, by FEM. The proposed method is validated with results available in the literature, and the calculated natural periods are compared with actual recorded data.

Chapter 3 presents a paper submitted to the journal “Earthquake Engineering and Structural Dynamics” in which the FEM-SBFEM hybrid technique is developed to obtain the linear crest amplification function (AF). The methodology is verified with results available in the literature. The effects of geometry and flexibility canyon on an AF are considered, and the calculated AF is compared with corresponding data recorded under an actual earthquake.

Chapter 4 presents a paper submitted to the journal “Géotechnique”. The finite element method (FEM) is a powerful tool for the nonlinear modeling of dynamic problems, and in this chapter, the equivalent linear method (EQL) is implemented in the FEM. To satisfy the radiation damping condition and rigorously model a canyon as an elastic unbounded domain, the scaled boundary finite element method (SBFEM) is utilized. The FEM is coupled with the SBFEM to take into consideration the effect of an earth dam’s nonlinear behavior. The linear and nonlinear amplification functions are compared, and the effects of canyon geometry and flexibility on the nonlinear amplification function and natural frequency are examined. The El Infiernillo dam was modeled by 3D nonlinear FEM-SBFEM, and the crest amplification function obtained by the proposed method is compared with recorded data.

Chapter 5 gives a summary of the thesis, followed by conclusions, and also provides directions for future work.

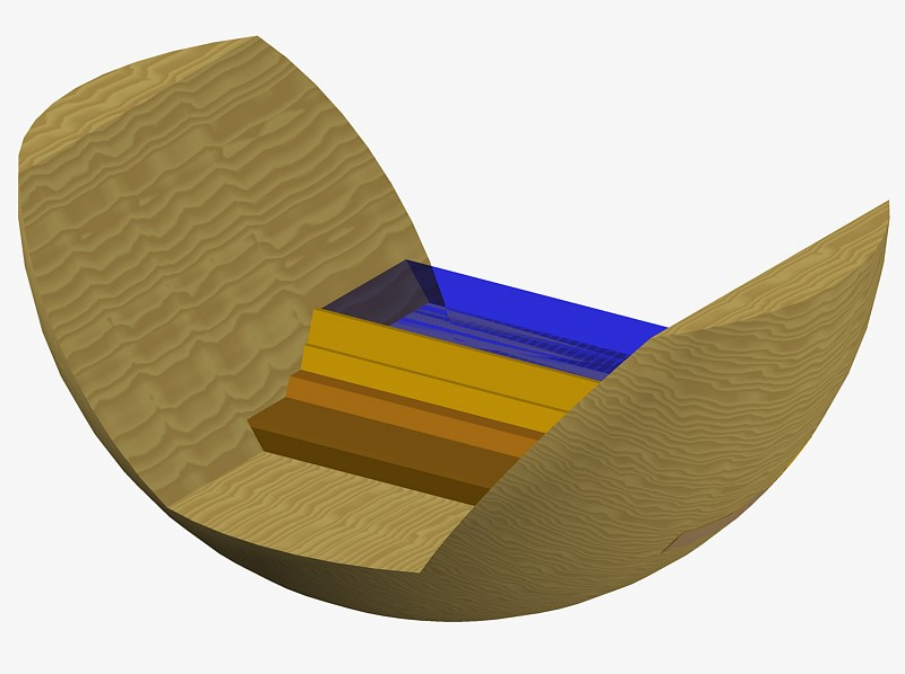

Figure 2 Schematic view of the proposed model

Chapter 1 A review of earth dam-canyon interaction

Until the 1960s, theoretical models were widely used to simulate the simplified behavior of earth dams under earthquakes. However, the emergence of high-performance computers has stimulated the development of numerical methods. The capability of numerical methods to solve complex problems has made them popular as highly efficient tools in engineering fields. The first analyses of earth dams under dynamic loadings by numerical methods were done in the 1960s [1], [2].

After over a half-century of developing numerical methods for the dynamic analysis of earth dams, numerous factors have been found to affect the responses of such dams. However, a few factors are considered as the most influential, and the remaining are treated as of secondary importance. The nonlinear behavior of an earth dam, earth dam-far field interaction, reservoir-earth dam interaction, and canyon (or foundation)-earth dam interaction effects have a great impact on the dynamic behavior of these dams, while the compressibility of water, absorption due to sediments, advanced soil models, etc., are of lower importance.

Although researchers have aimed to introduce the most accurate models possible, it should be noted that taking into consideration all influential effects results in a highly demanding computational problem. Furthermore, to reach an optimum model, the four more important effects must be taken into account. Therefore, the literature review is dedicated to considering these effects.

1.1 Unbounded domain

As mentioned earlier, earth dams have bounded media, and it is straightforward to solve dynamic analysis problems with existing numerical methods like the FEM and FDM (Finite Difference Method). However, in reality, an earth dam interacts dynamically with the surrounding soil, which is an unbounded domain. For example, a finite element model of an earth dam which is solved under dynamic loading, like an earthquake, when the inducing wave from the vibration of the earth dam reaches the fictitious boundary is reflected inside the discretized bounded domain while the wave should be passed through the boundary and goes toward infinity.

To solve this issue, various techniques have been suggested in the last few decades. These approaches are divided into two groups, i.e., local and global procedures. The local procedure, like absorbing layer, transmitting boundary conditions, and infinite elements, are simple techniques that enforce an artificial boundary to attenuate the outgoing waves, and are easily implemented in the FEM. Global procedures like the boundary element method (BEM), thin layer method (TLM), and SBFEM, however, are approaches that have their own equations and are independent of FEM. As global procedures provide the capability to model the unbounded domain and the stiffness and mass matrices could be obtained in the same way in the FEM, they can be coupled with the FEM to overcome the weakness of FEM in modeling the unbounded domain. Global procedures are well-known

for their accuracy in comparison with local methods, and the literature review of the local and global procedures is presented separately in the following sections.

1.1.1 Non-reflecting boundary conditions

Non-reflecting boundary conditions (NRBCs), which have been called by different names such as “absorbing boundary conditions”, were proposed in the late 1960s. The classical viscous boundary condition was proposed by Lysmer and Kuhlemeyer (LC ABS) [3], and both scalar and vector waves have been solved using the superposition boundary condition [4]. Viscous boundary conditions are simple and can be implemented in the FEM, and Sommerfeld-like NRBCs were widely used until the late 1970s [5]. Today, these boundary conditions are known as zero-order boundary conditions. Low-order NRBCs have been introduced from the late 1970s. Although accuracy is increased by increasing the order of approximation, only second-order equations can be implemented in the FEM. Today, second-order formulations are widely used, and Engquist–Majda NRBCs [6] are among the most well-known. Different types of NRBC are available in commercial software; e.g., the LC ABS technique is available in ABAQUS and ANSYS.

This technique only effectively absorbs waves arriving at the boundary with an angle larger than 30 degrees. Also, this method is suitable for soil-structure interaction problems, with the source of dynamic excitation inside the model. If the source is alongside the boundaries, the absorbing boundary cannot attenuate the waves properly, and consequently, the free boundary condition, which is a combination of a viscous boundary and a load history, has been introduced for earthquake loading. This approach is available in FLAC, DIANA, and PLAXIS, which are the most common software for seismic geotechnical engineering. Figure *1-1* shows the viscous boundary and free-field boundary that are utilized in FLAC.

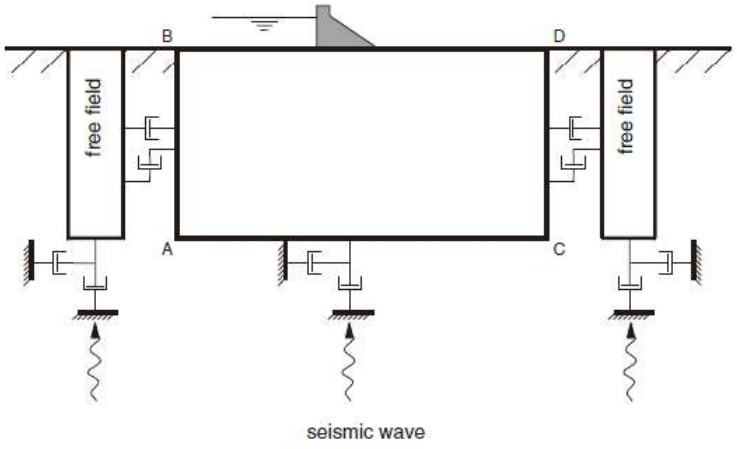

Figure 1-1. Model for seismic analysis of surface structures and free field [7]

These software are widely used by designers, engineers, and researchers for the dynamic analysis of earth dams, and FLAC and DIANA have been utilized for modeling of different types of earth dams, and the viscous and free field boundary conditions have been implemented in the models [8]–[10]. Similarly, ABAQUS has been utilized with using viscous dashpot element [11].

To sum up, although the viscous boundary technique is not an accurate approach, because of its simplicity and being straightforward to implement in commercial software, it is widely used. Also, this technique usually is used for unbounded domains with simple geometries.

1.1.2 Infinite Elements

The infinite element method (IEM) [12] is very similar to the FEM. This method was introduced in order to extend the FEM to satisfy the radiation condition. The IEM has been developed by many researchers, including Bettes [13], Valiappan and Zhao, Khalili et al. [14], and Astely [15] to model wave propagation in unbounded domains. In this approach, the bounded domain is modeled by the FEM and the unbounded domain by the IEM. In the IEM, the wave propagating toward infinity is represented by decay functions in shapes functions of displacements. As the equations cannot be directly derived in the time domain, the IEM has mostly been developed for time-harmonic analyses.

The IEM has been used to analyze gravity dam-foundation-reservoir interactions. Saini et al. [12] utilized the FEM-IEM to model the seismic behavior of a dam-reservoir system. The dam was assumed to be located on rigid bedrock, and the effect of the unbounded foundation was neglected. As well, Hariri-Ardebili and Mirzabozorg [16] conducted a time-domain analysis to take into account the effects of the reservoir and unbounded foundation in the FEM-IEM.

1.1.3 Perfectly matched layer technique

The perfectly matched layer (PML) technique was introduced by Bérenger [17] for the absorption of electromagnetic waves. In this technique, the unbounded domain is modeled by an absorbing layer with a finite thickness that reduces the reflected waves. The PML technique has been developed for the scalar wave equation and the Helmholtz equation [18], [19].

Basu and Chopra [20] employed a complex coordinate system in PLM for implementing in FEM elastodynamic equations. A dam-reservoir system has been solved using PLM [21], and it was shown that in order to achieve proper accuracy, the length of the reservoir should be two times greater than the height of the dam. This number is increased to six times when the excitation source has a vertical component. Hence, to absorb the waves, the reservoir should be sufficiently large which results in a time demand analysis. Different time and frequency domain problems have been solved, and results have been compared with obtained results by utilizing absorbing

boundaries [20], [22], [23]. For example, for the problem shown in Figure 1-2, with a 5 percent damping ratio, the computed results are shown in Figure *1-3*. While highly accurate results have been obtained from the PLM, the results of models utilizing the absorbing boundary conditions show appreciable inaccuracies. More examples can be found in the aforementioned references.

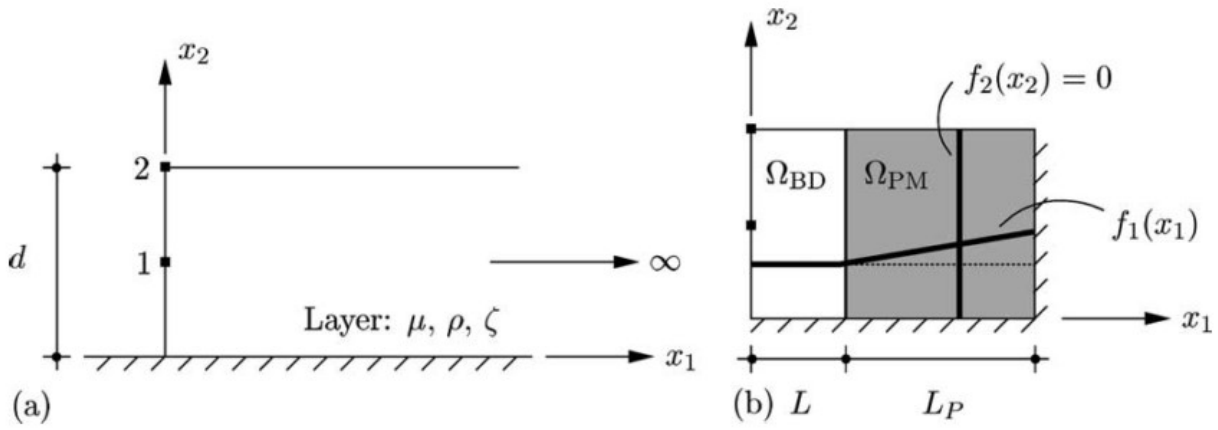

Figure 1-2. (a) Homogeneous isotropic, (b) a PML model [20]

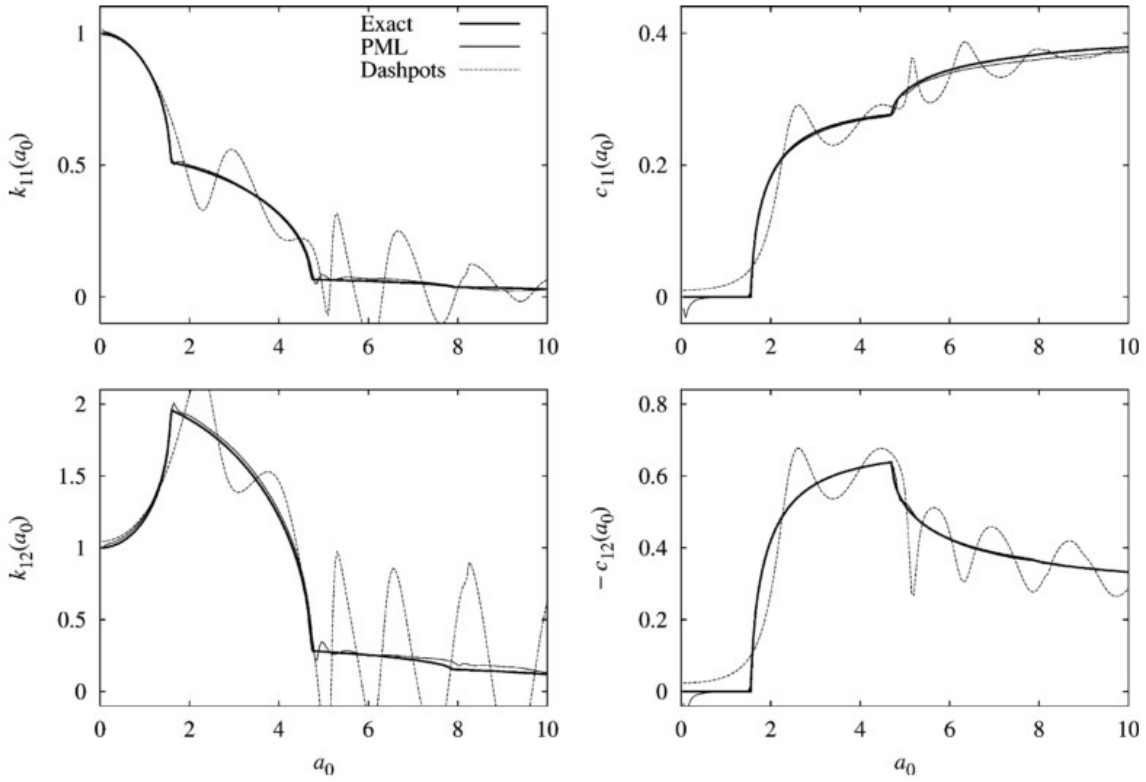

Figure 1-3. Dynamic stiffness coefficients of elastic semi-infinite layer on fixed base computed using a PML model, as well as a viscous dashpot boundary model: L = d/2, LP = d, nb = np = 15, nd = 15, f1(x1)= 10(x1 –L)/LP [20]

In conclusion, the PML method is highly accurate for problems with the source of excitation inside a bounded domain, such as moving loads, foundation vibration, etc. For loading on a boundary, such as earthquake loading, the method is more complicated. As stated in [24], "PML media only absorb waves generated in the bounded domain. Hence, a particular approach should be employed to incorporate incident waves generated in the exterior domain due to vertical ground motions at the reservoir bottom."

1.1.4 Thin layer method

The thin layer method (TLM) is a global procedures introduced by Lysmer and Wass [24]. As shown in Figure 1-4, the bounded finite element model is surrounded by the unbounded domain. The unbounded domain is constituted in three parts: the left and right parts, which are discretized consistent with the FEM domain, and the rigid bedrock located below the model. The two lateral parts are extended to infinity in the horizontal direction. The TLM is suitable for models with horizontal layers in which the material properties are constant for each layer and change with depth. The displacements vary linearly and exponentially in the vertical and horizontal directions, respectively. This technique has been developed for axisymmetric models [25], and has been extended for poroelastic materials [26], time-domain analysis [27], and layered strata with zigzag boundaries [28].

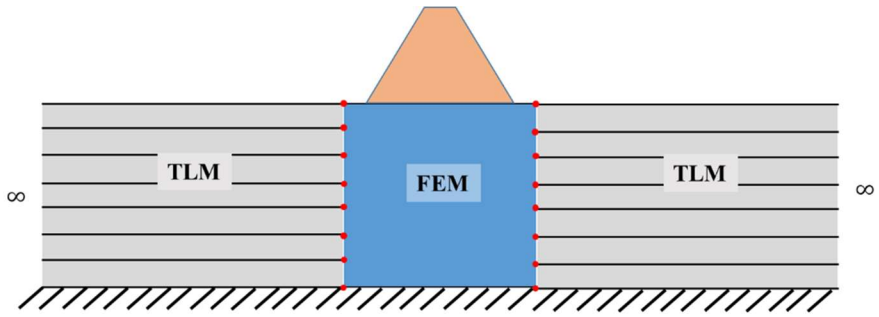

Figure 1-4. Schematic model discretized in TLM

Bougacha and Tassoulas [29] utilized this technique in their analysis of dam-reservoir-foundation interactions, taking into account the effects of a horizontally infinite foundation and a reservoir resting on rigid bedrock.

As a result, the TLM is easily implemented in the FEM and is well-suited for an unbounded domain with horizontal layers. However, the assumptions of horizontal and rigid bedrock limit the application of the method in practical geotechnical analyses.

1.1.5 Exact non-reflecting boundary conditions (ENRBCs)

Similar to the other global procedures, the exact solution is formulated exactly at the artificial boundary. Givoli and Keller [30] obtained an exact solution for 2D time-harmonic problems with a circular artificial boundary, while the technique has been developed for 3D spherical boundary conditions by Grote and Keller [31]. It has also

been implemented in the FDM and FEM [32]. The method has further been developed for non-circular and non-spherical boundaries by enclosing the actual artificial boundary between two addition boundaries, circular boundaries for 2D and spherical boundaries for 3D, and then applying the interpolation technique [33].

As a result, ENRBC is formulated based on an exact solution on the boundaries. As the exact solution is available only for boundaries with simple geometries and materials, the practical problems that can be solved with this method are limited.

1.1.6 Boundary element method (BEM)

Using the BEM, the radiation condition at infinity can be exactly satisfied through the use of suitable fundamental solutions; however, the fundamental solutions can be very complicated. The coupling of the FEM and BEM can be beneficial by obtaining the advantages of each. Linear and nonlinear models based on the coupled FEM-BEM technique have been successfully implemented to investigate the behavior of dams under seismic loading [34].

Yazdchi et al. [35] considered the transient responses of elastic dams by utilizing the FEM-BEM. For a block under transit loading, two different meshes for models with an absorbing boundary have been used (Figure 1-5). The results have been compared with the BEM and FEM-BEM results (Figure *1-6*); i.e., "This indicates that even though absorbing boundaries are efficient in absorbing the energy, the accuracy of the results is dependent on the extent of the mesh used. Naturally, this large number of elements in the FEM will increase the computational cost, especially in non-linear analysis in which coefficient matrices have to be evaluated at every time step" [35].

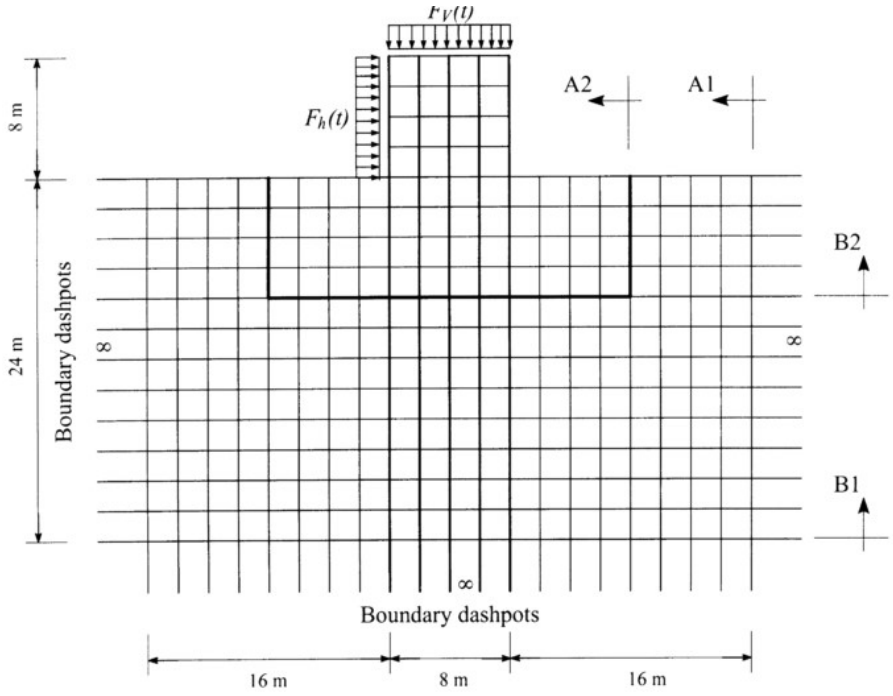

Figure 1-5. Finite element mesh using absorbing boundaries [35]

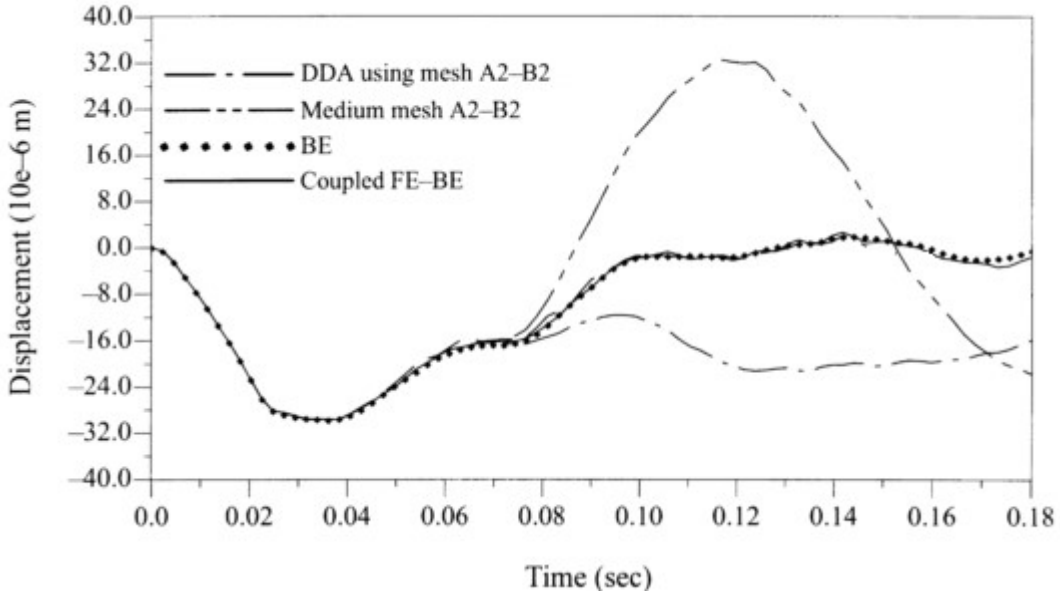

Figure 1-6. Vertical displacement at point A due to a vertical impulse load with different methods [35]

1.1.7 The scaled boundary finite-element method (SBFEM)

The SBFEM, a novel semi-analytical method in computational mechanics combining the advantages of both the FEM and BEM, was originally developed by Wolf and Song [36] for the dynamic analysis of unbounded domains. Only the boundary is discretized, no fundamental solution is necessary, and general anisotropic materials can be analyzed without additional efforts. The method proved far more versatile than initially envisaged, and was

extended successfully for static and bounded domains. It has also been extended for the dynamic analysis of non-homogeneous unbounded domains, with the elasticity modulus and mass density varying as power functions of spatial coordinates [37], [38]. In this method, the analytical nature of the solution in the radial direction allows accurate stress intensity factors in fracture mechanics to be determined directly from the definition. In statics, an eigenvalue problem is solved, leading to displacement and stress amplitudes. In the frequency domain, the SBFE equation is expressed regarding the dynamic-stiffness matrix, while in the time domain, the SBFE equation in acceleration unit-impulse response including convolution integrals are obtained. To increase the computational efficiency of the technique, a reduced set of base functions is constructed by excluding the higher-order modes determined from the eigenvalue problem used in static analysis [39]. The sparsity and the lumping of the coefficient matrices of the SBFEM are exploited to further reduce the computational costs [40]. A Padé series solution for the SBFEM equation in dynamic stiffness has also been developed for frequency-domain analyses [41].

Ekevid and Wiberg [42] and Ekevid et al. [43] used the SBFEM to simulate ground responses to high-speed trains moving over ground surfaces, and Syed and Maheshwari [44] improved the efficiency of the 3D FEM-SBFEM approach for soil-structure interaction (SSI) analysis in the time domain. The hybrid technique was used for the nonlinear analysis of a soil-pile system [45]. Xu et al. [46] and Seiphoori et al. [47] modeled CFRD-reservoir systems by FEM-SBFEM in order to consider the effects of hydrodynamic pressure on the dynamic stresses in slabs of high CFRD. Chen et al. [48] introduced an efficient nonlinear SBFEM with octree mesh for the dynamic analysis of some complicated geotechnical structures such as earth dams, while Lin et al. [49] proposed the SBFEM as an efficient method for dynamic dam-reservoir interaction systems. Also, Zhao et al. [50] used the FEM-SBFEM to consider the seismic responses of dams and offshore structures, with the SBFEM being applied at the water-structure interfaces.

The 3D SBFEM has been introduced as an appropriate tool for the dynamic analysis of geotechnical structures [51]. The SBFEM (Figure 1-7) and FEM (Figure 1-8) models have been compared for analysis of a tunnel under train-loading. While the SBFEM shows accurate results, the results of the FEM are only valid for times less than t=0.25s (early times of the response). After 0.25 s, the response obtained from the FEM deteriorates, as the enforced boundary conditions are not able to accurately capture the unbounded domain and absorb the energy of outgoing waves. The inducing waves from the vibration have been reached the fictitious boundary and reflected inside the domain and received at the observing points before 0.25s. It can be seen, the model with SBFEM has a small bounded domain. It leads to an effective computational model [51].

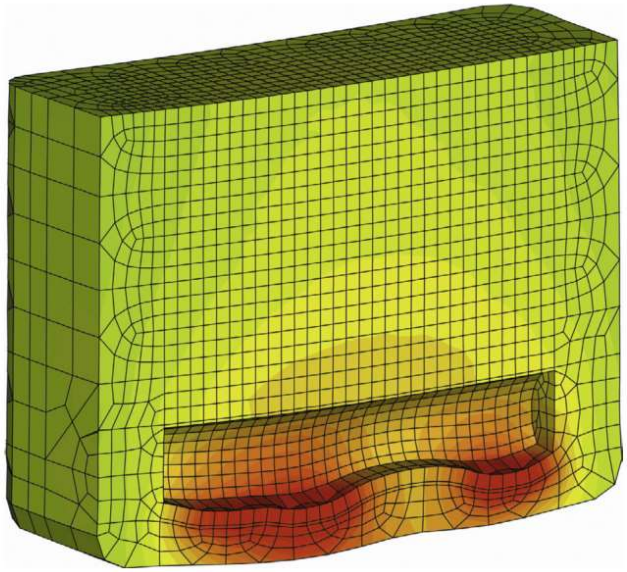

Figure 1-7. SBFE mesh for modeling the bounded half-space domains in the dynamic analysis of underground train-induced vibrations [51]

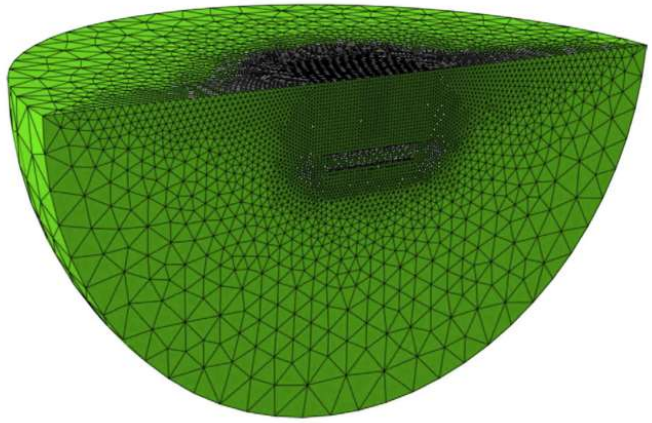

Figure 1-8. 3D FE extended mesh used for dynamic analysis of underground train-induced vibrations [51]

1.1.7.1 SBFEM equation

The SBFEM equation for modeling the unbounded domain is briefly presented here. The scaled boundary coordinate system is defined in a local coordinate system ξ, η, ζ. The radial coordinate ξ is measured from O (the scaling center), and the circumferential coordinates are defined by η and ζ.

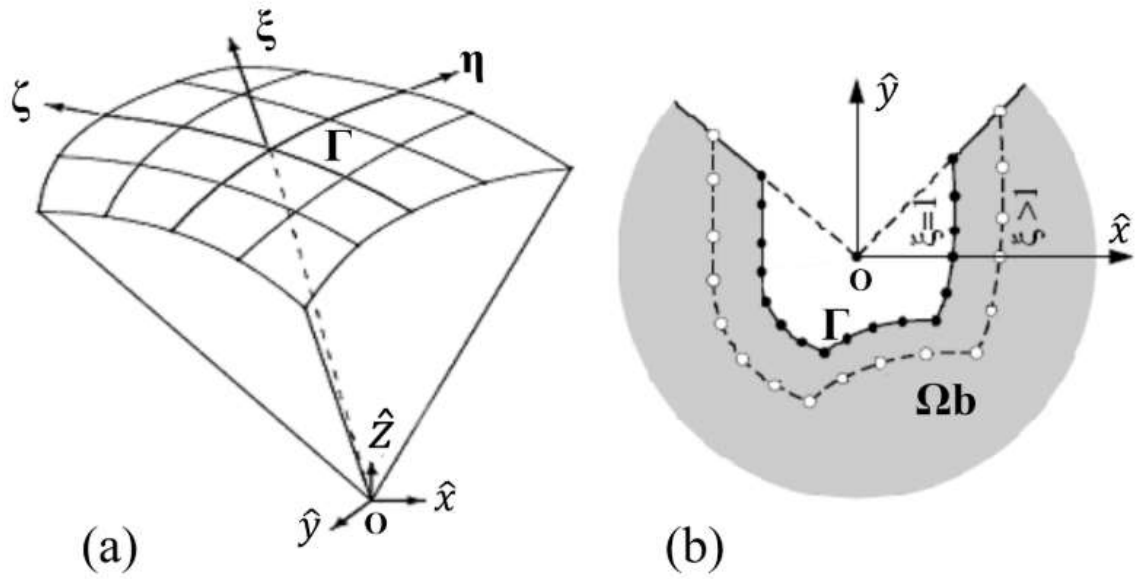

Figure 9 Scaled boundary coordinates: (a) scaling center O, radial coordinate ξ and boundary dis- cretization in circumferential coordinates η and for 3D modeling; (b) representation of the unbounded domain in 2D problems.

For 3D problems, only the doubly-curved surface boundary Γ is discretized. The unbounded domain Ω_b in radial coordinate ξ starts from ξ=1 on the boundary Γ to $\xi = \infty$. Each point $(\hat{x}, \hat{y}, \hat{z})$ is represented by scaling its corresponding point (x, y, z) on the surface boundary Γ and by using the mapping shape functions $[N(\eta, \zeta)]$ along the circumferential coordinates. While node positions are defined in the scaled boundary coordinate system, stresses, strains, and displacements are specified in the Cartesian coordinate system. Using the shape function $[N^u(\eta, \zeta)]$, the nodal displacements inside the domain at a node (ξ, η) from the displacement function. The displacement at a node (ξ, η) inside the domain is interpolated from the displacement functions $\{u(\xi)\}$ $\{\hat{T}(\xi)\}$.

$$\{u(\xi, \eta, \zeta)\} = [N^u(\eta, \zeta)]\{u(\xi)\} = [N_1(\eta, \zeta)[I], N_2(\eta, \zeta)[I], ...]\{u(\xi)\} \quad (1\text{-}1)$$

which [I] is a 3×3 identity matrix. By applying the virtual work method in the circumferential directions η, ζ [52] or by Galerkin's weighted residual technique [36], the scaled boundary finite-element equation is obtained. As the dynamic analysis in this work has been done in the frequency domain, only the SBFEM equations in the frequency domain are presented. The 3D scaled boundary finite-element equation in displacement for the frequency domain is presented as:

$$[E^0]\xi^2\{u(\xi)\}_{,\xi\xi} + (2[E^0] - [E^1] + [E^1]^{\mathrm{T}})\xi\{u(\xi)\}_{,\xi} + ([E^1]^{\mathrm{T}} - [E^2]\{u(\xi)\} + (\omega\xi)^2[M^0]\{u(\xi)\} = 0 \tag{1-2}$$

where ω denotes the excitation frequency and $[E^0]$, $[E^1]$, $[E^2]$, and $[M^0]$ represent the coefficient matrices achieved by assembling their corresponding coefficient matrices for each element, as in the finite-element method [36]. They are independent of ξ. The coefficient matrices $[E^0]$ and $[M^0]$ are positive-definite, $[E^1]$ is non-symmetric, and $[E^2]$ is positive-definite. Analogous to the standard finite element, the nodal force-displacement relationship is obtained. The internal nodal forces $\{q(\xi)\}$, which are the results of the surface tractions, are determined.

$$\{q(\xi)\} = \xi^2([E^0]\xi\{u(\xi)\}_{,\xi} + [E^1]^{\mathrm{T}}\{u(\xi)\}) \tag{1-3}$$

The internal nodal forces $\{Q(\xi)\}$ are equal to the external nodal loads $\{R(\xi)\}$.

$$\{R(\xi)\} = -\{q(\xi)\} = [S^{\infty}(\omega,\xi)]\{u(\xi)\} \tag{1-4}$$

Using Equations (1-2), (1-3), and (1-4) and eliminating $\{q(\xi)\}$ and $\{u(\xi)\}$ results in the scaled boundary finite element equation in dynamic stiffness in the frequency domain for unbounded domain:

$$([S^{\infty}(\omega)] + [E^1])[E^0]^{-1}([S^{\infty}(\omega)] + [E^1]^T) - (s-2)[S^{\infty}(\omega)] - [E^2] - \omega[S^{\infty}(\omega)]_{,\omega} + \omega^2[M^0] = 0 \tag{1-5}$$

where $[S^{\infty}(\omega)]$ is the dynamic-stiffness matrix of an unbounded domain.

1.1.7.2 Solution procedure

Equation (1-5) is a system of first-order nonlinear ordinary differential equations with respect to the frequency ω, which is solved numerically using a fourth-order Runge-Kutta method. An asymptotic expansion of the dynamic-stiffness matrix for high frequency is used to start numerical integration:

$$[S^{\infty}(\omega)] = [K_{\infty}] + \mathrm{i}\omega[C_{\infty}] + \sum_{i=1}^{m}[A^{(i)}](\mathrm{i}\omega)^{-i} \tag{1-6}$$

in which $[C_\infty]$, $[K_\infty]$, and $[A^{(i)}]$ are coefficient matrices [52]. $[S^\infty(\omega_h)]$ is obtained for a sufficiently high but finite value of the frequency ω_h and is used as an initial point to numerically solve Equation (1-5). Therefore, the dynamic-stiffness matrix of the unbounded domain is $[S^\infty(\omega)]$, calculated for the desired frequencies.

1.1.7.3 Coupling of bounded and unbounded domains

As discussed earlier, the coupling of FEM (Ω_s) and SBFEM (Ω_b) is done using the interface Γ. Using the obtained nodal force-displacement relationships for SBFEM (Equation (1-4)) and that of FEM, the assembled relationship is obtained as:

$$\begin{bmatrix}[S_{ss}] & [S_{sb}] \\ [S_{bs}] & [S_{bb}]+[S^\infty]\end{bmatrix}\begin{Bmatrix}\{u_s\} \\ \{u_b\}\end{Bmatrix}=\begin{Bmatrix}\{P_s\} \\ \{P_b\}\end{Bmatrix} \tag{1-7}$$

$[S]$ is the dynamic-stiffness matrix of the bounded domain, which is obtained as:

$$[S]=\begin{bmatrix}[S_{ss}] & [S_{sb}] \\ [S_{bs}] & [S_{bb}]\end{bmatrix}=[K]-\omega^2[M] \tag{1-8}$$

in which [K] and [M] are respectively the static-stiffness matrix and mass matrix of the eight-node hexahedral brick element [53].

1.2 Amplification function

Transfer function or amplification function are defined as the relationship between the input and output of a dynamic system, and shows how the system amplifies or deamplifies an input signal. For an earth dam-canyon system, the amplification function (AF) can be defined as the ratio of the crest motion to the canyon motion. The amplification function of an earth dam at the crest point determines how a ground motion like an earthquake in each frequency is amplified or deamplified. The amplification function represents the influence of an earth dam's and canyon's properties, including the geometry and material properties. Utilizing the superposition principle, the crest response of an earth dam due to an earthquake is obtained by the production of amplification function and the earthquake ground motion.

For the soil deposits (Figure 1-10), the amplification function is defined as the ratio of the free surface to the rigid bedrock motions. Kramer [54] proposed several AFs corresponding to different soil deposit conditions. K shows the wave number.

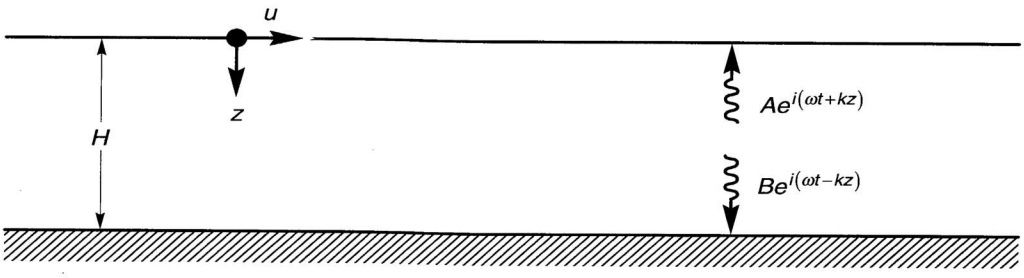

Figure 1-10. A linear elastic soil deposit [54]

For a linear elastic soil deposit, the AF was presented as [54]:

$$|AF(\omega)| = \frac{1}{|\cos(\omega H/V_s)|} \tag{1-9}$$

where is the circular frequency, H is the height of the soil layer, and V_s is the shear wave velocity of the layer.

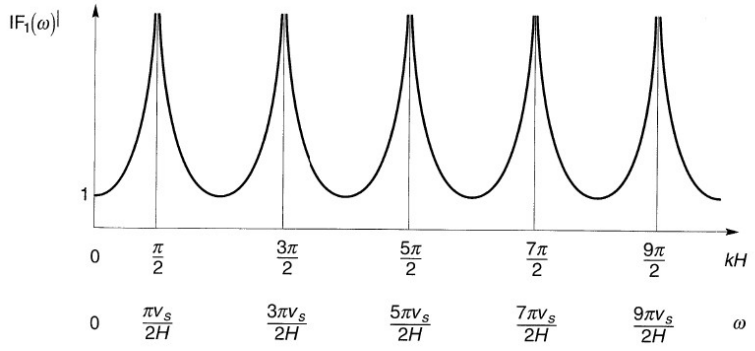

Figure 1-11. Amplification function of an elastic undamped soil layer [54]

Figure 1-25 shows that the surface displacement is always either greater than or equal to the bedrock displacement. When the denominator in Equation (1-9) approaches zero, the limit of AF is infinity. The corresponding ω that makes the denminator zero are the natural frequencies. This case never happens in a realistic problem where the soil layer has material damping and it always dissipates the energy. For a damped soil layer on rigid bedrock, AF was obtained in [54] as:

$$|AF(\omega)| = \frac{1}{\sqrt{\cos^2\left(\frac{\omega H}{V_s}\right) + (\beta\omega H/V_s)^2}} \tag{1-10}$$

where β is the material damping of the soil layer. Figure 1-12 indicates the AF of a damped soil layer. The local maximum represents the natural frequencies of the system. With increases in the material damping ratio, the AF is decreased.

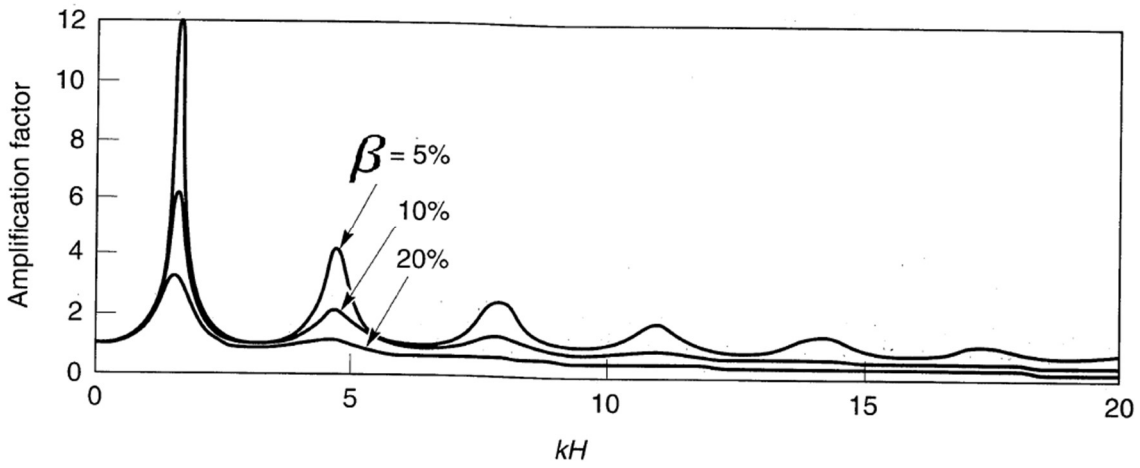

Figure 1-12. The AF of the damped soil on rigid bedrock [54]

The nth natural frequency of the soil layer is obtained by: [54]

$$\omega_n = \frac{V_s}{H}\left(\frac{\pi}{2} + n\pi\right) \tag{1-11}$$

The first natural frequency is presented as:

$$\omega_1 = \frac{V_s \pi}{2H} \tag{1-12}$$

However, the assumption of rigid bedrock is not realistic. In the equation, it is assumed that the boundary between the rigid bedrock and soil layer is fixed, and when the reflected wave from the surface reaches the fixed boundary, it is reflected into the soil layer. If the soil layer is on elastic bedrock, part of the wave will be transmitted into the rock layer (see Figure 1-13).

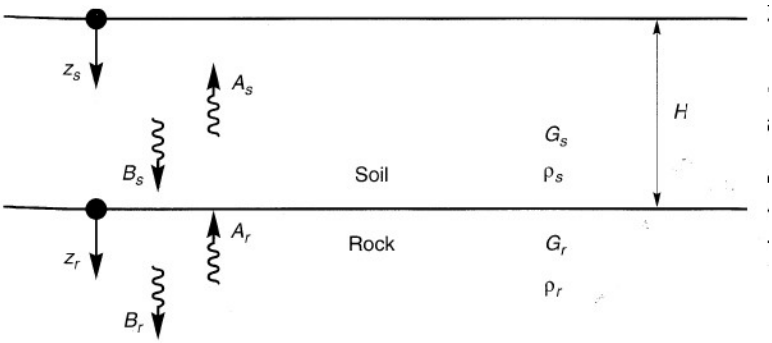

Figure 1-13. Elastic soil layer on elastic bedrock [54]

The amplification function for the soil layer on the elastic bedrock is obtained as: [54]

$$|AF(\omega)| = \frac{1}{\cos\left(\frac{\omega H}{V_s^*}\right) + i\alpha^* \sin(\omega H / V_s^*)} \tag{1-13}$$

where α^* is the complex impedance ratio defined as $\alpha = \frac{V_s^* * \rho_s}{V_r^* * \rho_r}$ and V_s^* shows the complex shear wave velocity. Figure 1-14 depicts the effect of the impedance ratio on the AF. With increases in the impedance ratio, the AF is decreased.

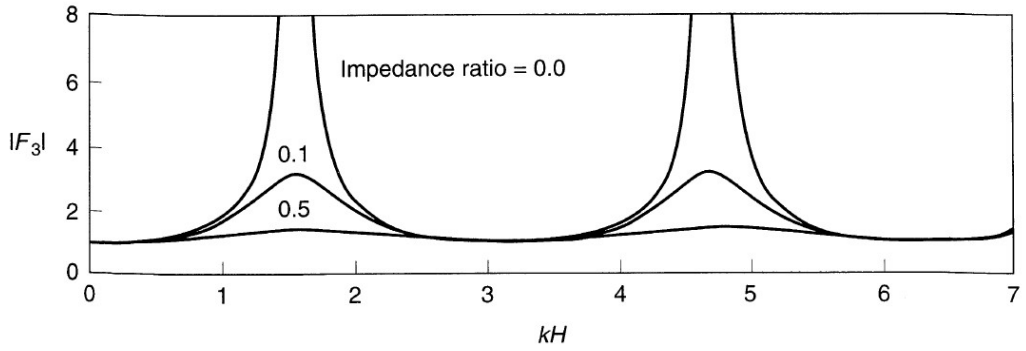

Figure 1-14. Effect of impedance ratio on the AF [54]

The amplification is greatly affected by the material damping and the radiation damping, which is related to the elasticity of the bedrock.

Several methodologies including analytical and numerical approaches have been developed to seek the geometry and flexibility effects of the canyon on the earth dam amplification function. The shear beam method was used by Ambraseys [55] to model an earth dam as a variable wedge-shaped cross-section, and a closed-form solution was presented to obtain different vibration modes of an earth dam in a rectangular canyon.

Dakoulas and Hashmi [56] presented an analytical approach for the steady-state response of earth dams in rectangular canyons. The dam was modeled as a 2D homogeneous triangular shear wedge with a linearly hysteretic material, and the canyon was idealized as a rectangle with elastic materials. Figure 1-15 portrays the dam cross-section and the perspective of the model.

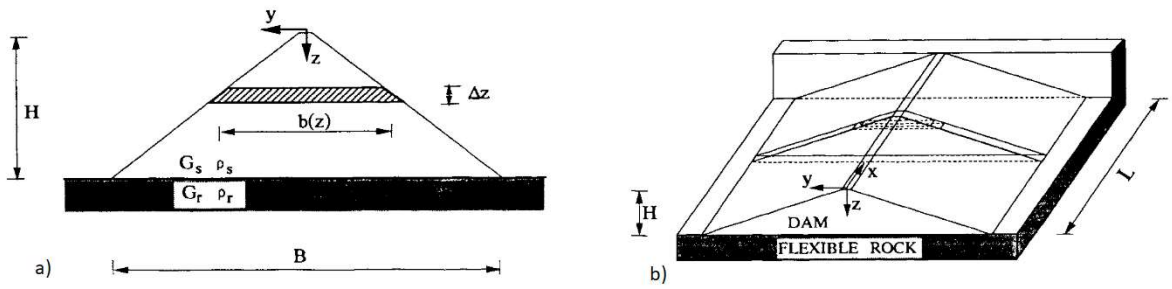

Figure 1-15. a) Dam Cross-Section; b) Perspective View of Dam Geometry [56]

Figure 1-16 illustrates the mid-crest amplification function of an earth dam located in a rectangular canyon under incident excitation, with the different θ angles defining the angle between the incident excitation and the vertical axis. A parametric study was done to investigate the effect of the impedance ratio on the response of the dam [57].

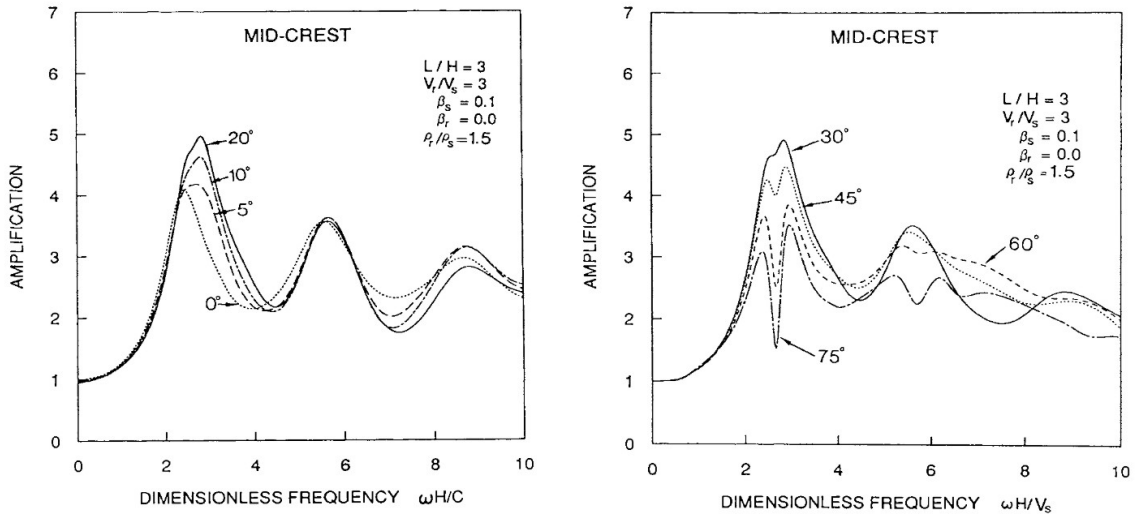

Figure 1-16. The mid-crest amplification function of an earth dam located in a rectangular canyon under incident excitation with different angles [56]

Dakoulas and Gazetas [57] suggested an analytical solution to estimate the steady-state response of earth dams in rigid semi-cylindrical canyons under harmonic base excitation (see Figure 1-17).

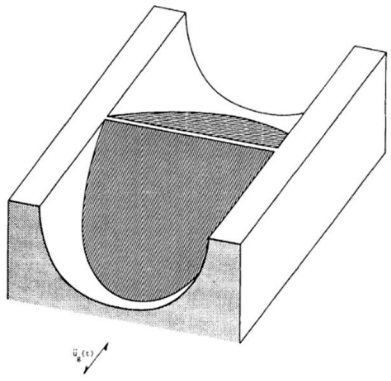

Figure 1-17. Three-dimensional view of darn in a rigid semi-cylindrical canyon [57].

In [57], it was shown that the presence of a rigid canyon enhances the seismic response. For the hysteretic damping ratio β=10%, the maximum amplification functions are obtained as $AF_{max} \approx 10$ and $AF_{max} \approx 8$ for the

3D developed theory and 2D plane strain shear beam, respectively (Figure 1-18(a)). As well, it was concluded that: “AF is independent of the exact canyon shape” (Figure 1-18(b)).

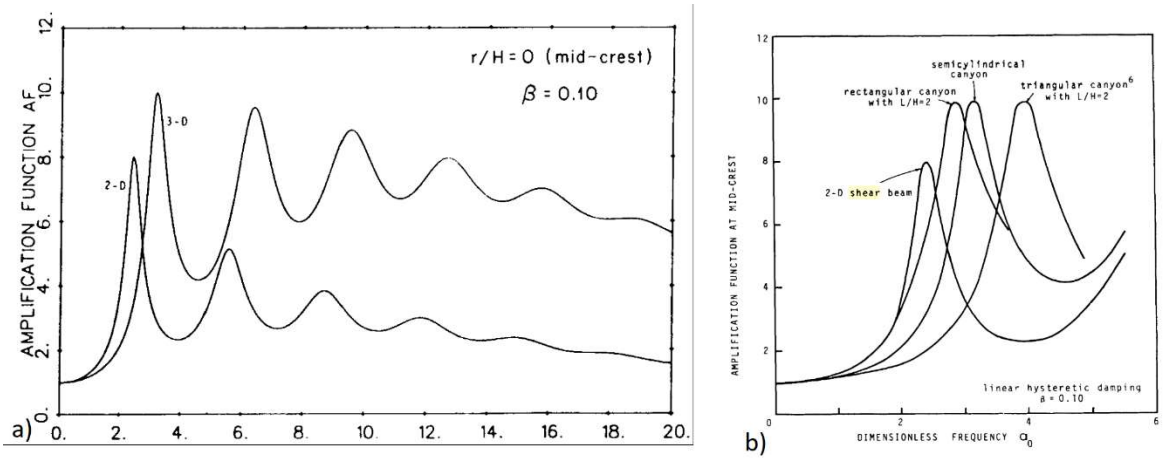

Figure 1-18. a) Steady-state response to harmonic base excitation for 2D and 3D models; b) effect of canyon shape on the mid-crest amplification function [57]

Dakoulas and Hsu [58] similarly proposed an analytical solution for semi-elliptical rigid canyons, and it was shown that the amplification effect is higher for a dam in narrow canyons compared to dams in wide canyons. Figure 1-19 shows the effect of the impedance ratio on the amplification function.

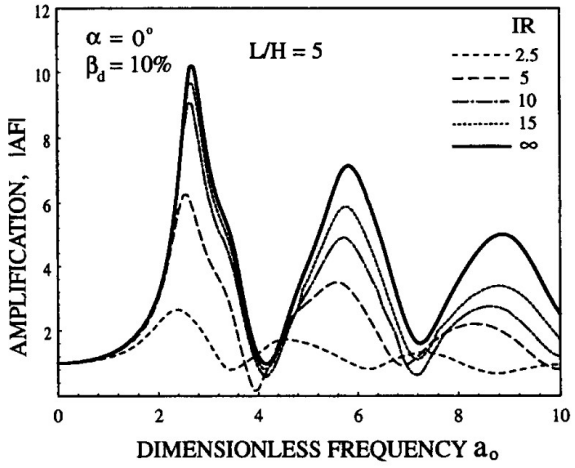

Figure 1-19. Effect of impedance ratio on the amplification function.

Abouseeda and Dakoulas [34] utilized an FEM to model earth dams and BEM to model their foundations as an elastic half-space for seismic soil-structure interactions in two dimensions (Figure 1-20). Figure 1-21 shows the horizontal crest amplification function for a 2D earth dam on an elastic foundation.

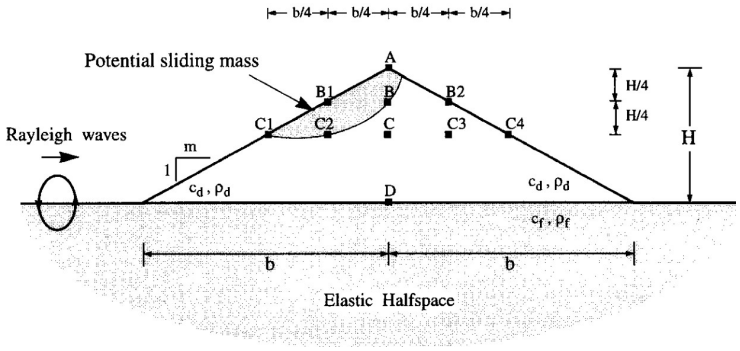

Figure 1-20. 2D dam on an elastic foundation [34]

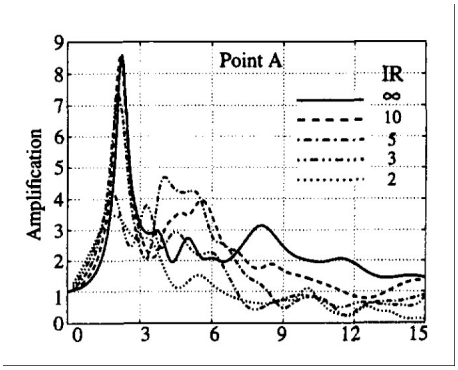

Figure 1-21. The horizontal crest amplification function for a 2D earth dam on an elastic foundation

1.2.1 Natural frequency

If an earth dam-canyon system experiences a seismic event with a fundamental frequency close to its natural frequency, the responses of the system are amplified. These amplifications may cause structural damage, and thus the natural frequency of dams has always been an important area of study. Ambraseys [59] initially utilized the shear beam method to investigate the natural frequencies and vibration modes of earth dams in the upstream-downstream direction, with the dam model being a truncated wedge (Figure 1-22).

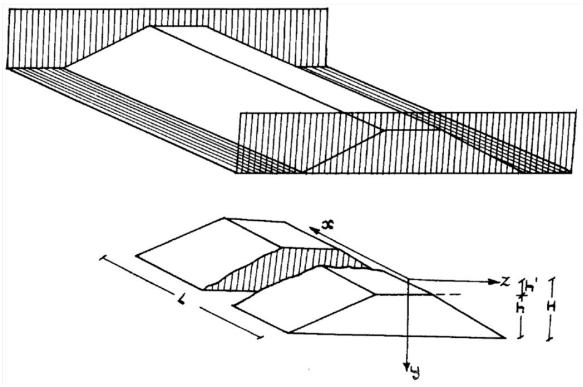

Figure 1-22. Model proposed by Ambraseys [59]

The undamped natural frequencies of the wedge were proposed as: [59]

$$\omega_{nr} = \frac{V_s}{H}\sqrt{\mathrm{A}_n{}^2 + \left(\frac{r\pi}{\mu}\right)^2} \tag{1-14}$$

where k' is the ratio of h' to H, V_s is the shear wave velocity; n and r are the mode numbers with respect to the y-axis and x-axis directions, respectively; and μ is the ratio of L to H. The A_n calculated for different mode numbers is chosen from Table 1-1.

Table 1-1. A_n [59]

k'	n=1	n=2	n=3	n=4	n=5	n=6
0.00	2.4	5.52	8.65	11.79	14.93	18.07
0.10	2.45	5.72	9.3	12.6	15.98	19.41
0.16	2.51	5.97	9.66	13.26	16.9	20.66
0.20	2.57	6.23	10.05	13.92	17.81	21.71
0.22	2.61	6.39	10.33	14.3	18.38	22.34
0.25	2.67	6.58	10.67	14.8	18.96	23.13
0.30	2.79	6.99	11.39	15.83	20.29	24.76
0.32	2.83	7.14	11.66	16.2	20.78	25.3
0.33	2.88	7.31	11.93	16.6	21.29	25.99
0.40	3.11	8.07	13.22	18.42	23.64	28.86
0.45	3.31	8.72	14.28	19.8	25.45	31.3
0.50	3.59	9.6	15.82	22.07	28.34	34.61
0.55	3.9	10.59	17.7	24.6	30.64	38.3
0.60	4.34	11.93	19.73	27.56	35.4	43.24
0.63	4.68	12.95	21.42	30.01	38.6	46.91
0.67	5.1	14.28	23.65	33.05	42.46	51.88
0.70	5.62	15.85	26.26	36.71	47.17	57.64
0.71	5.88	16.63	27.57	38.54	49.5	60.51

0.77	7.17	20.55	34.11	47.7	61.3	74.91
0.80	8.21	23.69	39.34	55.03	70.73	86.43
0.83	9.77	28.39	47.19	66.02	84.86	103.71
0.87	12.39	36.25	60.28	84.35	108.42	132.5
0.90	16	47.26	78.61	109.99	141.41	172.82
0.93	21.54	63.73	106.1	148.49	190.89	233.3
0.94	28.08	83.36	138.82	194.3	249.79	305.29
0.95	34.08	101.37	168.83	236.32	303.82	371.32
1.00	∞	∞	∞	∞	∞	∞

The first natural period in the upstream-downstream direction is obtained by:

$$T_1 = 2.61\frac{V_s}{H} \tag{1-15}$$

Chopra et al. [60] used the finite element method (FEM) to obtain the natural frequencies and mode shapes of earth dams with typical 2D cross-sections.

The 3D geometry of the canyon is an important factor with a great influence on a dam's response. Dams located in wider canyons show softer behaviors than dams in narrow canyons.

However, the assumption of a 2D plain strain is valid only for dams in rectangular canyons with infinitely long lengths [61]. Hatanaka et al. [62] investigated canyons' 3D geometry effects on the responses of dams. In an experiment comparing the natural frequencies of 2D and 3D earth dams in triangular and rectangular canyons by FEM. Martinez and Bielak [63] used a 2D FEM and a Fourier transform in the direction perpendicular to the cross-section in order to model a dam three-dimensionally, and they considered the effect of geometry on the natural frequencies. Figure 1-23 displays the natural frequencies of earth dams with different canyon shapes.

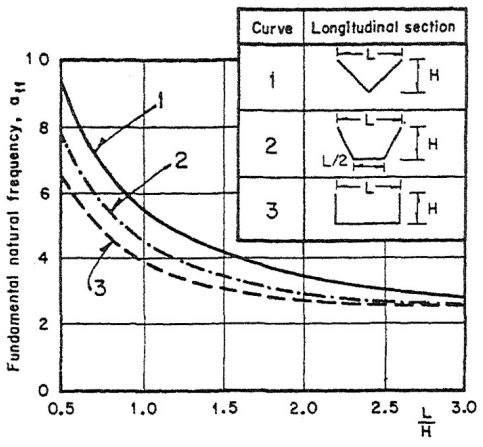

Figure 1-23. Natural frequencies of earth dams with different canyon shapes

Mejia and Seed [64] found that for narrow canyons, the 3D FEM natural frequencies obtained were 2.5 times higher than those for the 2D FEM models. Figure 1-24 depicts the ratio of 3D natural frequencies to 2D natural frequencies of an earth dam located in a rectangular and triangular canyon.

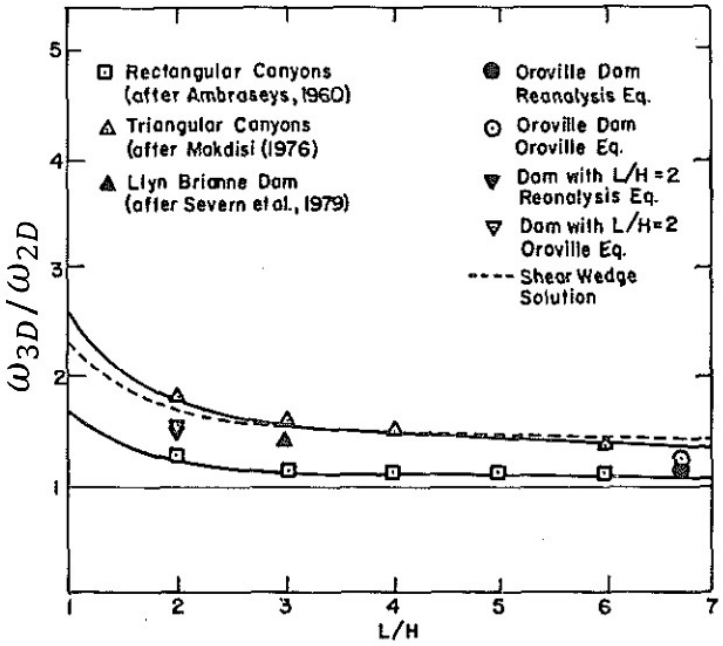

Figure 1-24. Ratio of 3D natural frequencies to 2D natural frequencies of an earth dam located in a rectangular and triangular canyon [64]

Comprehensive work was done by Dakoulas and Gazetas [65], with canyons of different geometries being considered. Figure 1-25 shows the findings in which T_1 is the fundamental period and $T_{1\infty}$ is the period of a dam in an infinitely wide canyon. As can be seen in Figure 1-25, the geometry of the canyon has a great impact on the response of dams. Dakoulas and Gazetas [65] found that for triangular canyons, the fundamental periods of earth dams in wide canyons were five times greater than for corresponding dams in narrow canyons. This suggests that the 3D geometry of a canyon effect greatly affects the fundamental periods of earth dams.

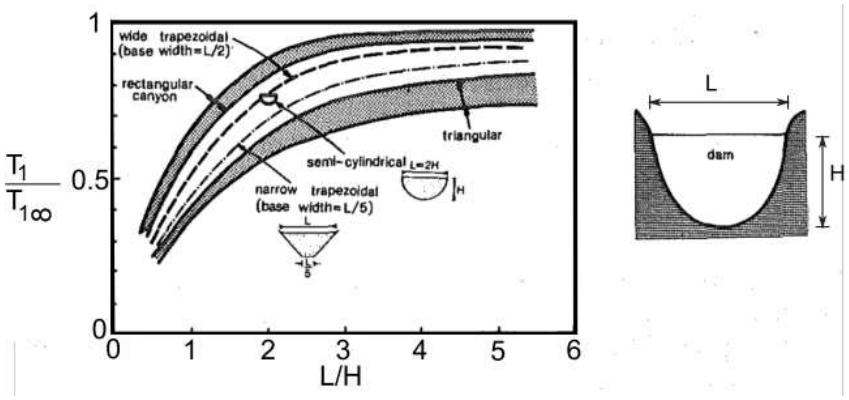

Figure 1-25. Effect of canyon geometry on the fundamental natural period, T1 of a dam [65]

Papalou and Bielak [9, 10] analyzed the La Villita earth dam in Mexico by using shear beams and FEM to model the dam and the canyon, respectively. The dynamic response of the dam was assessed for canyons with different material properties.

The assumption of a rigid canyon is not always close to the actual conditions, however. In reality, an earth dam interacts dynamically with the surrounding soil or rock, which is an elastic unbounded domain. Chopra and Perumalswami [68] used an analytical procedure and 2D FEM to show how the natural frequencies and mode shapes of earth dams surrounded by elastic half-spaces are influenced by the effects of the dam-foundation interaction.

1.3 Nonlinear behavior of earth dams

The nonlinear behavior of soil may affect the seismic response of earth dams, and a wide variety of nonlinear soil models have been applied for the dynamic analysis of earth dams under earthquakes. A hardening soil model was used in the FEM analysis of a homogeneous earth dam [69], while a tailing dam using PLAXIS was studied under seismic loading by applying the Mohr-Coulomb model [70]. Parish et al. [8] showed that plasticity should be considered in the study of earth dams under earthquake loading, as the seismic responses of earth dams are significantly affected by their plastic behavior; for example, “consideration of plasticity in the shell leads to a decrease of about 50% in the seismic amplification.”

Papalou and Bielak [67] considered the nonlinear behavior of earth dams under earthquake loading as well, and dams’ nonlinear behavior was studied using a multi-yield surface plasticity theory. As a result, it was shown that: “the effects of nonlinearity are most pronounced within the interior of the dam, where shear strains are largest. The reduction due to nonlinearity in the peak acceleration at a point 40 m below the crest of the dam is on the order of 25–30%, for a given canyon stiffness” (Figure 1-26).

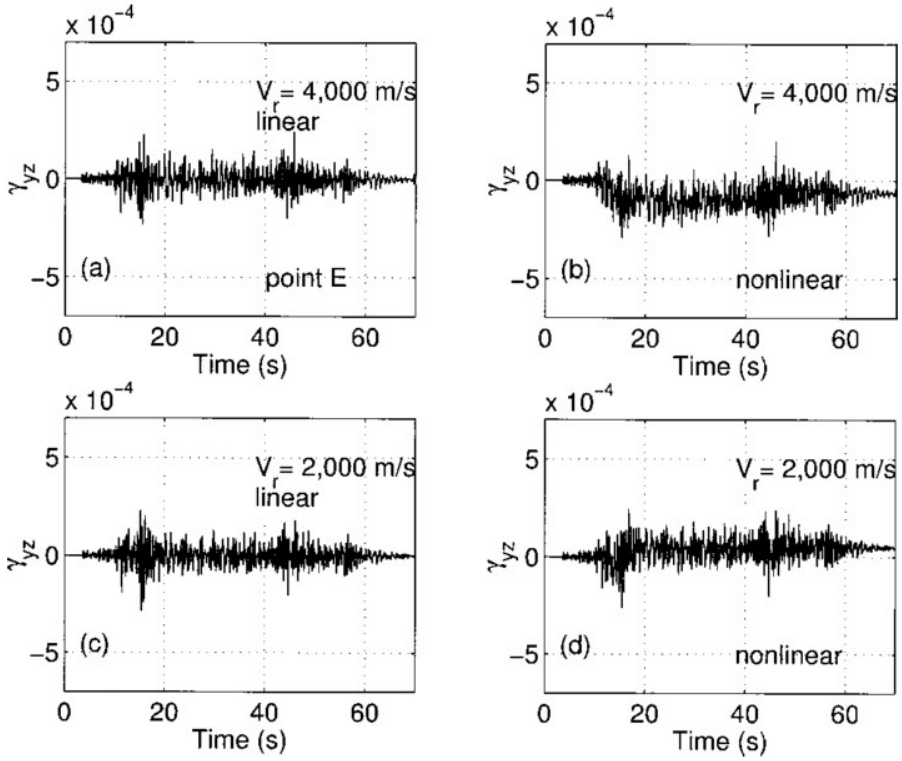

Figure 1-26. Time history of shear strain γyz at a point 40 m the crest of linear and nonlinear models of dam *[67]*

In a linear analysis, the shear modulus and damping ratio are used with the assumption of low strain, and the amplification function, natural frequency, and time-domain responses are calculated with this assumption. Under severe earthquakes, some parts of earth dams exhibit nonlinear behavior. Idriss and Seed [71] introduced the equivalent linear method (EQL) to take into consideration the effect of soil nonlinearity during strong earthquakes, and SHAKE [72] and FLUSH [73], which incorporate EQL, have been widely used in practical problems in geotechnical earthquake engineering.

In EQL first, with the assumption of small strain, $\gamma_{eff} < 10^{-6}$, the shear modulus G^1 and damping ratio β^1 are selected for each FEM element, and the maximum shear strain ($\gamma(\omega)_{max}$) for each element for each frequency is evaluated. Transferring the strain into the time domain and obtaining the maximum strain will be time-consuming. The maximum shear strain in the time domain is obtained by the root mean square of the maximum strain in the frequency domain as:

$$\gamma(t)_{max} = C * RMS(\gamma(\omega)_{max}) \tag{1-16}$$

where the constant C can be estimated by:

$$C = max|\{\ddot{u}^g(t)\}|/RMS(\{\ddot{u}^g(\omega)\}) \quad (1\text{-}17)$$

in which $\{\ddot{u}^g(t)\}$ and $\{\ddot{u}^g(\omega)\}$ are the input seismic acceleration excitations on the canyon in the time and frequency domains, respectively. The effective shear strain is estimated by:

$$\gamma(t)_{eff} = 0.65 * \gamma(t)_{max} \quad (1\text{-}18)$$

where 0.65, which is the strain ratio, is an empirical value. As the degradation curve ((1-18) is obtained in laboratory loading conditions, which are more severe than actual earthquake loading conditions, $\gamma(t)_{max}$ is multiplied by 0.65. The estimated shear strain $\gamma(t)_{eff}$ is used to obtain the corresponding shear modulus G and damping ratio β from Figure 1-27. The second iteration is done similarly. The results usually converge to the desired accuracy after 3 iterations.

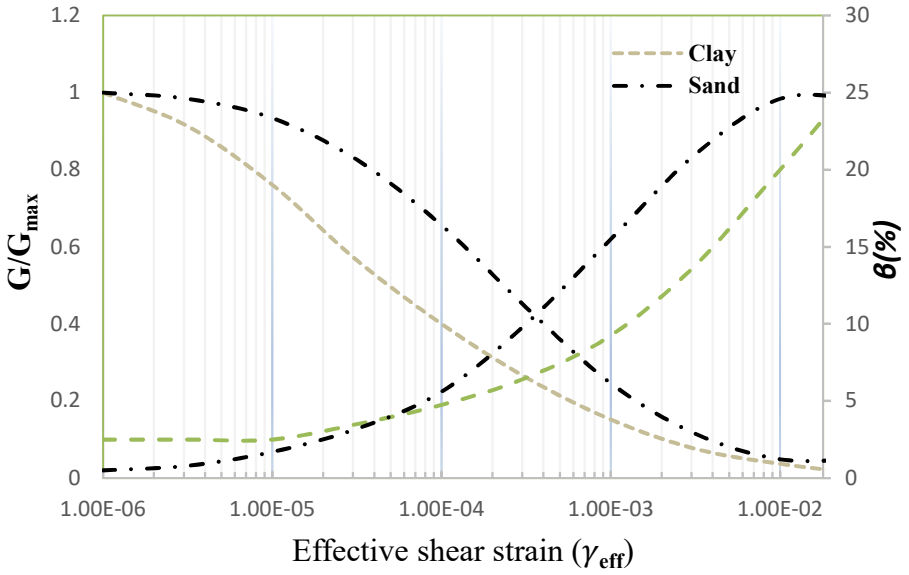

Figure 1-27. Strain-compatible soil properties [71]

Abdel-Ghaffar and Scott [74] developed EQL to analyze the Santa Felicia earth dam, which had been subjected to two strong earthquakes. Choudhury and Savoikar [75] carried out 1D equivalent-linear analysis utilizing DEEPSOIL software in order to model municipal solid waste landfills under earthquake loadings, while Mejia et al. [76] showed that the natural frequencies of earth dams modeled by the equivalent linear FEM vary with the intensity of the input motions. Cascone and Rampello [77] performed a seismic analysis of earth dams by decoupled displacement analysis, and the nonlinear behavior was incorporated by the EQL.

1.4 Conclusion

The research in the literature can be categorized into the following three groups:

I. In 2D-hybrid techniques, the approach can satisfy the radiation damping, but it does not take into consideration the 3D-geometry effect. Moreover, the surrounding soil is always modeled as a flexible foundation [34], [78].

II. In 3D models, the canyons are assumed to be constrained by rigid boundary conditions, while no influence of flexibility is examined [58], [79].

III. In 3D-hybrid models, the canyon behaves as an elastic half-space. The mathematical restrictions, however, limit the shape of the canyons to only some pre-determined profiles like semi-elliptical forms [80].

In this thesis, the 3D FEM-SBFEM equation is derived to conduct a comprehensive study of the effects of the flexibility and geometry of canyons on the seismic responses of earth dams, and the EQL has been implemented to consider the effect of earth dams' nonlinear behavior.

Chapter 2 Analysis of Earth Dam-Flexible Canyon Interaction with 3D Coupled FEM-SBFEM

2.1 Résumé

La géométrie et la flexibilité d'un canyon sont des paramètres qui affectent grandement la valeur des périodes naturelles de résonance dans les barrages en terre. Le canyon entourant un barrages peut être considéré comme un domaine illimité. Pour prendre en compte ces deux effets, le canyon a été modélisé par par la méthode des éléments finis de frontières à l'échelle (SBFEM) et le barrage en terre, à géométrie limitée, par la méthode des éléments finis (FEM). La technique hybride de SBFEM-FEM pour l'analyse tridimensionnelle dynamique de l'interaction sol-terre barrage a été validée avec les résultats disponibles dans la littérature. Comme la matrice de rigidité dynamique du domaine non borné est complexe et dépendante de la fréquence, la méthode classique de superposition de modes n'est pas simple pour le système d'interaction sol-structure. Ainsi, pour obtenir la fréquence propre fondamentale, le barrage a été sollicité en direction amont-aval. Les périodes naturelles de résonance des barrages en terre pour des canyons de formes géométriques et de coefficients d'impédance différents ont été obtenues. Elles se sont avérées avoir des effets significatifs sur la période naturelle de résonnance. Les résultats ont été comparés aux données enregistrées réelles pour des barrages existants. Il a été constaté que les graphiques proposés dans cette étude peuvent être utilisés par des concepteurs de barrages pour l'estimation des périodes naturelles des barrages en terre construits dans des canyons de formes et de propriétés des matériaux diverses.

2.2 Abstract

The geometry and flexibility of a canyon are the parameters that greatly affect the value of natural periods in earth dams. The canyon surrounding dams can be assumed as an unbounded domain. To take into account these two effects, the canyon was modeled by SBFEM and the earth dam, which has limited geometry, by FEM. The hybrid technique of SBFEM-FEM for dynamic three dimensional analysis of soil-earth dam interaction was validated with available results in the literature. Because the dynamic-stiffness matrix of the unbounded domain is complex and frequency dependent, the classical mode-superposition method is not straightforward for the soil-structure interaction system. Thus, to obtain the fundamental natural frequency, the dam was excited in the upstream-downstream direction. The natural period of the earth dam for canyons with different geometry shapes and impedance ratios were obtained. They were found to have significant effects on the natural period. The results were compared with actual recorded data. It was found that the proposed graphs in this study may be used by practical engineers for the estimation of natural periods of earth dams in canyons with different shapes and material properties.

2.3 Introduction

If an earth dam-canyon system experiences a seismic event with a fundamental frequency close to its natural frequency, the responses of the system are amplified. These amplifications may cause structural damage [81]. Thus, the natural frequency of dams have always been an important area of study. Ambraseys et al. [59] initially utilized the shear beam method to investigate the natural frequencies and vibration modes of earth dams in the upstream-downstream direction. Chopra et al. [60] used the finite element method (FEM) to obtain natural frequencies and mode shapes of earth dams with typical 2D cross sections.

However, the assumption of the 2D plain strain is valid only for dams in rectangular canyons with infinitely long lengths [61]. Hatanaka et al. [62] first investigated the canyon 3D geometry effects on the response of dams. In an experiment comparing the natural frequencies of 2D and 3D earth dams in triangular and rectangular canyons by FEM. Mejia and Seed [64] found that for narrow canyons, the 3D natural frequencies that are obtained are 2.5 times higher than those for the 2-D models. Dakoulas and Gazetas [57] obtained the fundamental periods of earth dams in rigid canyons with five different geometries. They found that for triangular canyons, the fundamental periods of earth dams in wide canyons were five times higher than for the corresponding dam in narrow canyons. This suggests that the 3D geometry canyon effect greatly affects the fundamental periods of the earth dams.

The assumption of a rigid canyon is not always close to the actual condition. In reality, the earth dam interacts dynamically with the surrounding soil which is an elastic unbounded domain. Chopra and Perumalswami [68] used an analytical procedure and 2D FEM to show how natural frequencies and the mode shapes of earth dams surrounded by elastic half spaces are influenced by dam-foundation interaction effects. Dakoulas and Gazetas [65] have utilized shear beams to model the earth dams on the elastic foundation with limited depth. Papalou and Bielak [9, 10] analyzed the La Villita dam in Mexico by using shear beams and FEM for modeling the earth dam and the canyon, respectively. The dynamic response of the dam was assessed utilizing canyons with different material properties.

FEM is not capable of modeling a half space to satisfy the radiation condition rigorously. Using the boundary element method (BEM), the radiation condition at infinity may be exactly satisfied through the use of suitable fundamental solutions. Abouseeda and Dakoulas [34] utilized FEM to model earth dam and BEM to model foundation as an elastic half space for seismic soil-structure interaction in two dimensions. Yazdchi et al. [35] considered the transient response of an elastic dam by utilizing the FEM-BEM.

Wolf and Song [36] proposed the scaled boundary finite-element method (SBFEM) for the dynamic analysis of unbounded domains. This novel semi-analytical method combines the advantages of BEM and FEM and also demonstrates the following benefits [82]:

- Reduction of the spatial dimension by one.
- No need for fundamental solutions.
- Radiation damping at infinity satisfied exactly for unbounded media.
- Exact and analytical solution in the radial direction for static problems.

Previous studies have extended this method to the dynamic analysis of non-homogeneous unbounded domains with the elasticity modulus and mass density varying as power functions of spatial coordinates [38], [83]. Futhermore, a Padé series solution for the SBFEM equation in dynamic stiffness was developed for frequency-domain analyses [41]. The sparsity and the lumping of the coefficient matrices of the scaled boundary finite-element equation were exploited to further reduce the computational costs [40]. A high-order local transmitting boundary constructed from a continued-fraction solution of the dynamic-stiffness matrix is developed [84]. SBFEM has been widely coupled with other numerical methods in different soil structure analyses [85] [86] and fracture mechanic problems [87] [88] [89]. Deeks and Augarde [90] coupled SBFEM with the meshless local Petrov–Galerkin modeling of the bounded domain.

Ekevid and Wiberg [42] and Ekevid et al. [43] used SBFEM to simulate ground response to high-speed trains moving on the ground surface. Syed and Maheshwari [44] improved the efficiency of the 3D FEM-SBFEM approach for soil-structure interaction (SSI) analysis in the time domain. The hybrid technique was used for nonlinear analysis of a soil-pile system [45]. Chen et al. [48] introduced an efficient nonlinear SBFEM with octree mesh to the dynamic analysis of some complicated geotechnical structures. Yaseri et al. [51] applied 3D FEM-SBFEM to analyze ground vibrations due to passing trains in tunnels. The equations of SBFEM for 2.5D numerical model were proposed for the dynamic analysis of moving trains [91]. The 2.5D is utilized for 3D models that have longitudinally invariant geometry and material properties.

Although this method has been used to model CFRD-reservoir systems [46], [47] and to be a useful tool for SSI problems, there are a lack of studies examining the natural frequency of earth dams using SBFEM. Most of the studies investigating the natural frequency of earth dams have been carried out assuming that the foundation and canyon are rigid or the radiation damping is not satisfying exactly. Therefore, the objective of this research is to (1) introduce the 3D FEM-SBFEM hybrid technique as an appropriate tool for dynamic analysis of an earth dam-canyon interaction system in the frequency domain; (2) examine the effects of flexibility and geometry of

canyons on natural periods and (3) propose new graphs for the estimation of natural periods in canyons with different shapes and material properties. In this study, the 3D canyon is modeled using fourth-node SBFEM surface elements. The FEM with eight-node hexahedral brick elements [53] is utilized for modeling the earth dam and the fundamental periods of an earth dam is expressed for canyons with four different geometry shapes.

2.4 Methodology

The 3D domain is decomposed as the bounded domain (earth dam) and the unbounded domain (surrounding foundation and canyon). The subscripts s (s for structure) denotes the nodes of the unbounded domain and b (b for base) indicates nodes associated with the generalized structure–soil interface, respectively (*Figure 2-1*). The bounded domain (Ω_s), including the earth dam, is discretized with FEM and the unbounded domain (Ω_b), including the canyon and foundation, is modelled using SBFEM to satisfy the radiation damping condition. With fulfilling equilibrium and compatibility conditions on the interface Γ the coupling of FEM (Ω_s)-SBFEM (Ω_b) is done.

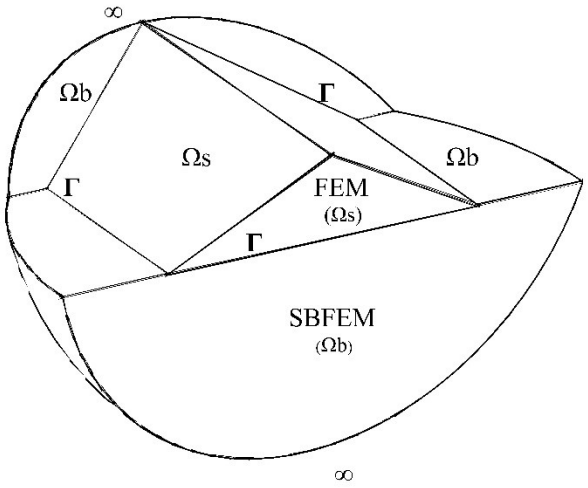

Figure 2-1. Schematic view of a symmetric soil-structure interaction system

2.4.1 SBFEM equation

The equation of SBFEM for modeling the unbounded domain is briefly presented. The scaled boundary coordinate system is defined in a local coordinate system ξ, η, ζ (*Figure 2-2* (a)). The radial coordinate ξ is measured from O (the scaling center) and the circumferential coordinates are defined by η and ζ. For 3D problems only the doubly-curved surface boundary Γ is discretized. The unbounded domain Ω_b in radial coordinate ξstarts from ξ*=1* on the boundary Γ to $\xi = \infty$. Each point ($\hat{x}$,$\hat{y}$, $\hat{z}$) is represented by scaling its corresponding point (*x ,y, z*) on the surface boundary Γ and by using the mapping shape functions [$N(\eta, \zeta)$] along the circumferential coordinates.

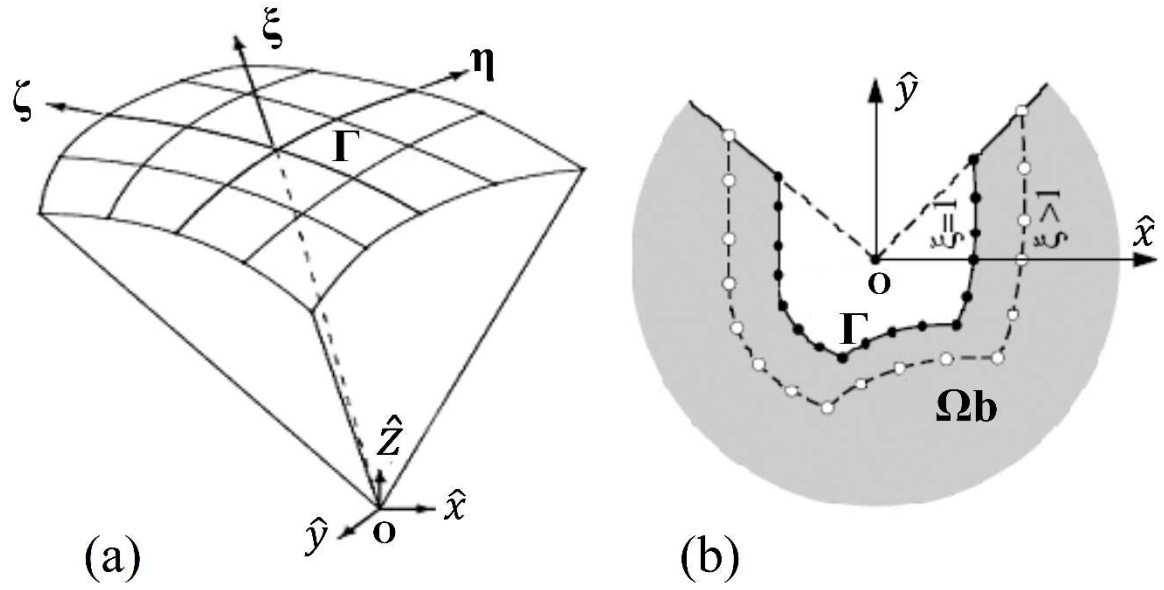

Figure 2-2. Scaled boundary coordinates: (a) scaling center O, radial coordinate ξ and boundary discretization in circumferential coordinates η and ζ for 3D modeling; (b) representation of the unbounded domain in 2D problems

While node positions are defined in the scaled boundary coordinate system, stresses, strains and displacements are specified in the Cartesian coordinate system. Using the shape function $[N^u(\eta,\zeta)]$, the nodal displacements inside the domain at a node (ξ,η) from the displacement function. The displacement at a node (ξ,η) inside the domain is interpolated from displacement functions $^{\{u(\xi)\}}\{\hat{\mathrm{T}}(\xi)\}$.

$$\{u(\xi,\eta,\zeta)\}=[N^u(\eta,\zeta)]\{u(\xi)\}=[N_1(\eta,\zeta)[I],N_2(\eta,\zeta)[I],...]\{u(\xi)\} \tag{2-1}$$

which [I] is a 3×3 identity matrix. By applying the virtual work method in the circumferential directions η, ζ [52] or the Galerkin's weighted residual technique [36], the scaled boundary finite-element equation is obtained. As the dynamic analysis in this work has been done in the frequency domain, only the equations of SBFEM in the frequency domain are presented. The 3D *scaled boundary finite-element equation in displacement* for frequency domain is presented as

$$\begin{aligned}[E^0]\xi^2\{u(\xi)\}_{,\xi\xi}+(2[E^0]-[E^1]+[E^1]^{\mathrm{T}})\xi\{u(\xi)\}_{,\xi}+\\ ([E^1]^{\mathrm{T}}-[E^2]\{u(\xi)\}+(\omega\xi)^2[M^0]\{u(\xi)\}=0\end{aligned} \tag{2-2}$$

where ω denotes the excitation frequency and $[E^0]$, $[E^1]$, $[E^2]$ and $[M^0]$ show coefficient matrices achieved by assembling their corresponding coefficient matrices for each element as in the finite-element method [36].

They are independent of ξ. The coefficient matrices $[E^0]$ and $[M^0]$ are positive-definite, $[E^1]$ is non-symmetric, $[E^2]$ is positive-definite. Analogous to standard finite element, the nodal force-displacement relationship is obtained. The internal nodal forces $\{q(\xi)\}$, which are the resultants of the surface tractions, are determined.

$$\{q(\xi)\} = \xi^2([E^0]\xi\{u(\xi)\}_{,\xi} + [E^1]^{\mathrm{T}}\{u(\xi)\}) \tag{2-3}$$

The internal nodal forces$\{Q(\xi)\}$are equal to the external nodal loads$\{R(\xi)\}$.

$$\{R(\xi)\} = -\{q(\xi)\} = [S^{\infty}(\omega,\xi)]\{u(\xi)\} \tag{2-4}$$

Using Equations (2-2), (2-3) and (2-4) and eliminating $\{q(\xi)\}$ and $\{u(\xi)\}$ results in the scaled boundary finite element equation in dynamic stiffness in the frequency domain for unbounded domain:

$$([S^{\infty}(\omega)]+[E^1])[E^0]^{-1}([S^{\infty}(\omega)]+[E^1]^T) - (s-2)[S^{\infty}(\omega)] - [E^2] - \omega[S^{\infty}(\omega)]_{,\omega} + \omega^2[M^0] = \tag{2-5}$$

where $[S^{\infty}(\omega)]$ is the dynamic-stiffness matrix of an unbounded domain.

2.4.1.1 Solution procedure

Equation (2-5) is a system of nonlinear ordinary differential equations of first order with respect to the frequency ω, which is solved numerically using a fourth-order Runge-Kutta method. An asymptotic expansion of the dynamic-stiffness matrix for high frequency is used to start numerical integration:

$$[S^{\infty}(\omega)] = [K_{\infty}] + \mathrm{i}\omega[C_{\infty}] + \sum_{i=1}^{m}[A^{(i)}](\mathrm{i}\omega)^{-i} \tag{2-6}$$

which $[C_{\infty}]$, $[K_{\infty}]$ and $[A^{(i)}]$ are coefficient matrices [52]. $[S^{\infty}(\omega_h)]$ is obtained for a sufficiently high but finite value of the frequency ω_h and used as an initial point for numerically solving the Equation (2-5). Therefore, the dynamic-stiffness matrix of the unbounded domain is $[S^{\infty}(\omega)]$ calculated for the desired frequencies.

2.4.1.2 Coupling of bounded and unbounded domains

As discussed earlier, the coupling of FEM (Ω_s)-SBFEM (Ω_b) is done using the interface Γ (Figure 2-1). Using the obtained nodal force–displacement relationships for SBFEM (Equation (2-4)) and that of FEM, the assembled relation is obtained as

$$\begin{bmatrix} [S_{ss}] & [S_{sb}] \\ [S_{bs}] & [S_{bb}] + [S^{\infty}] \end{bmatrix} \begin{Bmatrix} \{u_s\} \\ \{u_b\} \end{Bmatrix} = \begin{Bmatrix} \{P_s\} \\ \{P_b\} \end{Bmatrix} \tag{2-7}$$

$[S]$ is dynamic-stiffness matrix of the bounded domain which is obtained as

$$[S] = \begin{bmatrix} [S_{ss}] & [S_{sb}] \\ [S_{bs}] & [S_{bb}] \end{bmatrix} = [K] - \omega^2[M] \tag{2-8}$$

which [K] and [M] are, respectively, the static-stiffness matrix and mass matrix of the eight-node hexahedral brick element [53]. Figure 2-3 shows a flowchart for obtaining dynamic stiffness matrices by SBFEM and FEM and the coupling process.

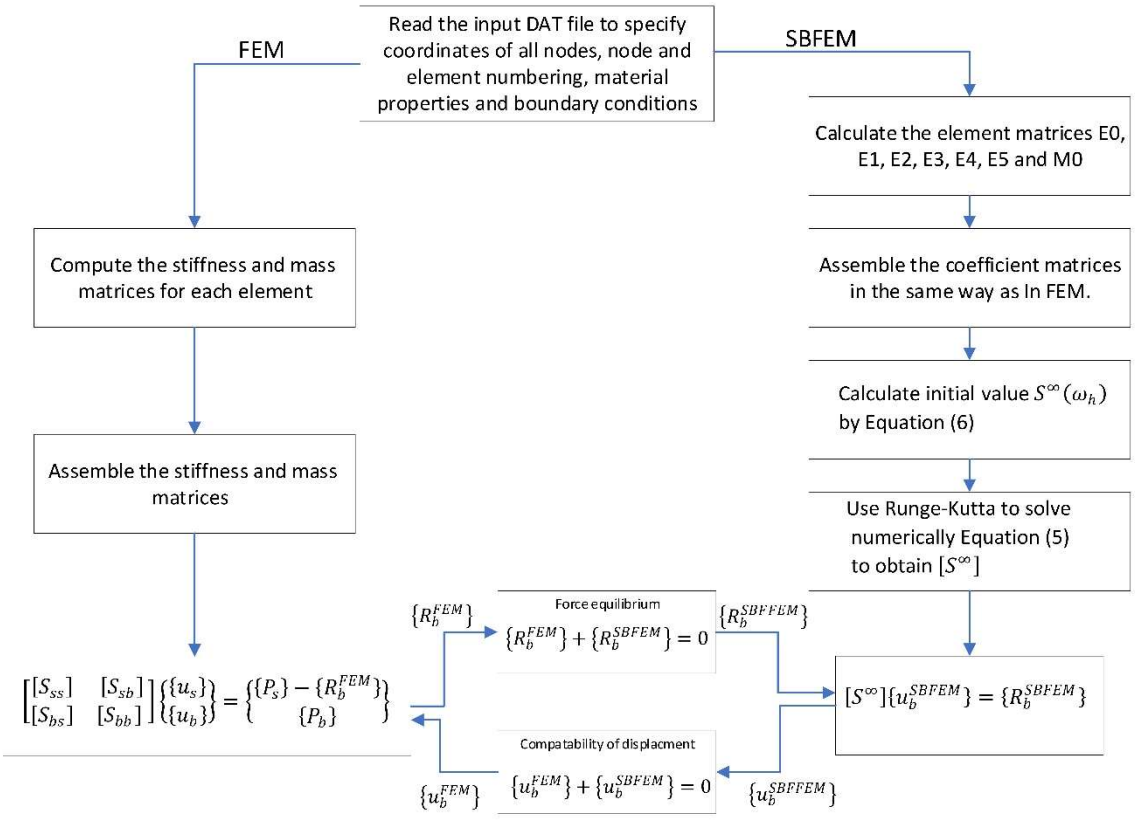

Figure 2-3. Algorithm for coupled FEM-SBFEM solution

2.5 Numerical examples

2.5.1 The rigid square massless plate on an isotropic homogeneous elastic half space

To validate the 3D FEM-SBFEM hybrid technique in the frequency domain, the popular example of the rigid square massless plate on an isotropic homogeneous elastic half space (Figure 2-4) is utilized. The obtained results of the proposed method are compared with available results in the literature. Only one quarter of the geometry is discretized by taking advantage of symmetry. As shown in Figure 2-4, the bounded and unbounded domains are discretized by FEM and SBFEM, respectively. The width of the plate is B = 30 m and the thickness is 0.1B. The bounded domain includes a domain with the size of 2B*2B*2B and the plate has a size of B*B*0.1B. The bounded domains of the soil and plate are discretized using an 8-node hexahedral brick element and the unbounded domain is modeled using 4-node surface elements.

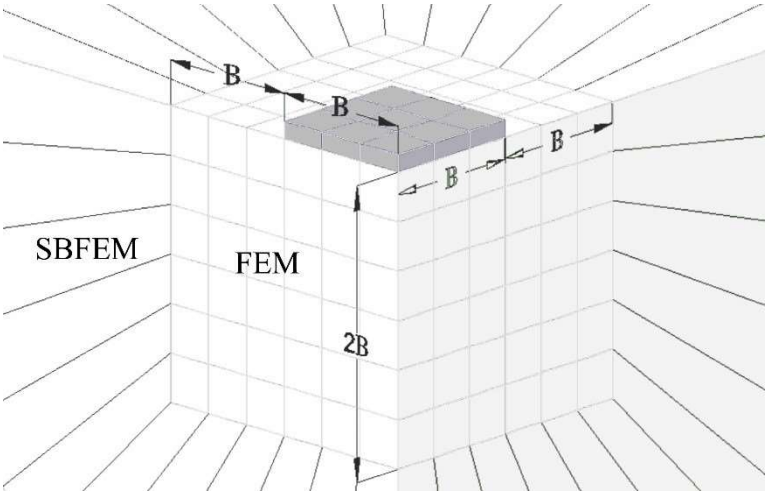

Figure 2-4. FEM-SBFEM mesh for a rigid square massless plate resting on an isotropic homogeneous elastic half-space

A vertical force P is applied at the center of the base of the plate. Vertical and horizontal compliance coefficients of the point O, due to vertical and horizontal loading *P* at point O, are obtained and are non-dimensionalized as $C_{VV}(a_0) = GBU_v/P$ and $C_{HH}(a_0) = GBU_H/P$ where G is the shear modulus of the soil domain and U_V and U_H are the vertical and horizontal displacements, respectively. $C_{MM}(a_0) = \frac{GB^3\theta}{M}$ is the rocking compliance. M and θ are the dynamic moment and the rotation of the plate around the horizontal axes, respectively. The non-dimensionalized compliance coefficients are decomposed into the dimensionless real and imaginary coefficients.Figure 2-5 compares the results from the present study with those obtained by Shahi and Noorzad [92], Zhao and Valliappan [14] and Wong and Luco [93]. The dimensionless frequency a_0 is defined

as $a_0 = \frac{\omega B}{c_s}$ where c_s is the shear wave velocity. Reasonable agreement is observed showing the accuracy and applicability of the hybrid method in modeling real 3D dynamic problems.

.

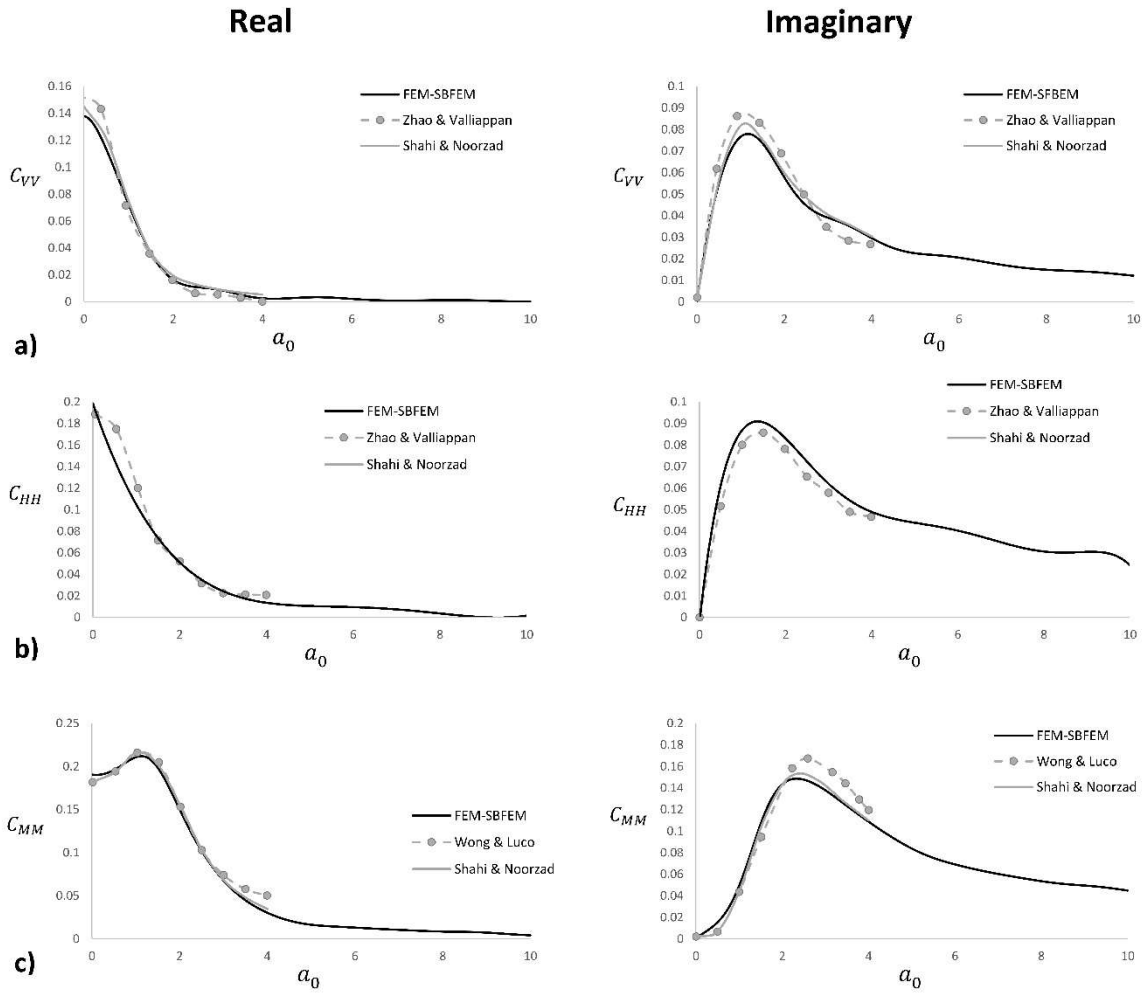

Figure 2-5. Vertical compliance of a rigid square massless plate resting on an isotropic homogeneous elastic half-space; (a) real part; (b) imaginary part

2.5.2 Earth dam foundation under an horizontal excitation

In this section, the earth dams are analyzed in three-dimension in order to consider the effects of 3D geometry and flexibility of canyon on dynamic behavior of earth dam. As discussed in the introduction, Dakoulas and Gazetas [65] showed how different geometries of canyons affect the natural periods of earth dams. Some graphs were proposed which are used for estimation of natural periods of earth dams in different canyon shapes. These graphs still are used by researchers [94]. It has been assumed that canyons are rigid. However, the assumption of a rigid canyon is not always close to reality. To take into account the effect of the flexibility of the canyon, the

impedance ratio $\alpha = \frac{V_{Sd}}{V_{S\infty}}$ is defined, which is the ratio of the shear wave velocity of the earth dam V_{Sd} and the shear wave velocity of the unbounded domain $V_{S\infty}$. The analysis is done for $\alpha = 0, 0.1, 0.2, 0.3, 0.4, 0.5, 0.6$. $\alpha = 0$ represents a rigid canyon.

It is assumed that the earth dam has a linear behavior. Therefore, the interface between FEM and SBFEM is located at the boundary between the earth dam and canyon. The earth dam is modeled by the FEM and the canyon by the SBFEM. Cross-section of the earth dam and its location in the canyon are sketched in Figure 2-6(a) and Figure 2-6(b). The geometries of four different canyons, a) rectangular canyon, b) wide trapezoidal canyon, c) narrow trapezoidal canyon and d) triangular canyon, are shown in Figure 2-7.

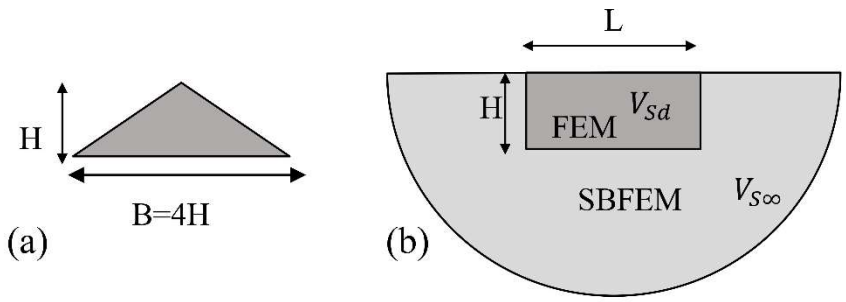

Figure 2-6. a) The geometry of the earth dam model; b) The location of earth dam in the canyon

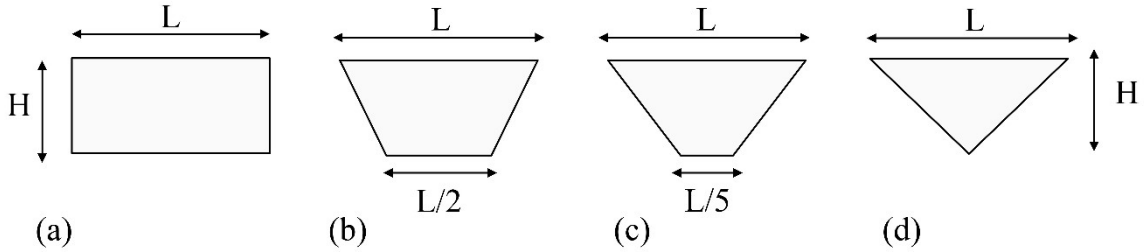

Figure 2-7. Different canyons geometries: (a) Rectangular Canyon; (b) Wide trapezoidal canyon; (c) Narrow trapezoidal canyon; (d) Triangular canyon

Full 3D analysis have been done for the 4 canyon geometry types, 8 different values of L/H and 7 values of α for each canyon geometry. In total, more than 224 3D model were created in Autocad and then the geometries were exported to GAMBIT to generate the mesh. The analyses were completed by a Fortran computer code in the Linux operating system. The obtained results were visualized in Tecplot. Figure 2-8 shows how different software were utilized in different stages as follows: 1) Autocad and Gambit as preprocessors; 2) Fortran as a solver and 3) Matlab and Tecplot as postprocessors. As the dynamic-stiffness matrix of the unbounded domain

is complex and frequency dependent, the classical mode-superposition method is not straightforward for the soil-structure interaction system. The dam is excited in upstream-downstream direction and the fundamental natural frequency of earth dam for the first mode of vibration is defined by the first peak in the acceleration amplification function at the crest of the dam [76]. The natural periods were obtained for different values of L/H and α.

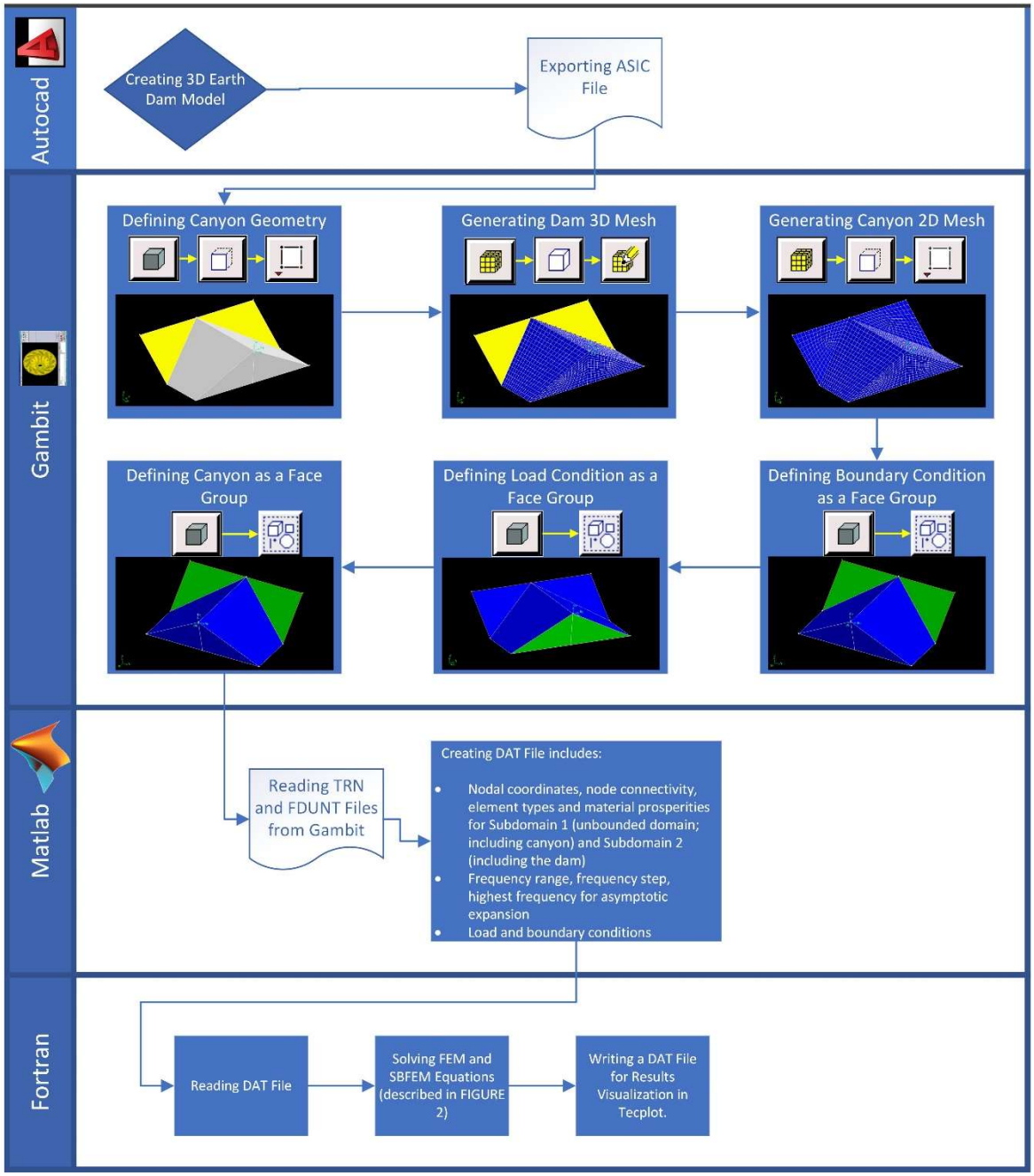

Figure 2-8. General algorithm of the study

Figure 2-9 shows that the two first peaks of amplitude correspond with the natural frequencies of the first and second modes of vibrations for the earth dam in the rectangular canyon with L/H=2.5 and impedance ratio α =0.4.

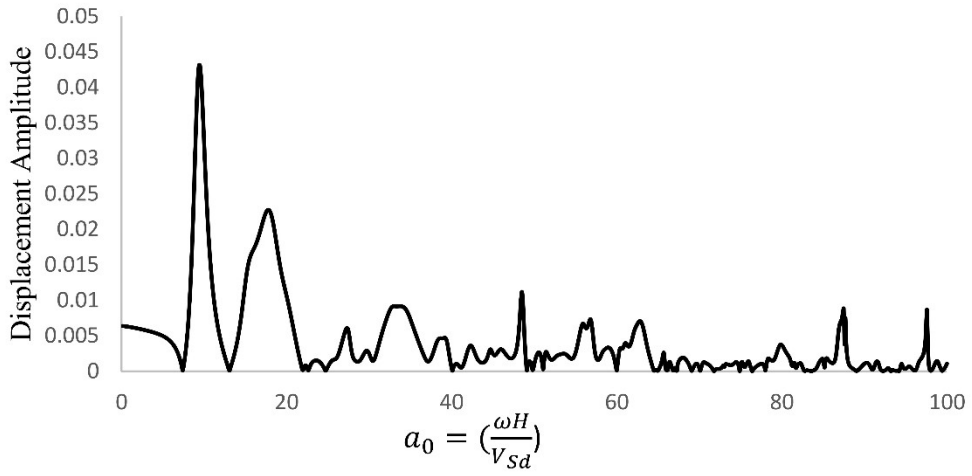

Figure 2-9. Displacement amplitude at the crest of dam in a rectangular canyon with L/H=2.5 and α =0.4

The calculated fundamental period of the earth dam (T_1) in the rectangular canyon for different values of α and L/H are shown in Figure 2-10. Fundamental period T_1 has been normalized by $T_\infty = 2.61\frac{H}{V_{sd}}$, which represents the fundamental period of an infinitely long dam [1, 6]. The solid lines represent the obtained results for different impedance ratio values and that of rigid canyon ($\alpha = 0$) is marked by asterisk. The results of the proposed technique, FEM by Martinez and Beilak [63] and the shear beam method by Gazetas [61] for the rigid canyon are depicted by the asterisk, dashed-dotted line and dotted line, respectively. While there is an excellent agreement between the obtained results and those of FEM, the results using shear beam analysis show underestimated values of the natural periods (Figure 2-10). Figure 2-10 shows that the fundamental natural period is highly influenced by the ratio α, representing the flexibility of the canyon. Increasing values of α leads to an increase in T_1. The effect of flexible canyon is more remarkable in wider canyons.

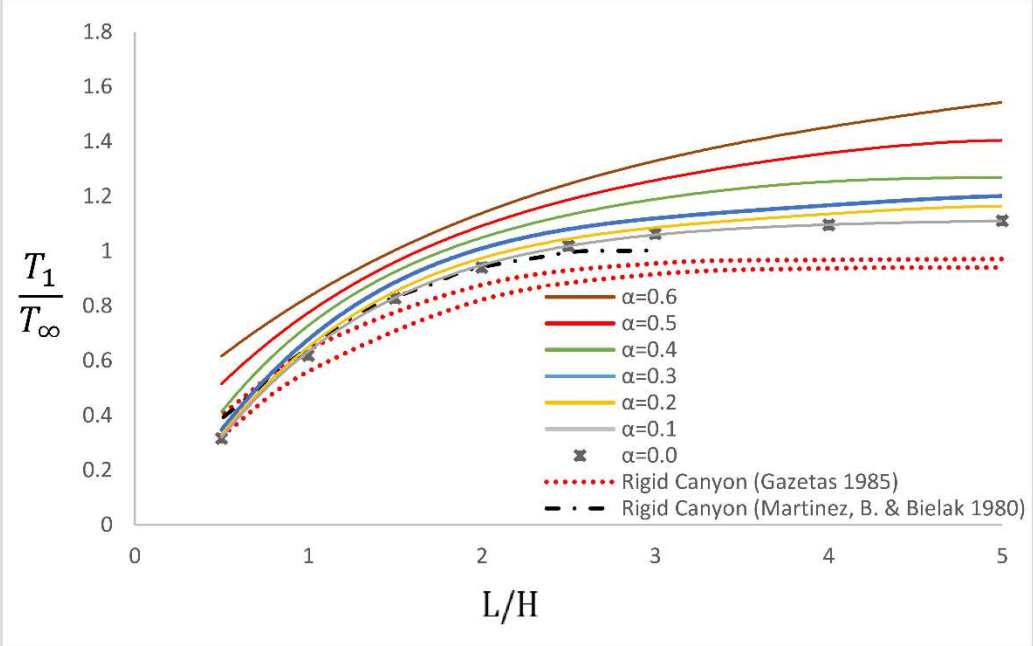

Figure 2-10. Effect of rectangular canyon geometry on the fundamental period

For the lower values of α and (L/H)>4, T_1 remains constant. Furthermore, the results of the wide enough rectangular canyon, with L/H=5 (Figure 2-11), were compared with the 2D available results in the literature. A reasonable agreement is observed between the results of the proposed technique 3D FEM-SBFEM (blue line and green dash line) and those of 2D FEM-BEM (red circle and black triangular) obtained by Touhei and Ohmachi [95] for the first and second modes of vibration for different values of α (Figure 2-12).The values of natural frequencies for 2D and 3D results are compared in Table 2-1, E is the differences percentage. The real and imaginary parts of the first mode of vibration have been shown respectively in Figure 2-13 (a) and Figure 2-13(b) for an earth dam in rectangular canyon with L/H=3 and α=0.6.

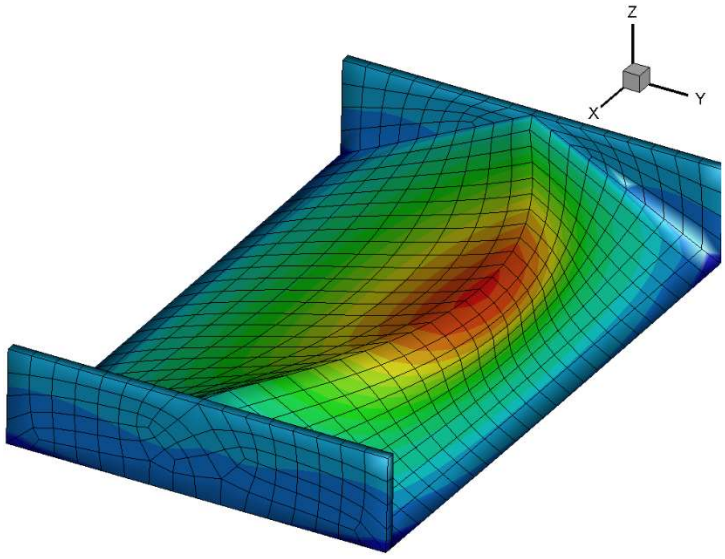

Figure 2-11. Deformation plot due to the excitation in direction of upstream-downstream(y direction) for the earth dam in the rectangular canyon with L/H=5

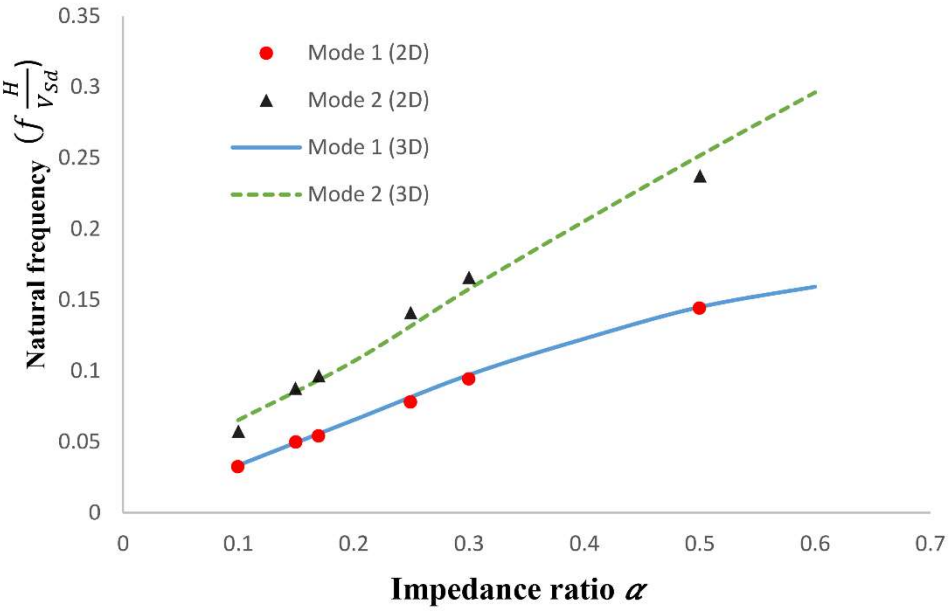

Figure 2-12. Comparison between natural frequencies of 2D and 3D models for the rectangular canyon with L/H=5

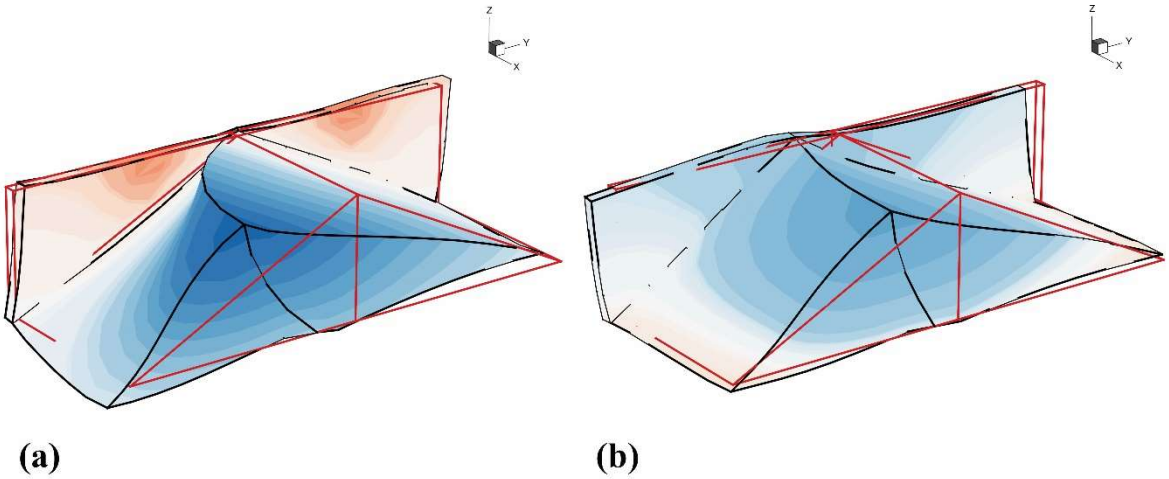

Figure 2-13. a) Real and b) imaginary parts of first mode shape of earth dam located in a rectangular canyon

Figure 2-14 shows how the flexibility of the wide trapezoidal canyon affects the fundamental natural period. For an earth dam in a wide trapezoidal canyon with L/H=5 and α=0.1, the real and imaginary parts of the first mode of vibration are shown, respectively, in Figure 2-15 (a) and Figure 2-15 (b).

Table 2-1. Comparison of obtained natural frequencies for 3D canyons with L/H=5 and 2D results

	Impedance ratio α					
	First Mode			Second Mode		
	0.1	0.3	0.5	0.1	0.3	0.5
3D	0.033	0.097	0.145	0.065	0.158	0.252
2D	0.033	0.094	0.144	0.057	0.166	0.238
E(%)	3%	3%	0%	12%	−5%	6%

Figure 2-7(c) shows the geometry of the narrow trapezoidal canyon. In the same way, the fundamental natural periods of the earth dam located in the narrow trapezoidal canyon are obtained (Figure 2-16). Figure 2-17(a) and Figure 2-17(b) represent the real and imaginary parts of the first mode, respectively, for an earth dam in a wide trapezoidal canyon with L/H=5 and α=0.1.

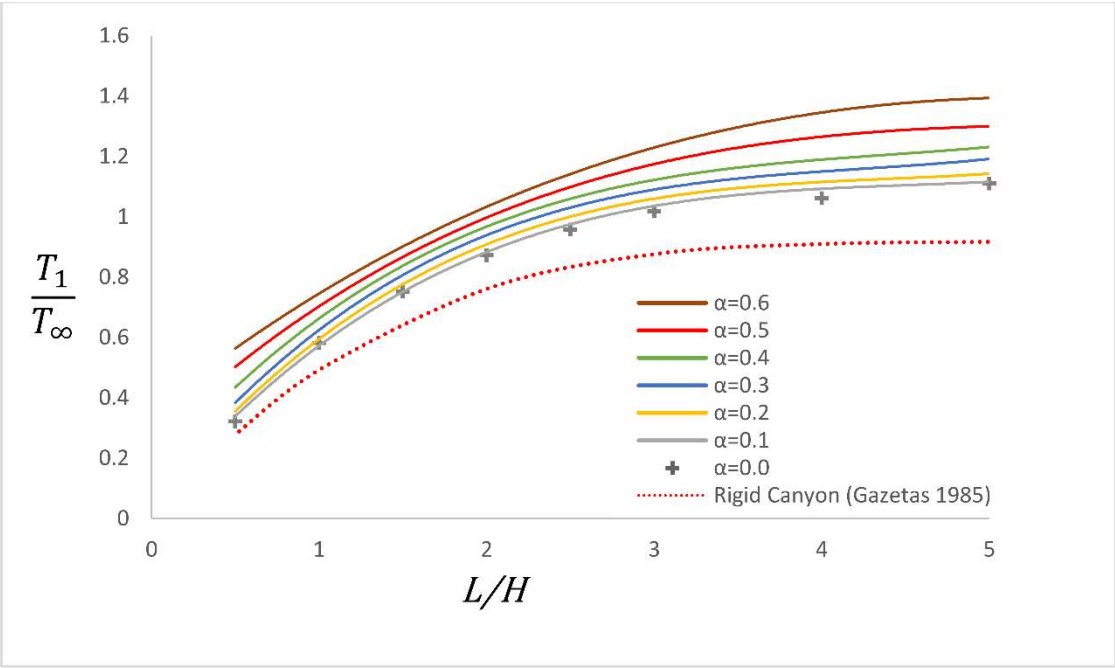

Figure 2-14. Effect of wide trapezoidal canyon geometry on the fundamental period

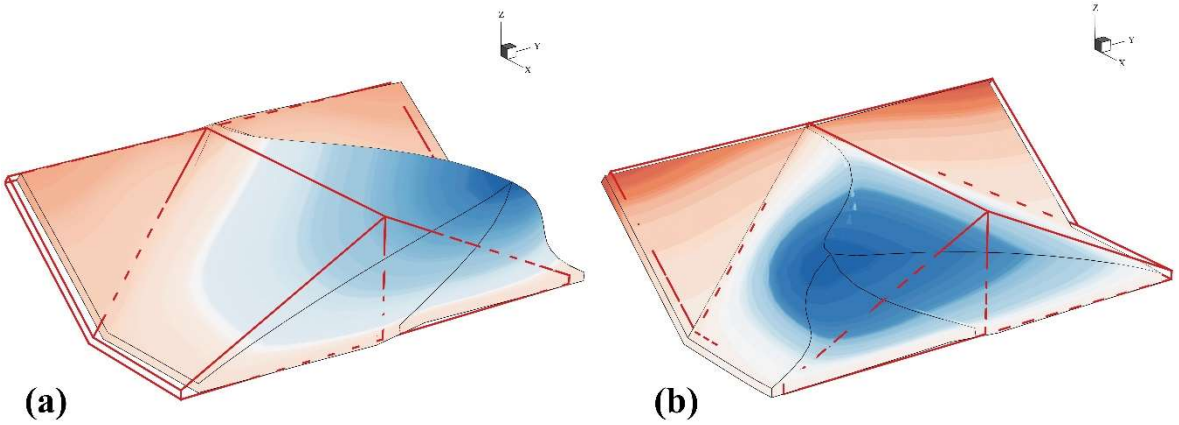

Figure 2-15. a) Real and b)imaginary parts of first mode shape of earth dam located in a wide trapezoidal canyon

The last canyon geometry is the triangular canyon Figure 2-7(d). Figure 2-18 shows the increasing fundamental natural periods with increasing L/H and α. The real and imaginary parts of the first mode of vibration of earth dam locating in the triangular canyon with L/H=5 and α=0 are shown in Figure 2-19(a) and Figure 2-19(b), respectively.

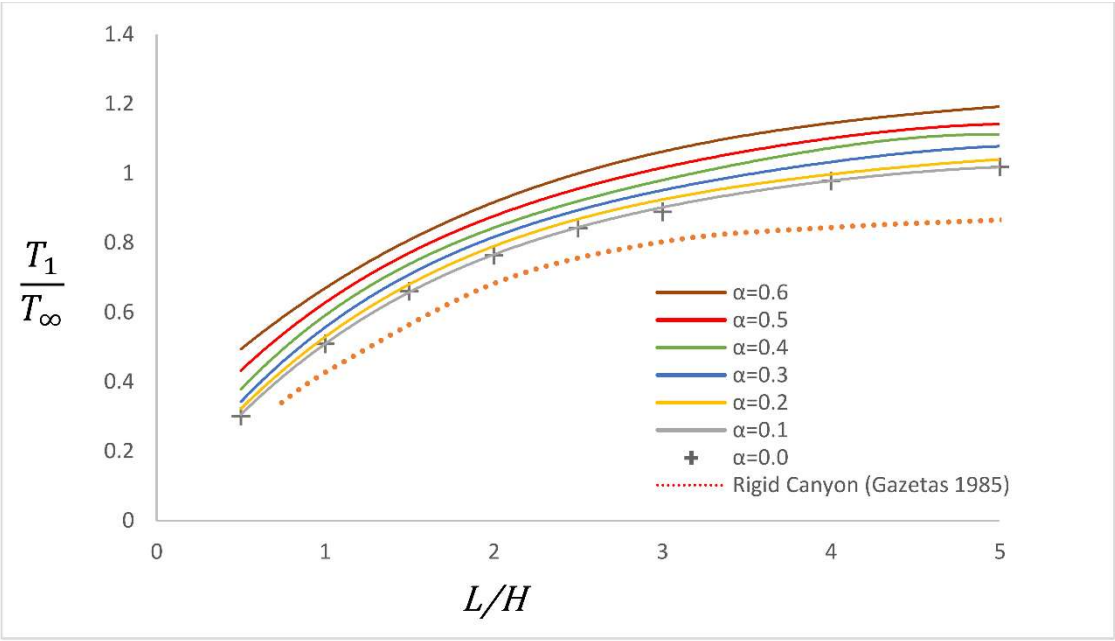

Figure 2-16. Effect of narrow trapezoidal canyon geometry on the fundamental period

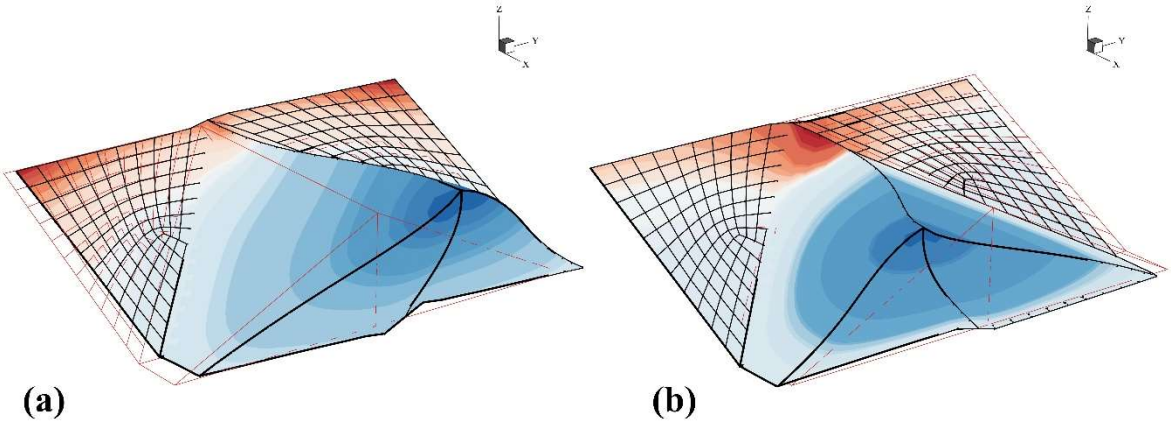

Figure 2-17 a) Real and b) imaginary parts of first mode shape of earth dam located in a narrow trapezoidal canyon.

A comparison of outcomes associated with the rigid canyon, between the proposed method (asterisks) and shear beam (dotted lines), reveals that the shear beam method always underestimates the values of natural periods (Figures 2-10, 2-14,2-16 and 2-18). This under prediction is approximately 15% at L/H=5 and is consistent across all four diverse canyon geometries.

A comparison of natural periods in different canyon geometries indicates that the earth dams behave more flexible in wider canyons. For $\mathrm{L/H} > 3$, the behavior of the natural periods of the rigid canyons plateaus,

whereas that of the relatively flexible canyon ($\alpha = 0.6$) continues to slightly increase (Figures 2-10, 2-14,2-16 and 2-18).

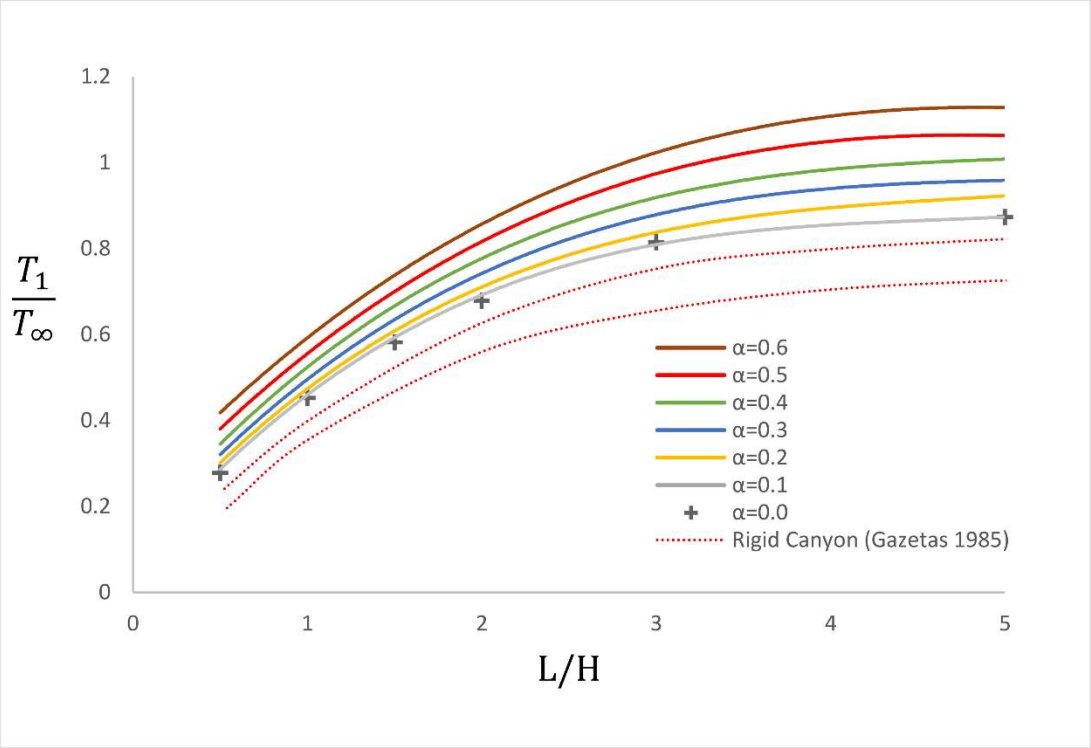

Figure 2-18. Effect of triangular canyon geometry on the fundamental period

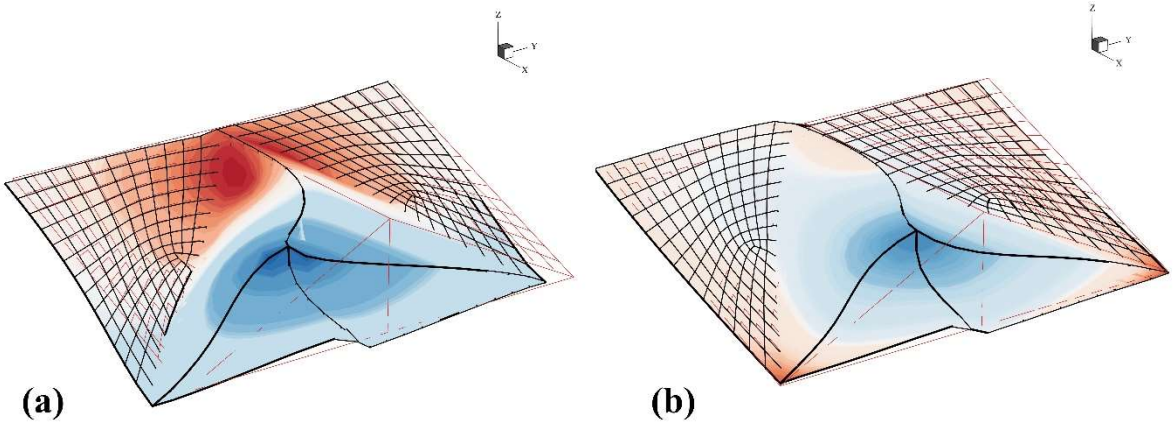

Figure 2-19. a) Real and b) imaginary parts of first mode shape of earth dam located in a triangular canyon

The effect of geometry on natural periods is shown in Figure 2-20. In comparison with the rectangular canyons, triangular canyons demonstrate stiffer responses. As apparent in Figure 2-20 (b), at L/H =5, triangular canyons demonstrate a 21% lower natural period compared to the rectangular ones. However, in the case of relatively flexible canyons, Figure 2-20 (a), their difference is approximately 29%. These results suggest that the effect of geometry is of more importance for flexible canyons.

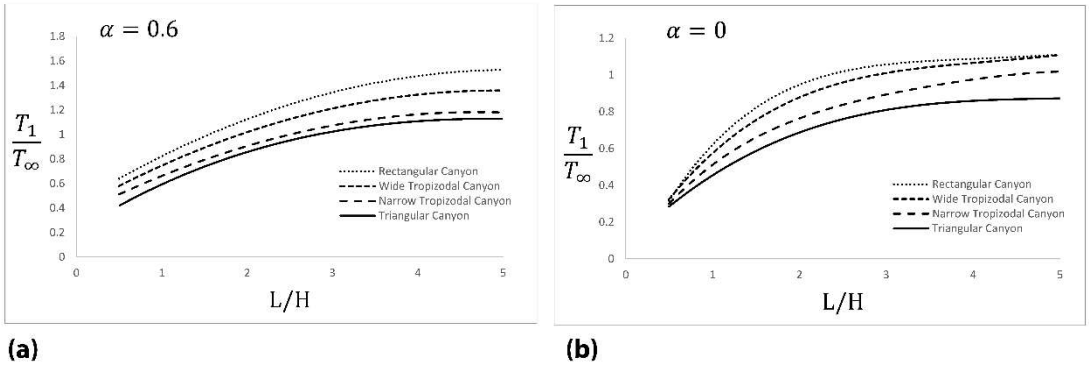

Figure 2-20. The effect of canyon geometry on natural periods of earth dams with $L/H = 5$ for: a) $\alpha = 0.6$ and b) $\alpha = 0$

The impedance ratio variations for different canyons with $L/H = 5$ is illustrated in Figure 2-21. For the $\alpha = 0.6$ in the wide rectangular canyon, it can be observed that the natural period increases by 39% compared with the results of the rigid canyons ($\alpha = 0.0$).

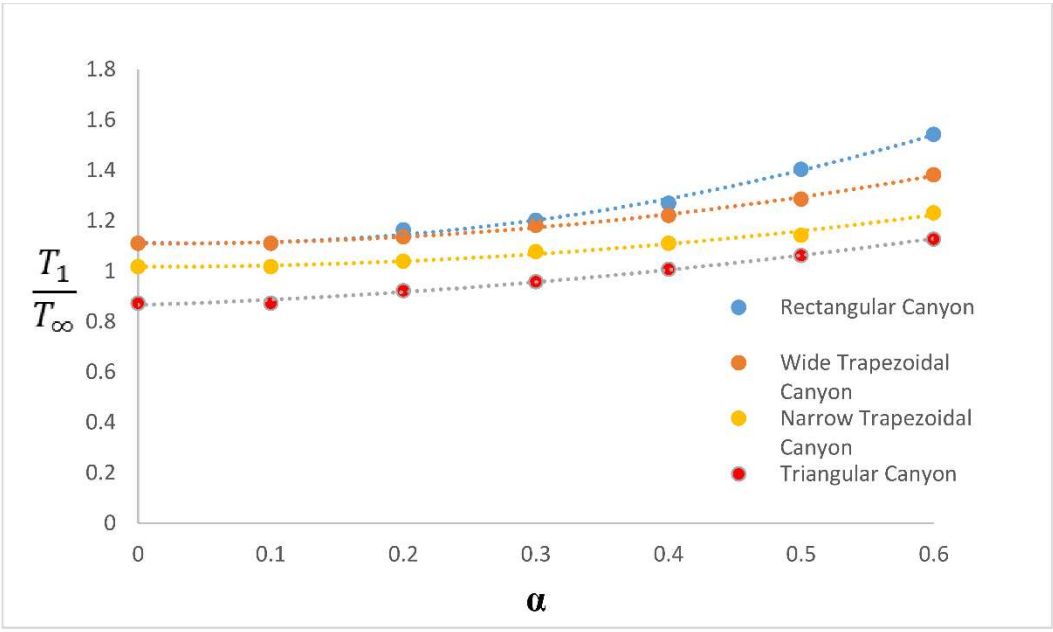

Figure 2-21. Comparison of natural periods for different values of α and L/H=5

The final example shows how the proposed graphs may be used to estimate the natural period of an actual dam. The calculated natural periods by FEM-SBFEM are compared with the actual recorded data. Cogswell is a rockfill dam located north of Whittier, California, in the San Gabriel Mountains. The crest length and maximum height of the dam are 175 m and 85 m, respectively. The shear wave velocity of the foundation rock mass is estimated to be about 1200-1500 m/s and 365 m/s for the rockfill. Based on the available data, α is determined to be around 0.2. As the canyon is an intermediate shape between narrow trapezoidal and triangular, the corresponding graphs of the case $\alpha = 0.2$ were chosen. For the L/H=0.2, the ratio of the fundamental natural period of the earth dam to the fundamental natural period of the infinitely long earth dam was estimated by $\frac{T_1}{T_\infty} = 0.75$ [black line and circle (Figure 2-23)]. This is in accordance with the fundamental natural period recorded during the Sierra Madre earthquake T_1=0.48, normalized by T_∞ [asterisk* (Figure 2-23])

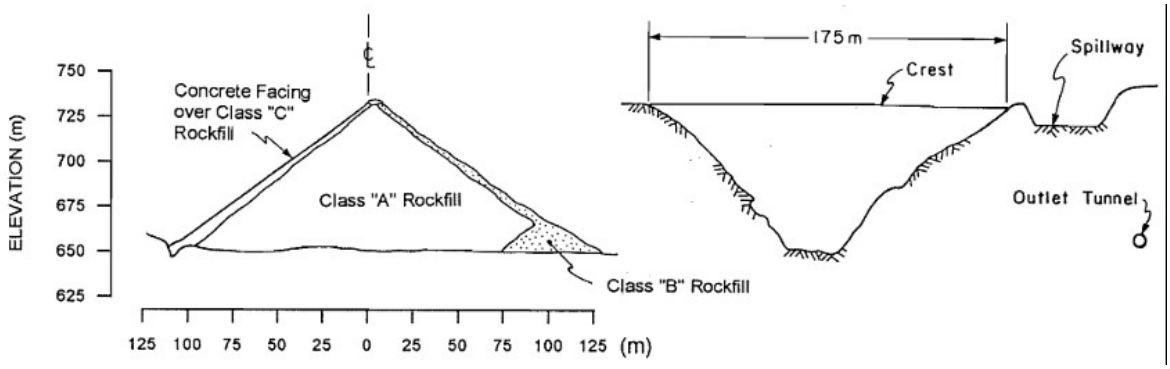

Figure 2-22. Transverse and longitudinal cross sections of Cogswell Dam [96]

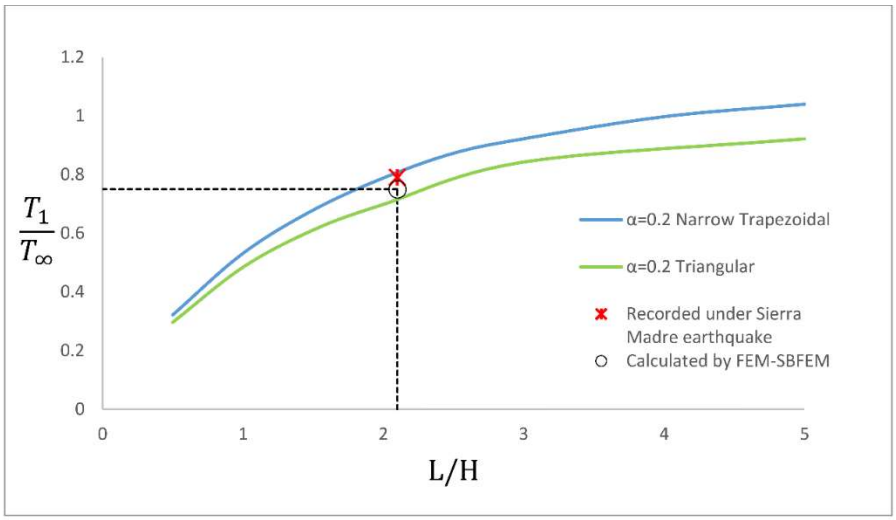

Figure 2-23. Comparison of obtained natural period by FEM-SBFEM and recorded natural periods under the Sierra Madre earthquake

2.6 Conclusion

The major objective of this research was developing the FEM-SBFEM hybrid technique to estimate natural periods of earth dams, incorporating the effects of 3D geometry and flexibility of canyon. The main conculision summarized as follow:

- The first-order nonlinear ordinary differential equations of SBFEM was solved numerically respect to the frequency ω using a fourth-order Runge-Kutta method. An asymptotic expansion of the dynamic-stiffness matrix for high frequency is used to start numerical integration.

- The equilibrium equations and the compatibility conditions were applied at boundary of canyon and earth dam to couple the dynamic stiffness obtained by FEM with the that of SBFEM.

- As the dynamic-stiffness matrix of the unbounded domain is complex and frequency-dependent, the classical mode-superposition method is not straightforward. Therefore, the dam was excited in the upstream-downstream direction.

- The results of the proposed technique were validated with available results in the literature. The natural periods of earth dams for different canyon geometries were obtained.

- It was observed that for the rigid rectangular canyons, the calculated fundamental natural periods are in agreement with the results of FEM in the literature. However, underestimations from the shear beam method were also observed.

- The role of flexibility and canyon geometry were also considered. These results suggest that the effect of geometry is of more importance for flexible canyons.

- Some graphs were proposed may be used by practical engineers for estimation of natural periods of earth dams in canyons with different shapes and material properties.

- Relationships were developed for obtaining the natural frequency of the earth dam based on the geometry and material properties of the canyon.

- A comparison of the calculated natural periods with actual recorded data demonstrates good agreement. In conclusion, the hybrid FEM-SBEFEM is an accurate approach for modeling earth dams under dynamic loadings.

2.7 Appendix

2.7.A

The equation of the fundamental period for the shear beam method, $T_{\infty} = 2.61 \frac{H}{V_{sd}}$, was improved to consider the effect of the flexibility of the canyon. The modified natural period equations for different shapes of canyon with L/H=5 are presented in Equations (A.2-9).

Triangular canyon $$T1 = (0.45\,\alpha 2 + 0.17\,\alpha + 0.87)\ 2.61 \frac{H}{V_{sd}} \quad \text{(A.2-9)}$$

Narrow trapezoidal canyon $$T1 = (0.58\,\alpha 2 + 0.1\,\alpha + 1.01)\ 2.61 \frac{H}{V_{sd}} \quad \text{(A.2-10)}$$

Wide trapezoidal canyon $$T1 = (0.79\,\alpha 2 - 0.03\,\alpha + 1.11\,)\ 2.61 \frac{H}{V_{sd}} \quad \text{(A.2-11)}$$

Rectangular canyon $$T1 = (1.38\,\alpha 2 - 0.12\,\alpha + 1.11\,) 2.61 \frac{H}{V_{sd}} \quad \text{(A.2-12)}$$

2.7.B

A modified equation for the natural periods is proposed which may take into the account the effect of the flexibility of canyon:

$$T1 = \beta\ 2.61 \frac{H}{V_{sd}} \quad \text{(B.1)}$$

where β is obtained form Table 2-2, which is based on the calculated results.

Table 2-2. β parameter for different values of impedance ratio and L/H for different canyon shapes

			α						
			0	0.1	0.2	0.3	0.4	0.5	0.6
Rectangular Canyon	L/H	5	1.11	1.11	1.16	1.2	1.27	1.4	1.54
		4	1.09	1.11	1.14	1.18	1.25	1.36	1.45
		3	1.06	1.06	1.09	1.13	1.19	1.26	1.33
		2.5	1.02	1.02	1.04	1.08	1.13	1.19	1.24
		2	0.94	0.94	0.98	1	1.05	1.09	1.14
		1.5	0.83	0.84	0.86	0.88	0.93	0.96	1
		1	0.62	0.63	0.64	0.69	0.72	0.77	0.83
		0.5	0.32	0.32	0.33	0.34	0.41	0.52	0.62
Wide Trapezoidal Canyon	L/H	5	1.11	1.11	1.14	1.18	1.25	1.31	1.38
		4	1.06	1.06	1.09	1.13	1.18	1.22	1.29
		3	1.02	1.02	1.04	1.06	1.1	1.13	1.19
		2.5	0.96	0.98	1	1.02	1.05	1.08	1.13
		2	0.87	0.87	0.91	0.94	0.96	1	1.05
		1.5	0.75	0.76	0.79	0.82	0.86	0.89	0.92
		1	0.58	0.58	0.6	0.64	0.68	0.72	0.75
		0.5	0.32	0.33	0.35	0.37	0.42	0.48	0.55
Narrow Trapezoidal Canyon	L/H	5	1.02	1.02	1.04	1.08	1.11	1.14	1.19
		4	0.98	0.98	1	1.03	1.07	1.1	1.15
		3	0.89	0.91	0.92	0.95	0.98	1.02	1.06
		2.5	0.84	0.84	0.87	0.89	0.92	0.95	1
		2	0.76	0.76	0.79	0.81	0.84	0.87	0.92
		1.5	0.66	0.66	0.68	0.71	0.74	0.78	0.81
		1	0.51	0.51	0.53	0.56	0.59	0.62	0.66
		0.5	0.3	0.31	0.32	0.34	0.38	0.43	0.5
Triangular Canyon	L/H	5	0.87	0.87	0.92	0.96	1.01	1.06	1.13
		4	0.85	0.85	0.88	0.92	0.97	1.02	1.08
		3	0.81	0.81	0.84	0.88	0.92	0.98	1.03
		2.5	0.75	0.76	0.78	0.8	0.85	0.9	0.95
		2	0.68	0.68	0.7	0.73	0.77	0.81	0.85
		1.5	0.58	0.6	0.61	0.63	0.66	0.7	0.74
		1	0.47	0.47	0.48	0.51	0.53	0.57	0.6
		0.5	0.28	0.28	0.3	0.31	0.34	0.38	0.42

2.8 Acknowledgements

This work was supported by the Natural Sciences (NSERC) and Hydro-Québec Industrial Research Chair for lifecycle optimization of embankment dams. The authors also thank their industrial partners: Hydro-Québec, SNCLavalin, Qualitas, WSP, Golder Associates, Klohn Crippen Berger, ConeTec, and Hatch. All calculations were carried out on the Mammouth High Performance Computing (HPC) cluster under the administration of Calculquebec and Compute Canada.

Chapter 3 Computation of Amplification Functions of Earth Dam-Flexible Canyon Systems by the Hybrid FEM-SBFEM Technique

3.1 Résumé

Les effets de géométrie et de flexibilité du canyon environnant peuvent amplifier la réponse du barrage. Pour modéliser le canyon comme un domaine élastique non borné, la condition d'amortissement du rayonnement doit être satisfaite. En conséquence, la méthode des éléments finis de frontières à l'échelle (SBFEM) s'avère être un outil puissant à cet égard. Dans cet article, une méthode de sous-structure a été utilisée pour enchevêtrer FEM-SBFEM. La technique hybride traite le barrage en terre en utilisant FEM et le canyon élastique non borné par SBFEM. L'approche proposée a été vérifiée par quelques données disponibles dans la littérature. La réponse sismique du système de canyon flexible de barrage de terre a été étudiée en utilisant 3D FEM-SBFEM. Plusieurs fonctions d'amplification correspondant à différentes conditions de canyon ont été obtenues en appliquant un déplacement uniforme à la limite du canyon. Une étude approfondie a été réalisée pour examiner les effets de la géométrie et de la flexibilité du canyon sur la réponse en régime permanent du barrage. Ces deux effets ont influencé de manière importante les fonctions d'amplification. Alors que la flexibilité du canyon affecte de manière significative la valeur de la fonction d'amplification maximale, cette valeur ne change pas pour les barrages en terre dans lesquels les canyons ont des formes différentes pour une même longueur. De plus, la réponse latérale du barrage de terre dans le domaine temporel a été calculée pour analyser les effets susmentionnés lors d'un tremblement de terre réel. Les fonctions d'amplification proposées ont été utilisées pour comparer les spectres de réponse enregistrés du barrage d'El Infiernillo lors des tremblements de terre de 1966 avec la fonction d'amplification calculée. Un accord raisonnable a été observé entre eux.

3.2 Abstract

A dam's responses can be amplified by the geometry and flexibility of its surrounding canyon. To modeling a canyon as an elastic unbounded domain, the radiation damping condition should be satisfied, and in this regard, the Scaled Boundary Finite Element Method (SBFEM) is a powerful tool. In this article, a substructure method was used to combine the standard Finite Element Method (FEM) with the SBFEM, resulting in the hybrid FEM-SBFEM technique. This hybrid technique treats an earth dam by using FEM and a corresponding elastic unbounded canyon by SBFEM. The proposed approach was verified by data available in the literature. The seismic response of an earth dam-flexible canyon system was investigated by employing a 3D FEM-SBFEM method. Several amplification functions corresponding to different canyon conditions were obtained by applying a uniform displacement for the canyon boundary, and a comprehensive study was performed to examine the effects of canyon geometry and flexibility on the steady-state response of the dam, as these two effects

influenced the amplification functions. While the flexibility of the canyon significantly affects the maximum amplification function value for a dam, this value does not change for earth dams in canyons with different shapes but the same length. In addition, the lateral response of earth dams in the time domain was computed in order to analyze the aforementioned effects under an actual earthquake. The proposed amplification functions were used to compare the recorded response spectra of the El Infiernillo dam under the 2 earthquakes in 1966 with the calculated amplification function, and a reasonable agreement was observed between them.

3.3 Introduction

The amplification function is defined as the relationship between the input and output of a dynamic system, and reflects how the system amplifies or deamplifies the input signal. For an earth dam-canyon system, the amplification function (AF) can be defined as the ratio of the crest motion to the canyon motion. The amplification function of an earth dam at the crest point determines how ground motion like an earthquake is amplified or de-amplified for a given frequency. The amplification function represents the influence of earth dam and canyon properties, including their geometry and material properties. Utilizing the superposition principle, the crest response of an earth dam due to an earthquake is obtained by the production of amplification function and the earthquake ground motion.

Several methodologies, including analytical and numerical approaches, have been developed to try to determine the geometry and flexibility effects of a canyon on the earth dam amplification function. The shear beam method was used by Ambraseys [55] to model an earth dam as a variable wedge-shaped cross-section, and a closed-form solution was presented to obtain different vibration modes of an earth dam in a rectangular canyon. Dakoulas and Gazetas [57] suggested an analytical solution to estimate the steady-state response of earth dams in rigid semi-cylindrical canyons under harmonic base excitation, and it was shown that the presence of a rigid canyon enhances the seismic response. For the hysteretic damping ratio β=10%, the maximum amplification functions were obtained as $AF_{max} \approx 10$ and $AF_{max} \approx 8$ for the 3D developed theory and 2D plane strain shear beam, respectively. Also, Dakoulas and Gazetas [57] concluded that: "AF is independent of the exact canyon shape." Dakoulas and Hsu [58] similarly proposed an analytical solution for semi-elliptical rigid canyons, and it was shown that the amplification effect is higher in dams in narrow canyons compared to dams in wide canyons. Further, Dakoulas and Hashmi [56] presented an analytical approach for examining the steady-state response of earth dams in rectangular canyons. The dam was modeled as a 2D homogeneous triangular shear wedge with a linearly hysteretic material, and the canyon was considered to be a rectangle with elastic materials, with a parametric study being done to investigate the effect of impedance ratio on the response of the dam.

A 2D finite element method (FEM) was used by Clough and Chopra [1] to conduct a linear dynamic analysis of a homogenous earth dam on a rigid foundation. Similarly, 2D FEM was applied by Hall and Chopra [97] for the prediction of dynamic reservoir-dam interactions. In comparison with gravity dams, the presence of a reservoir does not significantly influence an earth dam's responses. The calculated AF_{max} for both situations, i.e., with and without the reservoir, was almost 8. To resolve the erroneous rigid foundation assumption, a finite element model of the earth dam was coupled with an analytical solution to simulate earth dam-flexible foundation interactions [68], with the foundation being assumed to be a linear elastic half-space.

Domínguez [98] was the first to apply the boundary element method (BEM) for the dynamic soil-structure interaction (SSI) problem. BEM accurately simulates the soil medium as a half-space, and also rigorously satisfies the Sommerfeld radiation condition [99]. BEM has been used for different SSI problems, including gravity dams [100] and arch dams [101]. The coupling of FEM and BEM [102] can be beneficial through gaining the advantages of both. Touhei and Ohmachi [103] determined the impulsive crest responses of a dam-foundation system by using the FEM-BEM approach in the time domain, and the effect of a flexible foundation with different impedance ratios was considered. Guan and Moore [104] coupled FEM and a layer transfer matrix for the 2D frequency domain analysis of an earth dam on a multi-layer foundation, while Dakoulas and Abouseeda [105] employed 2D FEM-BEM to obtain the seismic responses of an earth dam-foundation system. The hybrid methodology was developed to consider the inelastic response of the earth dam [34].

A fundamental solution satisfying the governing equation in BEM is often complicated to obtain and sometimes impossible, as it shows singularities and may not exist for some anisotropic problems [82]. Wolf and Song [36], [106] developed a novel semi-analytical approach for calculating the dynamic stiffness matrix of a half-space, which is called the scaled boundary finite element method (SBFEM). As SBFEM is independent of the fundamental solution, it does not have the difficulty of BEM and rigorously satisfies the radiation damping by combining the advantages of FEM and BEM. Equations for SBFEM have also been promoted by other researchers; for example, Bazyar and Song [38] extended the SBFEM equation for non-homogeneous elastic unbounded domains in time-harmonic and transient domains. SBFEM has also been used for other geotechnical problems, including steady-state confined and unconfined seepage problems [20], [21], transient seepage [109], and non-linear problems [110]. Further, Chen et al. [111] advanced the polygon-scaled-boundary finite element method for the nonlinear analysis of concrete-faced rockfill dams.

A renewed interest has been seen in applying the FEM-SBFEM method for different SSI problems with dynamic loadings [45], [47], [112], [113]. Yaseri et al. [51], [91] coupled FEM with SBFEM to analyze induced ground vibration due to passing trains, and Lin et al. [49] proposed SBFEM as an efficient method to evaluate dynamic dam-reservoir interaction systems. Zhao et al [50] used FEM-SBFEM to consider the seismic responses of dams and offshores structures, with SBFEM being applied at the water-structure interfaces. The authors of [114] successfully utilized the hybrid FEM-SBFEM technique for estimating the natural periods of different earth dam-canyon systems, with several graphs and equations being produced to obtain the natural period of earth dams while taking into account the geometry and flexibility effects of the canyon.

The research in the literature can be categorized into three groups, as follows:

- In 2D-hybrid techniques, the approach can satisfy the radiation damping, but it does not take into consideration the 3D-geometry effect. Moreover, the surrounding soil has always been modeled as a flexible foundation [34], [78].

- In 3D models, canyons have been assumed to be constrained by rigid boundary conditions, while no influence of flexibility has been examined [58], [79].

- In 3D-hybrid models, the canyon behaves as an elastic half-space. The mathematical restrictions, however, have limited the shapes of canyons to only some pre-determined profiles like semi-elliptical forms [80].

In this work, a 3D FEM-SBFEM equation is derived to conduct a comprehensive study of the effects of canyon flexibility and geometry on the seismic responses of earth dams. The objectives of the current work are as follows:

- Introducing the FEM-SBFEM technique as a powerful tool for the dynamic analysis of earth dam-flexible canyon interactions.

- Studying the flexibility and geometry effects of a canyon on dam-crest seismic responses.

3.4 Formulation

Utilizing the substructure method, the soil-earth dam interaction system is divided into two simpler sub-models (see Figure 3.1) and the bounded domain (ΩF) of the earth dam is discretized for analysis by FEM. The mesh is built with the nodes of the earth dam Γ^e and the interface Γ^i. In the same way, the unbounded domain (Ωs) of the canyon is meshed by SBFEM, including canyon nodes Γ^i and interface nodes Γ^i. While FEM is simulated by 3D brick elements, the surface element is utilized in SBFEM. To take into account the flexibility effect of the canyon, the impedance ratio is defined as $\alpha = \frac{\rho_e V_e}{\rho_c V_c}$, where V_e and V_c are the shear wave velocities of the earth dam and the canyon, respectively. ρ is the mass density and S.C represents the scaling center in the scaled boundary finite element coordinate system.

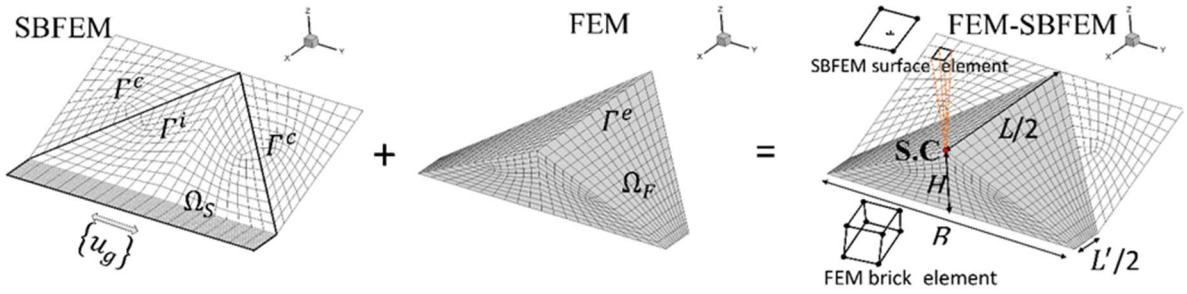

Figure 3-1. Symmetric earth dam-canyon interaction system

3.4.1 FEM formulation

The equation of motion for the bonded domain is presented as Equation (3-1). The bounded domain is an earth dam including the interface nodes Γ^e and ones of the earth dam having no contact with the canyon Γ^e (Figure *3-1*).

$$[S^F(\omega)]\{u(\omega)\} = \{P(\omega)\} \tag{3-1}$$

where ω is frequency, and $\{u\}$ and $\{P\}$ are the displacement and the load vectors, respectively. $[S^F]$ is the dynamic-stiffness matrix of the bounded domain. If it is decomposed into two parts, Γ^i and Γ^e, it will be converted into:

$$[S^F] = \begin{bmatrix} [S^F_{ee}] & [S^F_{ei}] \\ [S^F_{ie}] & [S^F_{ii}] \end{bmatrix} = [K^F](1 + 2i\beta) - \omega^2[M^F] \tag{3-2}$$

where $[K^F]$ is the stiffness matrix, $[M^F]$ is the mass matrix and β is the material hysteretic damping ratio.

3.4.2 SBFEM formulation

For 3D problems, the SBFEM equation of the dynamic stiffness matrix is presented as:

$$([S^S(\omega)] + [E^1])[E^0]^{-1}(+[S^S(\omega)] + [E^1]^T) - ([E^2]) - \omega[S^S(\omega)]_{,\omega} + \omega^2[M^0]\,\xi^2 = 0 \tag{3-3}$$

where $[E^0]$-$[E^2]$ and $[M^0]$ are the coefficients matrices of SBFEM; their derivations are discussed in references [36], [52], [82], [115]. These are obtained by the assemblage of the corresponding coefficient matrices of every individual element, similar to the standard FEM methodology. Equation (3-3) is a non-linear first-order ordinary differential equation in which the variable ω is the only independent variable. The Runge- Kutta scheme

is used for the numerical integration of Equation (3-3). To obtain an initial value, an asymptotic expansion is used:

$$\left[S^{\mathrm{S}}(\omega)\right] = [K^S] + i\omega[C^S] + \sum_{i=1}^{m}[A^i](i\omega)^{-1} \tag{3-4}$$

$[C^S]$, $[K^S]$ and $[A^i]$ are the coefficient matrices [52]. $\left[S^{\mathrm{S}}(\omega_h)\right]$ is calculated for sufficiently high (but not infinite) values of the frequency ω_h. The solution algorithm uses initial value $\left[S^{\mathrm{S}}(\omega_h)\right]$ as an initial value and solves Equation (3-4) step-by-step with respect to ω. There will be a stiffness matrix of the unbounded domain resulted from each ω. the lower band, ω_l, would approach zero.

3.4.3 Coupled FEM-SBFEM formulation

Equation (3-5) indicates the equations of motion for earth dam-canyon interaction in the frequency domains.

$$[S(\omega)]\{u(\omega)\} = \{P(\omega)\} \tag{3-5}$$

If the above equation is decomposed into two domains $\Gamma^c$and Γ^i (Figure 3-1), it is rewritten as:

$$\begin{bmatrix}[S_{ee}^F] & [S_{ei}^F]\\ [S_{ie}^F] & [S_{ii}^F]\end{bmatrix}\begin{Bmatrix}\{u_e\}\\ \{u_i\}\end{Bmatrix} = \begin{Bmatrix}\{P_e\}\\ \{P_i\}\end{Bmatrix} \tag{3-6}$$

The seismic excitation input motion $\{u^g(\omega)\}$ is applied to all nodes of the canyon, $\Gamma^c$and Γ^i (Figure 3-1). Superscript *g* indicates the ground system. The interaction force on the interface nodes obtained from the product of Equation (3-3) by relative motion as illustrated by:

$$\{\{R_i(\omega)\}\} = \begin{bmatrix}[S_{ii}^S] & [S_{ci}^S]\end{bmatrix}\begin{Bmatrix}\{u_i^t(\omega)\} - \{u_i^g(\omega)\}\\ \{u_c^t(\omega)\} - \{u_c^g(\omega)\}\end{Bmatrix} \tag{3-7}$$

Subscript *t* shows the total displacement with respect to a fixed reference. The seismic motion $\{u^g(\omega)\}$ is converted to an equivalent load which applies to the interface nodes Γ^i. The equation of motion for the canyon nodes that do not have contact with the earth dam (Γ^c) is as follows:

$$[S_{cc}^S]\left(\{u_c^t(\omega)\} - \{u_c^g(\omega)\}\right) + [S_{ci}^S]\left(\{u_i^t(\omega)\} - \{u_i^g(\omega)\}\right) = 0 \tag{3-8}$$

By substituting $\{R_i(\omega)\}$ (Equation (3-7)) for $\{P_i\}$ (Equation (3-6)) and utilizing Equation (3-8), Equation (3-6) is rearranged as:

$$\begin{bmatrix} [S_{ee}^F] & [S_{ei}^F] & 0 \\ [S_{ie}^F] & [S_{ii}^F]+[S_{ii}^S] & [S_{ci}^S] \\ 0 & [S_{ic}^S] & [S_{cc}^S] \end{bmatrix} \begin{Bmatrix} \{u_e^t\} \\ \{u_i^t\} \\ \{u_c^t\} \end{Bmatrix} = \begin{Bmatrix} 0 \\ [S_{ii}^S]\{u_i^g(\omega)\}+[S_{ci}^S]\{u_c^g(\omega)\} \\ [S_{ic}^S]\{u_i^g(\omega)\}+[S_{cc}^S]\{u_c^g(\omega)\} \end{Bmatrix} \tag{3-9}$$

which is the equation of motion of an earth dam-canyon system under seismic excitation. This equation can be solved for each frequency.

3.4.4 Amplification Function

To calculate the amplification function, a unit displacement $\{u^g(\omega)\}$ applied at all nodes of the canyon (Γ^i and Γ^c). Equation (3-9) is solved for $\{u^g(\omega)\}=1$; then, the displacement at the crest of the dam is obtained in the upstream-downstream direction and is introduced as the amplification function (AF) of the crest (point S.C in Figure 3-1). As can be seen from Figure 3-2, by multiplying the amplification function by the Fourier amplitude spectrum of a seismic event ($\{\ddot{u}^g(\omega)\}$), the crest dam response $\{\ddot{u}^{cr}(\omega)\}$ is obtained. The corresponding response to the seismic event in the time domain is obtained by using the inverse Fourier transform $\{\ddot{u}^{cr}(t)\}$.

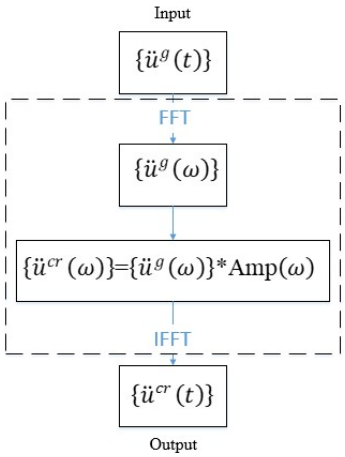

Figure 3-2. Diagram of AF application

3.5 Verification

To validate the proposed methodology, the example of a rigid massless foundation on an elastic half-space is used. More details can be found in the companion paper [114]. The width equals B=30 m and the thickness is 0.1B. The bounded domain, a cube with the size 2B*2B*2B, is modeled by FEM and the half-space is discretized by SBFEM. The FEM and SBFEM are constituted by 216 8-nodes brick elements and 108 four-node surface

elements, respectively. The material properties are chosen as modulus of elasticity =24 *10^6 kPa, Poisson's ratio = 0.33 and unit weight = 24 kN/m3. The material properties for the bounded and the unbounded domains are the same (impedance ratio=1).

Figure 3-3 compares the results calculated by FEM-SBFEM with results available in the literature [40, 41] for different loading conditions. Figure 3-3(a) and Figure 3-3(b) represent the real and imaginary parts of the vertical and horizontal compliances (C_{VV} and C_{HH}), respectively. a_0 is dimensionless frequency $a_0 = \frac{\omega B}{c_s}$, where c_s is the shear wave velocity. Equations (3-10) and (3-11) indicate the non-dimensionalized vertical and horizontal compliance coefficients, respectively.

$$C_{VV}(a_0) = \frac{GBU_v}{P_v} \tag{3-10}$$

$$C_{HH}(a_0) = \frac{GBU_H}{P_H} \tag{3-11}$$

where G is the shear modulus and, U_V and U_H are the vertical and horizontal displacements under the loading P, respectively. Figure 3-3(c) depicts the rocking compliance results normalized as:

$$C_{MM}(a_0) = \frac{GB^3\theta}{M} \tag{3-12}$$

where which M is the dynamic moment and θ is the rotation of the plate around the horizontal axe. The good agreement between the results of the proposed method and the available data in the literature shows the applicability and accuracy of FEM-SBFEM under different loading conditions (Figure 3-3).

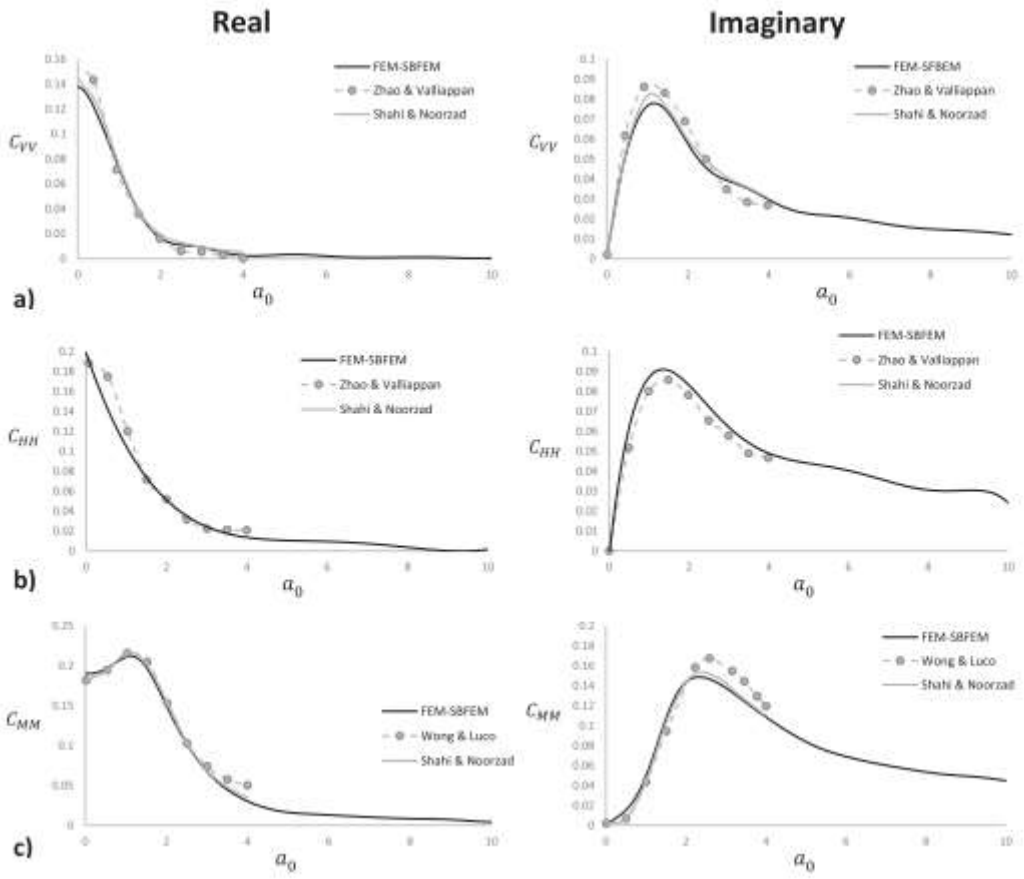

Figure 3-3. (a) Vertical compliance; (b) Horizontal compliance; and (c) Rocking compliance of a rigid square massless plate resting on an isotropic homogeneous elastic half-space [114]

Figure 3-4 compares the obtained maximum amplification function with other results available in the literature [65], [116]. AF_{max} changes with variations of the rigidity factor IR, which is the inverse of the impedance ratio. The results of FEM-SBFEM for the earth dam in a rectangular canyon with L/H=5 show a reasonable agreement with the results by Dakoulas (1993) for a semi-cylindrical canyon. When the IR approaches 10, the AF max also approaches 10, which is approximately equal to the value reported in [116] for a rigid canyon with different shapes. In addition, the AF_{max} for higher values of IR for a rectangular canyon with L/H=10 approaches 8, which is close to the value obtained by 2D models.

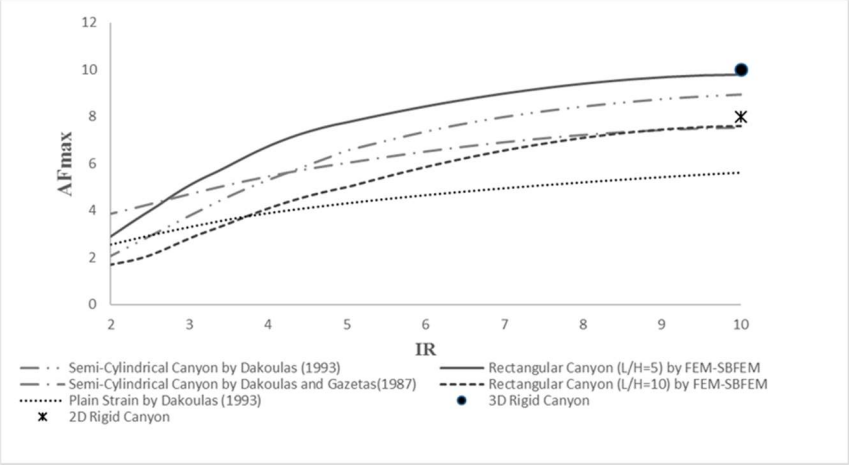

Figure 3-4. Amplification value for the first natural frequency

3.6 Numerical Examples

The programming was written in FORTRAN and run on the Linux CentOS 7 operating system and the analysis was carried out on the Niagara High-Performance Computing (HPC) cluster under the administration of Compute Canada. The machine configuration was 2 x CPU: Intel Sylake 2.4GHz, 20 cores each, a total of 40 cores, and 202 GB of RAM. The calculation time for a model as depicted in Figure 3-5 was almost 8 hours.

To obtain the effect of the impedance ratio (α) on the amplification function (AF), the wide ranges of α are defined as α=0, 0.1, 0.2, 0.3, 0.4, 0.5 and 0.6. Figure 3-1 depicts the geometry of the model, where. L is the length of the canyon, H is the height of the dam, and B is the width of the dam (which is B=2*H). Also, to for considering the effect of canyon geometry, the L/H ratios of 2.5, and 5, as well as four shape types (rectangular canyon, wide trapezoidal canyon, narrow trapezoidal canyon, and triangular canyon) are chosen. The length L' (Figure 3-1) is $L/2$ and $L/5$ for the wide and the narrow trapezoidal canyons, respectively. For the triangular canyon, $L' = 0$. The damping ratios for the earth dam are β=0%, 5%, and 10%, and 0% for the unbounded domain (i.e., the foundation and the canyon).

For the narrow trapezoidal canyon (L/H=5) the generated mesh is shown in Figure 3-5 and the symmetric boundary condition is assigned. For this model, the number of nodes is 3,568, and the unbounded canyon consists of 664 4-nodes surfaces elements (Figure 3-5(a)). The model also comprises an earth dam with 2,626 hexahedral elements having 8 nodes (Figure 3-5(b)). Figure 3-5 represents the downstream-upstream direction displacement under harmonic excitation in the same direction.

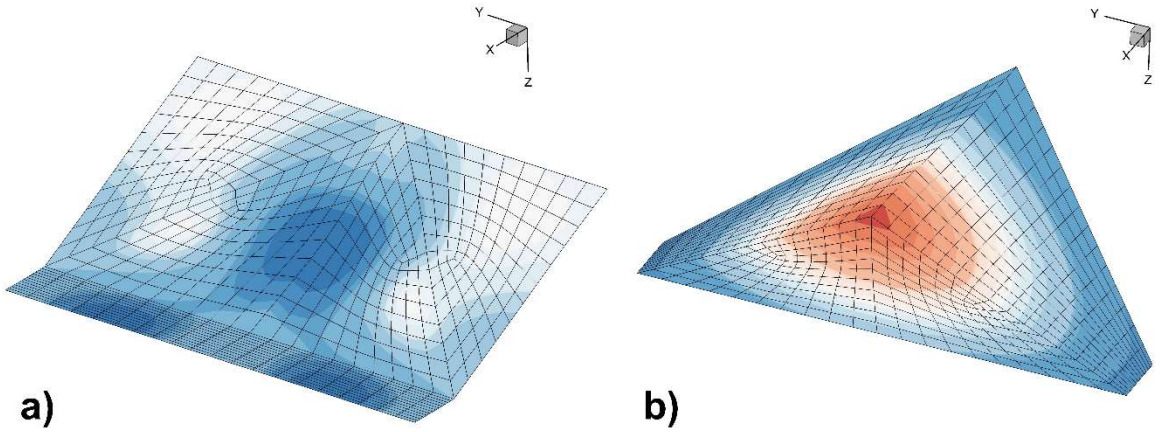

Figure 3-5. Displacement contours in upstream-downstream direction under harmonic canyon excitation for: a) the canyon mesh; b) the assembled earth dam-canyon mesh

3.6.1 Results and discussions

In this part, the amplification functions calculated by FEM-SBFEM are presented. First, the effects of canyon flexibility of (α) and the material damping ratio (β) on the amplification function are studied. Secondly, Two parameters are studied in order to consider the effect of geometry: 1) the length of the canyon for L/H=2.5 and 5 (Figure 3-6-Figure 3-9); and 2) the shape of the canyon (Figure 3-10).

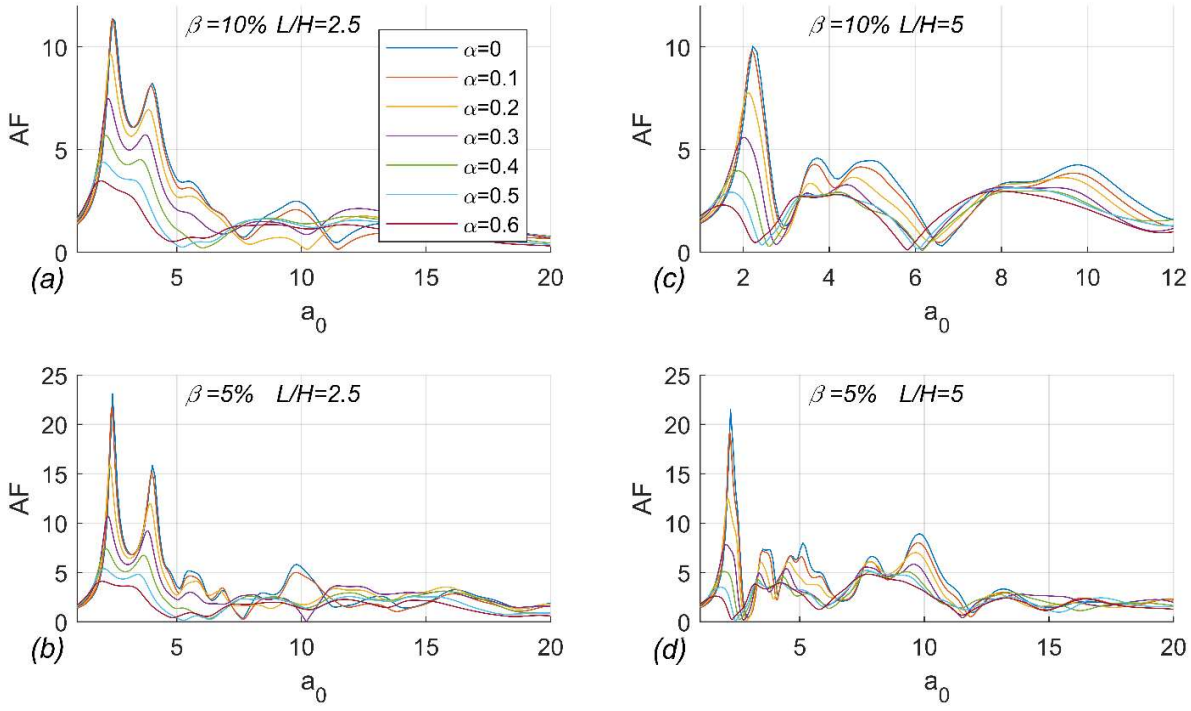

Figure 3-6. Amplification function of the earth dam in a rectangular canyon with different values α, L/H and β

Figure 3-6 indicates the AF of the earth dam located in a rectangular canyon. The AF_{max} values of the stiff canyon (α=0) for L/H=5 are 21.5 and 10 with regard to the damping ratios β=5 and 10%, respectively, and the corresponding AF_{max} magnitudes are 23.12 and 11.38 for L/H=2.5. The decreasing effect of β on the wider canyon is more noticeable; doubling *L* leads to a 12% decrease in AF_{max} (Figure 3-6(a),(c)), while for higher values of α (more flexible canyons), the material damping effect is lighter. To clarify, for α=0.6, if L/H=5, Figure 3-6(d, c) yields AF_{max} values of 2.6 and 2.29 for β=5% and 10% respectively.

The amplification functions are similarly computed for an earth dam located in a wide trapezoidal canyon, as shown in Figure 3-7.

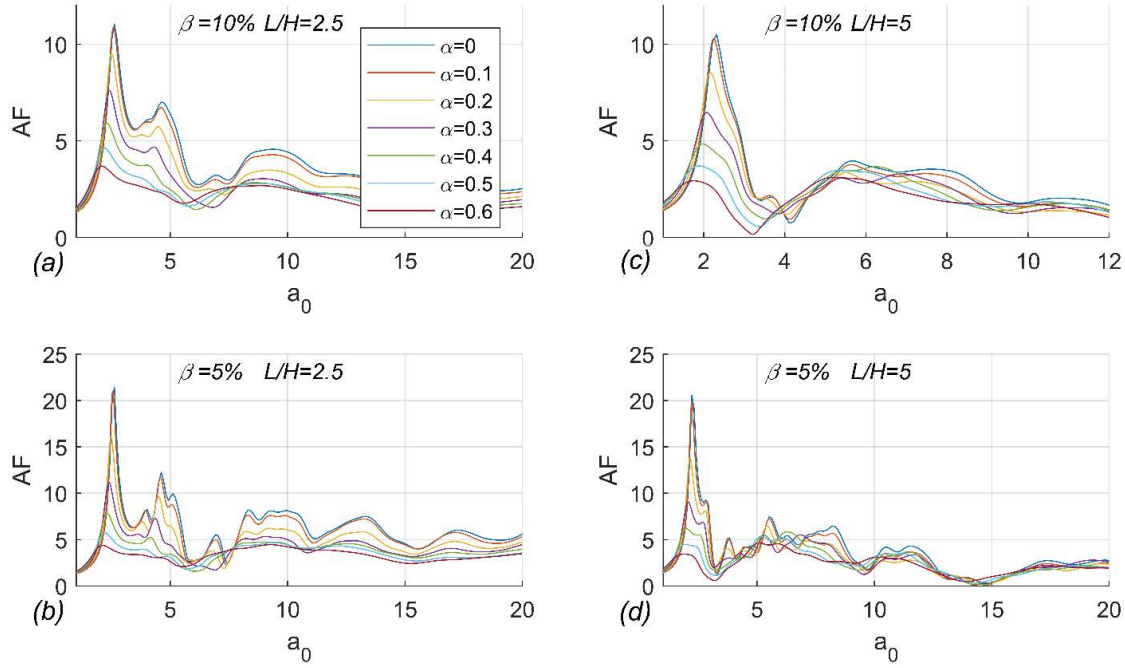

Figure 3-7. Amplification function of an earth dam in a wide trapezoidal canyon with different α, L/H and β

Figure 3-8 represents the amplification function for a narrow trapezoidal canyon with L/H=2.5 and L/H=5 and β= 5% and 10%.

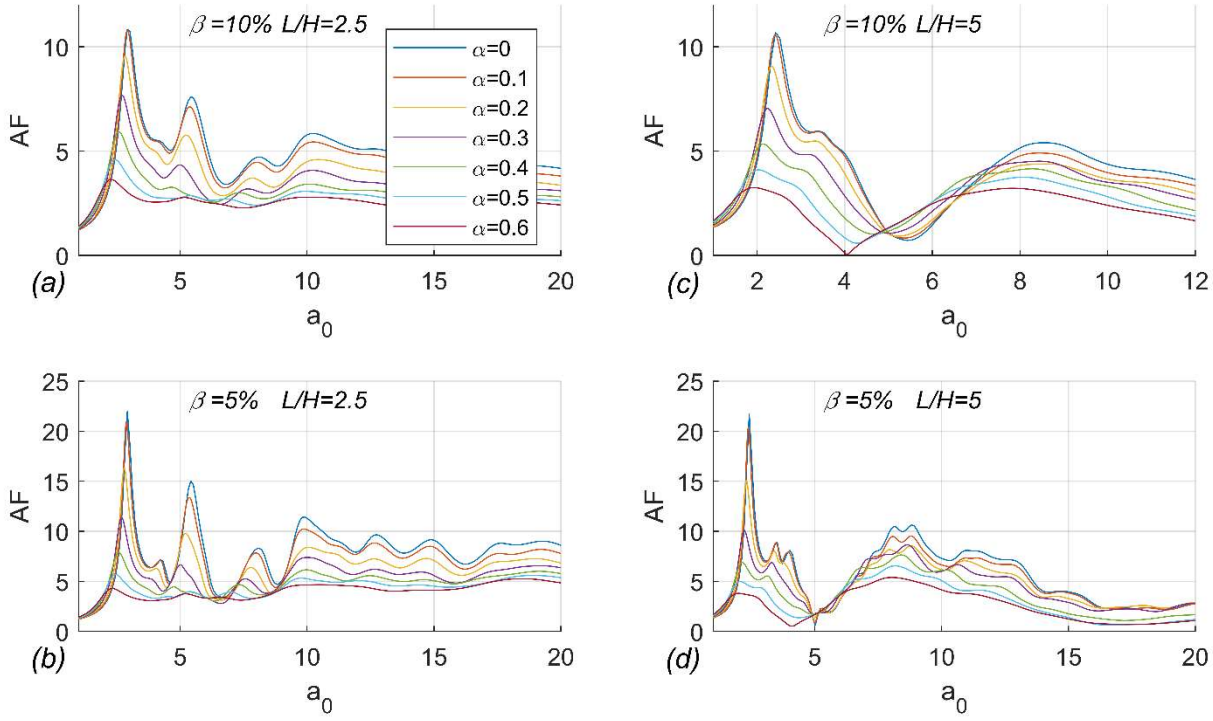

Figure 3-8. Amplification function of an earth dam in a narrow trapezoidal canyon with different α, L/H, and β

For the sake of completeness, the amplification function of an earth dam located in a triangular canyon is presented in Figure 3-9.

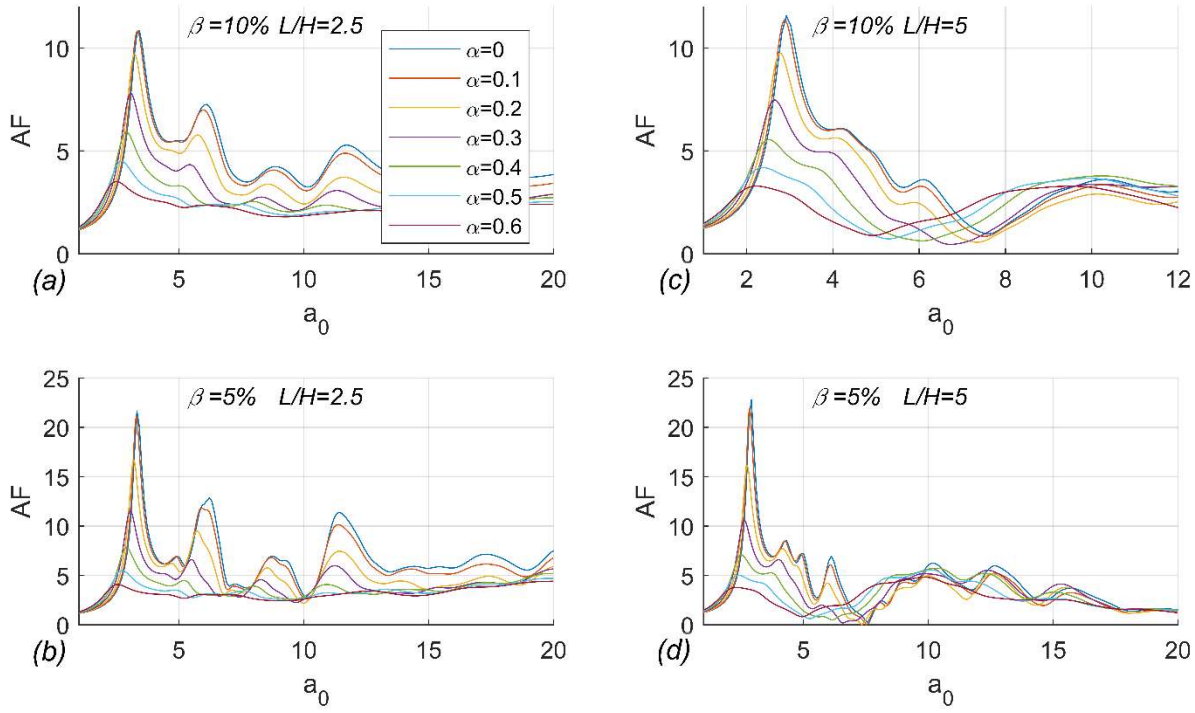

Figure 3-9. Amplification function of an earth dam in a triangular canyon with different values α, L/H and β

Figure 3-10 compares the effect of canyon geometry on the amplification function for canyons of L/H=2.5 associated with β= 10%. The calculated AFs for the rectangular, wide trapezoidal, narrow trapezoidal, and triangular canyons are shown in sequence by (-), (- -), (.-), and (.). Each color corresponds to a specific impedance ratio.

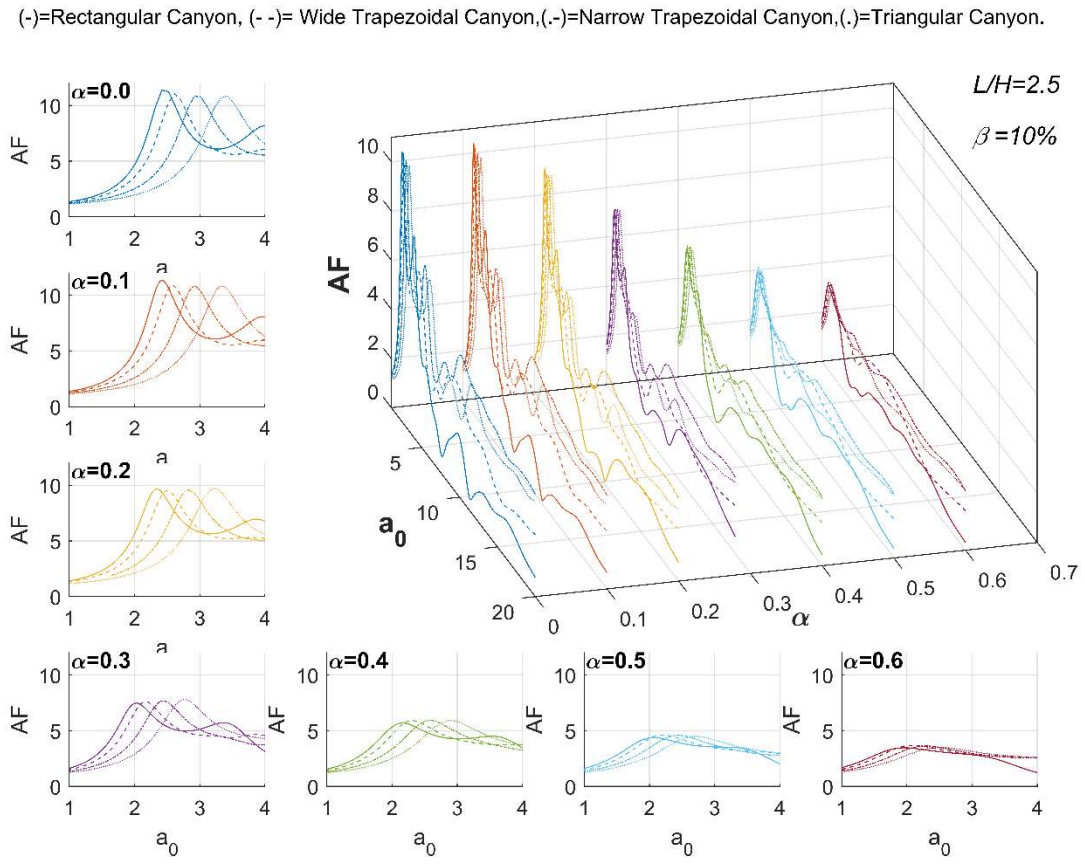

Figure 3-10. Comparison of the effect of canyon geometry on the first amplitude for an earth dam located in a canyon with L/H=2.5 and β=10%

3.7 Application of the calculated amplification functions

The amplification function can be utilized to obtain a wide variety of crest response parameters, including acceleration, velocity, displacement, etc. As mentioned above, the amplification function is the ratio of the amplitude of the crest motion to the amplitude of the canyon motion. By applying the ground vibration as an input for the canyon, the crest response is calculated based on the superposition principle. First, the time history of an earthquake is converted to the frequency domain by a fast Fourier transform. Then, the seismic vibration in the frequency domain is multiplied by the amplification function to obtain the crest response in the frequency domain. Using the inverse Fourier transform for the crest response yields the time domain response. Each earthquake frequency is amplified based on the amplification function.

As an example, the response of an earth dam located in a narrow trapezoidal canyon with L/H=5 is calculated step by step. In this case, the following specifications are considered: H=100, B=200, β=5%, and earth dam shear wave velocity=300 m/s. The S90W El-Centro earthquake (1940) horizontal ground motion is applied in

this example (Figure 3-11(a)), and the Fourier series of the input motion on the canyon is computed (Figure 3-11(b)). Figure 3-11(c) represents the amplification function of the earth dam obtained in the previous section by FEM-SBFEM for α=0.1. The product of each term of the amplification function (Figure 3-11(c)) and the Fourier series of the input motion (Figure 3-11(b)) results in the crest response in the frequency domain (Figure 3-11(d)). Figure 3-11(e) portrays the crest response of the dam in the time domain under the El Centro earthquake.

3.7.1 The El Infiernillo dam

As the last example, a calculated AF is used as an estimate in order to find the crest response of an existing earth dam under an actual earthquake. The El Infiernillo dam is an earth dam on the Balsas River in Mexico. The dam is situated in a high seismicity region in a narrow valley. It has been subjected to several precisely monitored earthquakes [61], [117], [118]. The dam's height and length are 148m and 350m, respectively (Figure 3-12). The material properties of the three sections of the dam are shown in Table 3-1 [117]. These properties include the shear modulus, mass density, and passion ratio. The sections of the dam are made of: (1) compacted rockfill; (2) impervious core; and (3) dumped rockfill (Figure 3-12(a)).

Table 3-1. Material Properties of the El Infiernillo dam

	Material	Shear Modulus (MPa)	Mass Density (Kg/m3)	ν
1)	Compacted Rockfill	682	2100	0.42
2)	Impervious Core	227	2000	0.49
3)	Dumped Rockfill	245	2100	0.38

To be able to use the calculated amplification functions, a simplified model with volume-averaged properties was used, and it is assumed that the dam is homogenous. Therefore, the average shear modulus and mass density are respectively estimated as 404 MPa and 2100 kg/m^3. The canyon is simplified as a narrow trapezoidal canyon with L/H=2.5.

The impedance ratio and damping ratio are chosen respectively α=0.3 and β=8% [61]. Two earthquakes shook the dam in the year 1966, and the earthquake motions were recorded at two stations, one at the dam crest and one near the base. The ratio of the crest response to the base response is defined as the response spectra ratio. Similar to the site effect in soil deposits, the response spectra ratio can be used as an estimation for the steady-state AF [61].

Figure 3-13 shows the response spectra recorded by the accelerograms at the canyon during the 1966 events. There is a reasonable agreement between the AF obtained by FEM-SBFEM (dash-dot-dot line line) and the response spectra (dash-dot line and dot line) recorded at the crest. The solid line shows the results of FEM-

SBFEM for β=10%, which have a smaller discrepancy with the recorded data for the maximum amplitude in comparison with the results for β=8%.

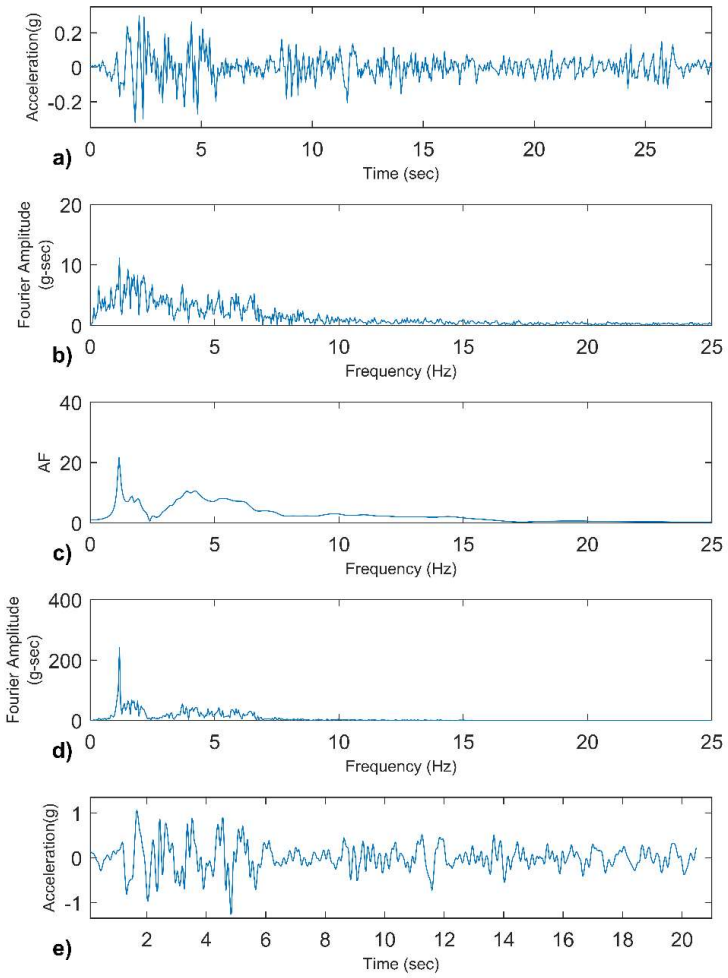

Figure 3-11. Different steps to obtain the crest response due to an earthquake: a) The S90W El-Centro earthquake (1940) horizontal ground motion; b) Fourier amplitude spectrum of the earthquake; c) The transfer function obtained by FEM-SBFEM for α=0.1 and L/H=5; d) product of the amplification function (c) and the Fourier series of the input motion (b); e) time history of the crest under the earthquake obtained by inverting the Fourier series from (d)

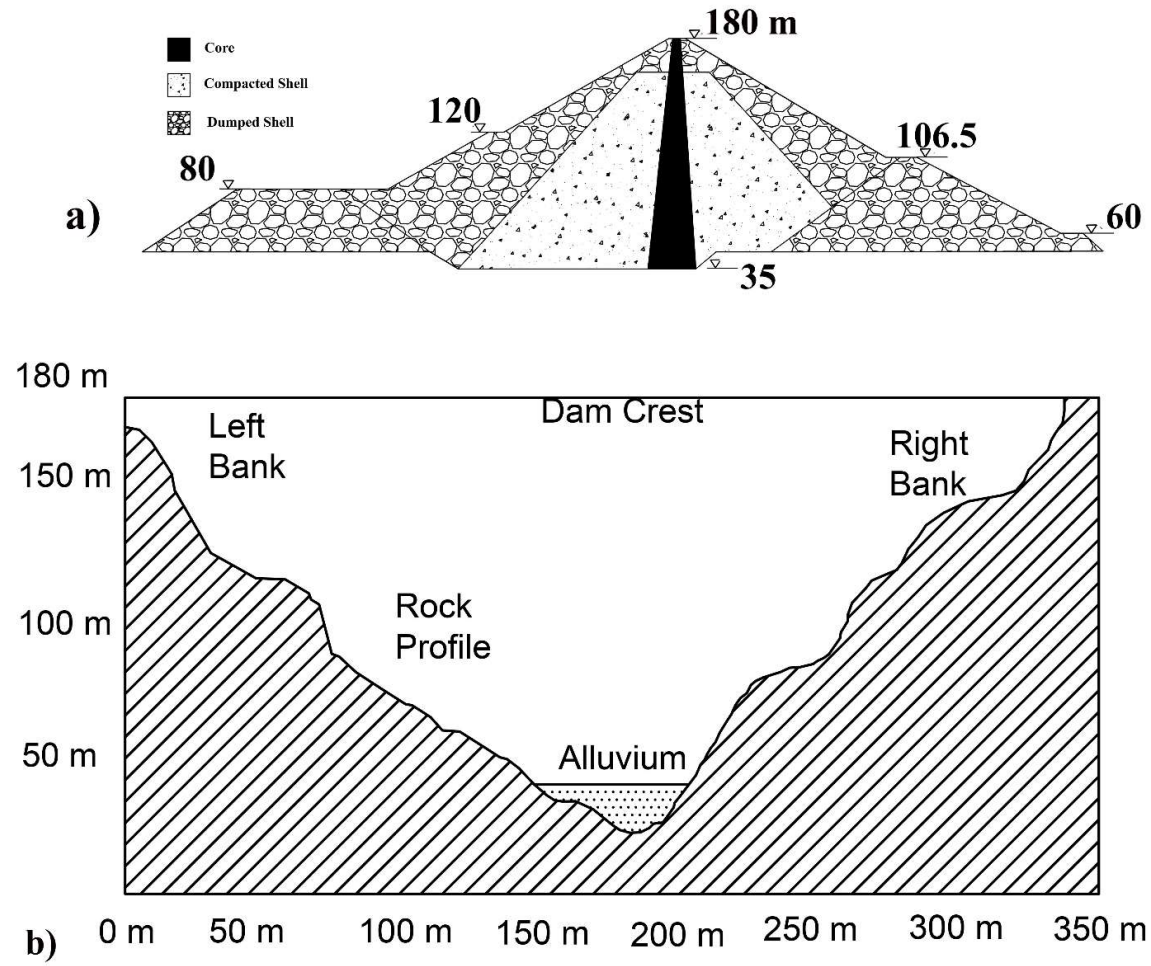

Figure 3-12. El Infiernillo dam: (a) maximum cross section; (b) geological profile [117]

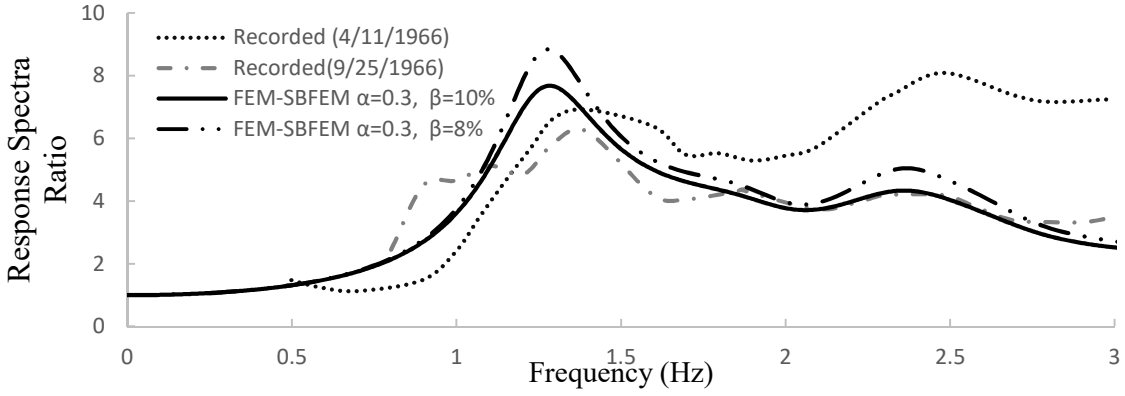

Figure 3-13. Response Spectra of El Infiernillo rockfill dam due to two earthquakes during the year 1966

3.8 Conclusion

This work introduced the 3D FEM-SBFEM equation in order to investigate the seismic responses of earth dams. FEM represents the earth dam domain, while SBFEM models unbounded canyon domains. The hybrid technique

was validated through a benchmark example and available 2D results. A comprehensive study was done in order to seek the flexibility and geometry effects of canyons, and 112 3D models were created corresponding to 2 different material damping ratios, 2 different canyon lengths, 7 different impedance ratios, and 4 canyon geometry shapes. Dam crest acceleration due to an actual earthquake was obtained using a fast Fourier transform. The recorded response spectra of the El Infiernillo dam under the 1966 earthquakes were utilized for comparison with a proposed amplification function, and a reasonable agreement was seen between the recorded data and the FEM-SBFEM results.

.

3.9 Acknowledgments

This work was supported by the Natural Sciences and Engineering Research Council of Canada (NSERC) through Grant No. PCIPJ 395213-3 and the Hydro-Québec Industrial Research Chair for the lifecycle optimization of embankment dams. The authors also thank their industrial partners Hydro-Québec, Hatch, SNC-Lavalin, WSP, Qualitas, Golder Associates, Klohn Crippen Berger, and ConeTec. All calculations were carried out on the Niagara High-Performance Computing (HPC) cluster under the administration of Compute Canada.

Chapter 4 Shear Strain Dependent Amplification Function of Earth Dam-Flexible Canyon system by the Hybrid FEM-SBFEM Technique

4.1 . Résumé

La méthode linéaire équivalente (EQL) a été implémentée dans la FEM. La technique FEM-SBFEM a été étendue pour prendre en compte l'effet du comportement non linéaire des barrages en terre. Il a été observé que le comportement non linéaire affecte grandement la fréquence naturelle de résonnance, la fonction d'amplification et l'accélération de crête maximale d'un barrage en terre situé dans un canyon. Les effets de la géométrie et de la flexibilité du canyon sur le comportement non linéaire ont aussi été examinés. En augmentant la flexibilité du canyon, il a été montré que l'effet de la non-linéarité diminuait. Le barrage d'El Infiernillo a été modélisé par FEM-SBFEM non linéaire 3D, et une comparaison de la fonction d'amplification de crête obtenue par la méthode proposée avec les données enregistrées montre la précision de la méthode FEM-SBFEM non linéaire.

4.2 Abstract

The finite element method (FEM) is a powerful tool for the nonlinear modeling of dynamic problems. In the present work, the equivalent linear method (EQL) has been implemented into the FEM. For stratifying the radiation damping condition and rigorously modeling canyon as an elastic unbounded domain, the scaled boundary finite element method (SBFEM) was utilized. The FEM-SBFEM technique, wherein FEM is coupled with SBFEM, has been extended to take into consideration the effect of earth dam nonlinear behavior. It was observed that the nonlinear behavior greatly affects the natural frequency, the amplification function, and peak crest acceleration of the earth dam located in canyons. The effects of canyon geometry and flexibility on the nonlinear behavior were examined, and it was seen that by increasing the flexibility of the canyon, the effect of nonlinearity was decreased. The El Infiernillo dam was modeled by 3D nonlinear FEM-SBFEM, and comparison of the crest amplification function obtained by the proposed method with the recorded data shows the accuracy of the nonlinear FEM-SBFEM.

4.3 Introduction

The dynamic response of an earth dam is highly affected by the shape, geometry, and flexibility of a canyon, and an earth dam-flexible canyon system may amplify or deamplify the canyon's seismic acceleration. The crest amplification is represented by a frequency-dependent amplification function, and the first peak in the amplification function corresponds to the natural frequency.

Generally, dams located in narrow canyons show a stiffer behavior than dams in wider canyons. This stiffening effect leads to smaller natural periods [119]. Mejia and Seed [120] compared the natural frequencies of 2D and 3D dams in triangular and rectangular canyons, and it was concluded that by decreasing the length to height ratio, the 3D natural frequency is increased in comparison with the 2D natural frequency. For a triangular dam with a length to height ratio of one, the 3D natural frequency is 2.5 times higher than for a 2D dam. Dakoulas and Gazetas [65] studied more canyon geometries. For the lower value of the length to height ratio, the fundamental period of a dam in a narrow canyon was obtained a fifth of the corresponding value for the dam in a wide canyon. It was also shown that the amplification function is greatly affected by the geometry of the canyon, and that the amplification function in narrow canyons is higher than for dams in wide canyons.

The amplification function of a dam located in a flexible semi-cylindrical canyon was calculated, and it was shown by Dakoulas and Gazetas [65] that by increasing the flexibility of the canyon, the amplification function is decreased. Papalou and Bielak [66] modeled earth dams and canyons by the shear beam method and FEM, respectively, and it was concluded that by reducing the canyon stiffness, the acceleration response of the dam decreases. Touhei and Ohmachi [103] utilized the 2D FEM-BEM hybrid technique to investigate the effects of foundation flexibility on the crest response. Abouseeda and Dakoulas [121] studied the seismic behavior of earth dams with a flexible foundation by the 2D FEM-BEM method, and the amplification functions of earth dams under earthquakes with different peak accelerations were compared.

In the linear analysis, the shear modulus and damping ratio are used with the assumption of low strain ($\gamma_{eff} < 10^{-6}$). The amplification function, natural frequency, and time-domain response are calculated with this assumption. Under severe earthquakes, some parts of earth dams exhibit nonlinear behavior. Idriss and Seed [71] introduced the equivalent linear method (EQL) to take into consideration the effect of soil nonlinearity during strong earthquakes, and SHAKE [72] and FLUSH [73], which incorporate EQL, have been widely used in practical problems in geotechnical earthquake engineering. Abdel-Ghaffar and Scott [74] developed EQL to analyze the Santa Felicia earth dam which was subjected to two strong earthquakes. Choudhury and Savoikar [75] carried out 1D equivalent-linear analysis utilizing the DEEPSOIL software in order to model municipal solid waste landfills under earthquake loadings, while Mejia et al. [76] showed that the natural frequencies of earth dams modeled by the equivalent linear FEM vary with the intensity of the input motions. Cascone and Rampello

[77] performed a seismic analysis of earth dams by the decoupled displacement analysis and the nonlinear behavior was incorporated by the EQL.

The scaled boundary finite element method (SBFEM) is a semi-analytical fundamental solution-less boundary element method introduced by Song and Wolf [52],[36]. It combines the advantages of FEM and BEM while it avoids their shortcomings. The unbounded domain has been modeled by SBFEM to satisfy the radiation damping condition, and it has been widely used in different dynamic problems: dam-reservoir interaction analysis [46], [122]–[125], moving loads [43], [51], [91], pile-soil interaction [45], concrete dam-foundation interaction [113], and earth dam-canyon interaction [29],[30].

FEM is a powerful tool for the nonlinear modeling of dynamic problems. In the present work, the EQL has been implemented into the FEM. For stratifying the radiation damping condition and rigorously modeling a canyon as an unbounded domain, FEM has been coupled with SBFEM. The FEM-SBFEM technique has been extended to take into consideration the effect of earth dams' nonlinear behavior. The canyon is modeled by SBFEM to study the effect of flexibility and geometry of the canyon, and how nonlinear behavior affects the natural frequency, amplification function, and peak crest acceleration of earth dam located in canyons with different material and geometry conditions has been examined.

4.4 Formulation

Figure 4.1 illustrates an earth dam-canyon interaction system. The substructure method is utilized in which the domain is divided into two subdomains: a bounded domain (ΩF) and an unbounded domain (Ωs). The subscripts F and S denote the finite element method (FEM) and the scaled boundary finite element method (SBFEM) respectively. It is assumed that the canyon has a linear elastic behavior and that under severe loadings, the dam experiences nonlinearity in its material behavior. Therefore, the earth dam is modeled by FEM and the canyon by SBFEM. Coupling of FEM and SBFEM is done on the interface Γ^i. The earth dam mesh nodes and canyon meshes not contacted by the earth dam are shown by domains Γ^e and Γ^c, respectively. To quantitatively examine the effect of an elastic canyon, the impedance ratio is defined as $\alpha = \frac{{V_e}^1}{V_c}$, where ${V_e}^1$ and V_c are the shear wave velocities of the earth, for the initial shear modulus, and the canyon, respectively.

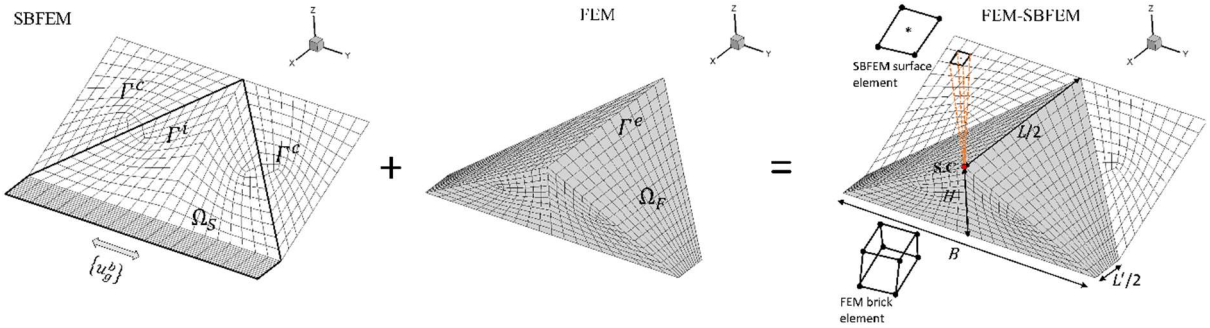

Figure 4-1. a symmetric earth dam-canyon interaction system

4.4.1 FEM formulation

The equation of motion for an earth dam is expressed by the dynamic stiffness matrix $[S^F(\omega)]$, the displacement vector$\{u(\omega)\}$, and load vector $\{P(\omega)\}$ as:

$$[S^F(\omega)]^j\{u(\omega)\} = \{P(\omega)\} \tag{4-1}$$

where ω is the frequency. $[S^F]$ is decomposed into two parts, Γ^i and Γ^e:

$$[S^F]^j = \begin{bmatrix} [S^F_{ee}] & [S^F_{ei}] \\ [S^F_{ie}] & [S^F_{ii}] \end{bmatrix}^j = [K^F]^j(1 + 2i\beta^j) - \omega^2[M^F] \tag{4-2}$$

where $[M^F]$ and $[K^F]^j$ are the mass and stiffness matrices, respectively, and β^j is the material hysteretic damping ratio. The coefficient matrices are obtained by the classical FEM equation for each element, and assembling them results in $[S^F]^j$. The superscript j shows the iteration number in the nonlinear analysis that will be discussed in detail in section 1.4.

4.4.2 SBFEM formulation

The SBFEM equation in displacement for 3D problems in the time domain is expressed as [126]:

$$\begin{aligned}[E^0]\xi^2\{u\,(\xi,t)\}_{,\xi\xi} + (2[E^0] - [E^1] + [E^1]^T)\xi\{u\,(\xi,t)\}_{,\xi} \\ + ([E^1]^T - [E^2])\{u(\xi,t)\} - [M^0]\,\xi^2\{\ddot{u}(\xi,t)\} + \{F(\xi)\} = 0\end{aligned} \tag{4-3}$$

where $[E^0]$, $[E^1]$, $[E^2]$, and $[M^0]$ are coefficient matrices and ξ is the dimensionless radial coordinate. Analogous to FEM, the coefficient matrices are achieved by assembling the coefficient matrices of each element [36]. Applying the harmonic excitation $u\,(\xi,t) = u\,(\xi)e^{i\omega t}$ in Equation (4-1) results in:

$$\begin{aligned}[E^0]\xi^2\{u\,(\xi)\}_{,\xi\xi} + (2[E^0] - [E^1] + [E^1]^T)\xi\{u\,(\xi)\}_{,\xi} + ([E^1]^T - [E^2])\{u(\xi)\} \\ + \omega^2[M^0]\,\xi^2\{u(\xi)\} + \{F(\xi)\} = 0\end{aligned} \tag{4-4}$$

which represents the SBFEM equation in displacement for the frequency domain. The boundary tractions are defined as equivalent boundary nodal forces:

$$\{R(\xi)\} = \xi^2[E^0]\{u(\xi)\}_{,\xi} + \xi[E^1]^T\{u(\xi)\} \tag{4-5}$$

The amplitudes of the nodal displacement and those of the force are related as:

$$\{R(\xi)\} = [S^S(\omega)]\{u(\xi)\} \tag{4-6}$$

where $[S^S(\omega)]$ is the dynamic stiffness matrix of an unbounded domain. Substituting Equations (4-5) and (4-6) in Equation (4-4) leads to:

$$([S^S(\omega)] + [E^1])[E^0]^{-1}(+[S^S(\omega)] + [E^1]^T) - ([E^2]) - \omega[S^S(\omega)]_{,\omega} + \omega^2[M^0]\xi^2 = 0 \tag{4-7}$$

The Runge-Kutta scheme is utilized for the numerical solution of Equation (4-7), which is a non-linear 1st-order ODEs with an independent variable of ω. Asymptotic expansion of the unbounded dynamic-stiffness matrix provides an initial condition for the numerical solution [126]. The asymptotic expansion is obtained for a high (but finite) value of ω_h.

$$\left[S^S(\omega_h)\right] = [K^S] + i\omega_h[C^S] + \sum_{i=1}^{m}[A^i](i\omega_h)^{-1} \tag{4-8}$$

where $[C^S]$, $[K^S]$ and $[A^i]$ are the coefficient matrices [52].

4.4.3 Coupled FEM-SBFEM formulation

Equation (4-1) is decomposed into two domains, $\Gamma^c$and Γ^i, as:

$$\begin{bmatrix}[S^F_{ee}] & [S^F_{ei}]\\ [S^F_{ie}] & [S^F_{ii}]\end{bmatrix}^j \begin{Bmatrix}\{u_e\}\\ \{u_i\}\end{Bmatrix} = \begin{Bmatrix}\{P_e\}\\ \{P_i\}\end{Bmatrix} \tag{4-9}$$

Equation (4-6), the interaction force, for the interface nodes (Γ^i) is rewritten for the decomposed unbounded stiffness matrix as:

$$\begin{Bmatrix}R_i(\omega)\\ R_C(\omega)\end{Bmatrix} = \begin{bmatrix}[S^S_{ii}] & [S^S_{ci}]\\ [S^S_{ic}] & [S^S_{cc}]\end{bmatrix}\begin{Bmatrix}\{u^t_i(\omega)\} - \{u^g_i(\omega)\}\\ \{u^t_c(\omega)\} - \{u^g_c(\omega)\}\end{Bmatrix} \tag{4-10}$$

where the subscripts *t* and *g* show the total and the ground system, respectively. The displacement vector represents the relative motion. $\{u^g(\omega)\}$ is the seismic excitation input motion acting on all nodes of the canyon, $\Gamma^c$and Γ^i (Figure *4-1*). By substituting $\{R_i(\omega)\}$ for $\{P_i\}$ in Equation (3-6), it is then formulated as:

which is the algebraic equations of motion amplitudes in the frequency under seismic excitation domain for earth

$$\begin{bmatrix} [S_{ee}^F]^j & [S_{ei}^F]^j & 0 \\ [S_{ie}^F]^j & [S_{ii}^F]^j + [S_{ii}^S] & [S_{ci}^S] \\ 0 & [S_{ic}^S] & [S_{cc}^S] \end{bmatrix} \begin{Bmatrix} \{u_e^t\} \\ \{u_i^t\} \\ \{u_c^t\} \end{Bmatrix} = \begin{Bmatrix} 0 \\ [S_{ii}^S]\{u_i^g(\omega)\} + [S_{ci}^S]\{u_c^g(\omega)\} \\ [S_{ic}^S]\{u_i^g(\omega)\} + [S_{cc}^S]\{u_c^g(\omega)\} \end{Bmatrix} \quad (4\text{-}11)$$

dam-unbounded canyon system.

4.4.4 Amplification function

The amplification function (AF), or the transfer function, is defined as a system's ratio of output to input. For the earth dam-canyon system, the AF is obtained by setting $\{u^g(\omega)\}$ as equal to 1. The crest displacement is considered as the crest amplification function. The AF can be utilized to obtain other response types, including acceleration and velocity. Benefiting from the amplification function, the response of a linear elastic earth dam-canyon system to any load combination is achieved by multiplying the AF with the load combination. The amplification functions also expresses how the input canyon motion is amplified or de-amplified for each frequency. If $\{u^g(\omega)\} = 1$ in Equation (4-11), it is rewritten as:

$$\begin{bmatrix} [S_{ee}^F]^j & [S_{ei}^F]^j & 0 \\ [S_{ie}^F]^j & [S_{ii}^F]^j + [S_{ii}^S] & [S_{ci}^S] \\ 0 & [S_{ic}^S] & [S_{cc}^S] \end{bmatrix} \begin{Bmatrix} \{AF_e^t\} \\ \{AF_i^t\} \\ \{AF_c^t\} \end{Bmatrix} = \begin{Bmatrix} 0 \\ [S_{ii}^S] + [S_{ci}^S] \\ [S_{ic}^S] + [S_{cc}^S] \end{Bmatrix} \quad (4\text{-}12)$$

Solving equation (4-12) will result in the amplification functions. By multiplying the amplification function of the desired points (crest for instance) by the Fourier amplitude spectrum of a seismic event, the response of the dam is computed:

$$\{\ddot{u}^{crest}(\omega)\} = \{AF(\omega)\}\{\ddot{u}^g(\omega)\} \quad (4\text{-}13)$$

The inverse Fourier transform is used to obtain the corresponding response in the time domain:

$$\{\ddot{u}^{crest}(t)\} = IFFT(\{\ddot{u}^{crest}(\omega)\}) \quad (4\text{-}14)$$

4.4.5 Equivalent linear analysis

Under severe seismic events, some parts of an earth dam experience large strains that cause nonlinear behavior. The equivalent linear method is used to take the nonlinear effect into account. Figure *4-2* depicts the different steps in the proposed methodology. First, with the assumption of small strain, $\gamma_{eff} < 10^{-6}$, the shear modules G^1 and damping ratio β^1 are selected for each FEM element. The superscripts refer to the iteration number. $[S^F(\omega)]^1$ and $[S^S(\omega)]$ are calculated for the earth dam and the canyon, respectively. The

unit displacement, $\{u^g(\omega)\} = 1$, is applied on the canyon nodes. The maximum shear strain ($\gamma(\omega)_{max}$) for each element for each frequency is evaluated. Transferring the strain into the time domain and obtaining the maximum strain will be time-consuming. The maximum shear strain in the time domain is obtained by the root mean square of the maximum strain in the frequency domain as:

$$\gamma(t)_{max} = C * RMS(\gamma(\omega)_{max}) \tag{4-15}$$

where the constant C can be estimated by:

$$C = max|\{\ddot{u}^g(t)\}|/RMS(\{\ddot{u}^g(\omega)\}) \tag{4-16}$$

in which $\{\ddot{u}^g(t)\}$ and $\{\ddot{u}^g(\omega)\}$ are the input seismic acceleration excitations on the canyon in the time and frequency domains, respectively. The effective shear strain is estimated by:

$$\gamma(t)_{eff} = 0.65 * \gamma(t)_{max} \tag{4-17}$$

where 0.65, which is the strain ratio, is an empirical value [73]. As the modulus reduction curve (Figure 4-3) is obtained in the laboratory loading conditions, which are more severe than actual earthquake loading conditions, $\gamma(t)_{max}$ is multiplied by 0.65. The estimated shear strain $\gamma(t)_{eff}$ is used to obtain the corresponding shear modulus G^2 and damping ratio β^2 from Figure 4-3. The second iteration is done similarly. The results usually converge to the desired accuracy after 3 iterations.

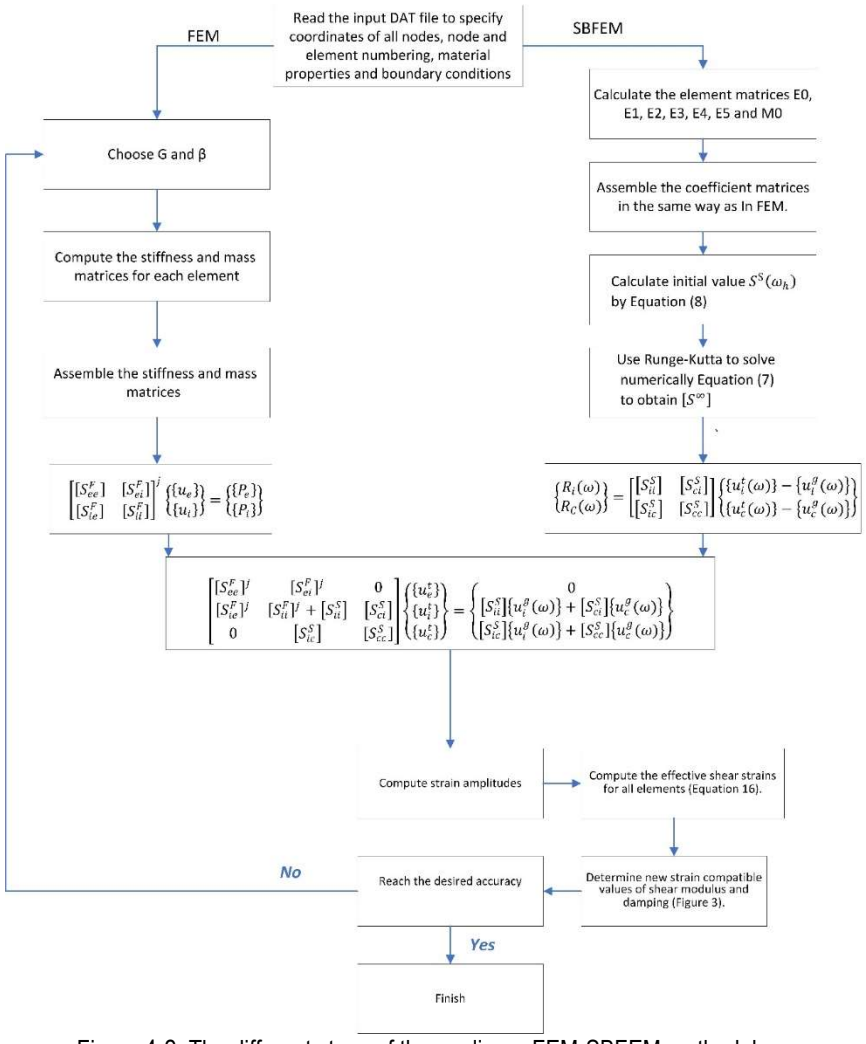

Figure 4-2. The different steps of the nonlinear FEM-SBFEM methodology

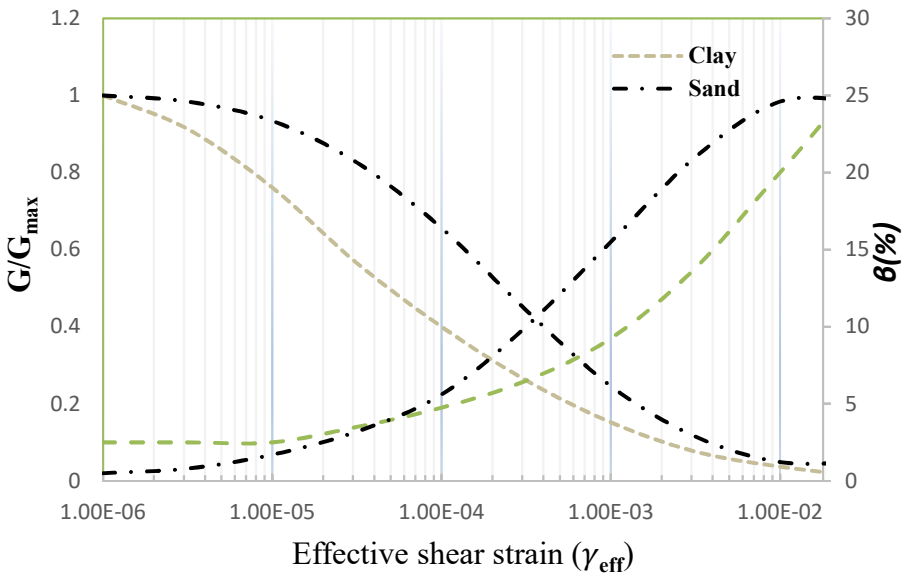

Figure 4-3. Strain-Compatible Soil Properties [71]

4.5 Numerical examples and discussion

It is of interest to first validate the coupled hybrid technique and then validate the 3D modelling. It should be noted that the FEM-SBFEM has already been validated by authors with several examples in [114]; however, for the sake of completeness, the example of a rigid foundation on an half-space is reviewed here. More details can be found in the mentioned article. A comparison of the FEM-SBFEM with results available in the literature for different loading conditions shows that the methodology is correctly implemented in this work (Figure 4-4).

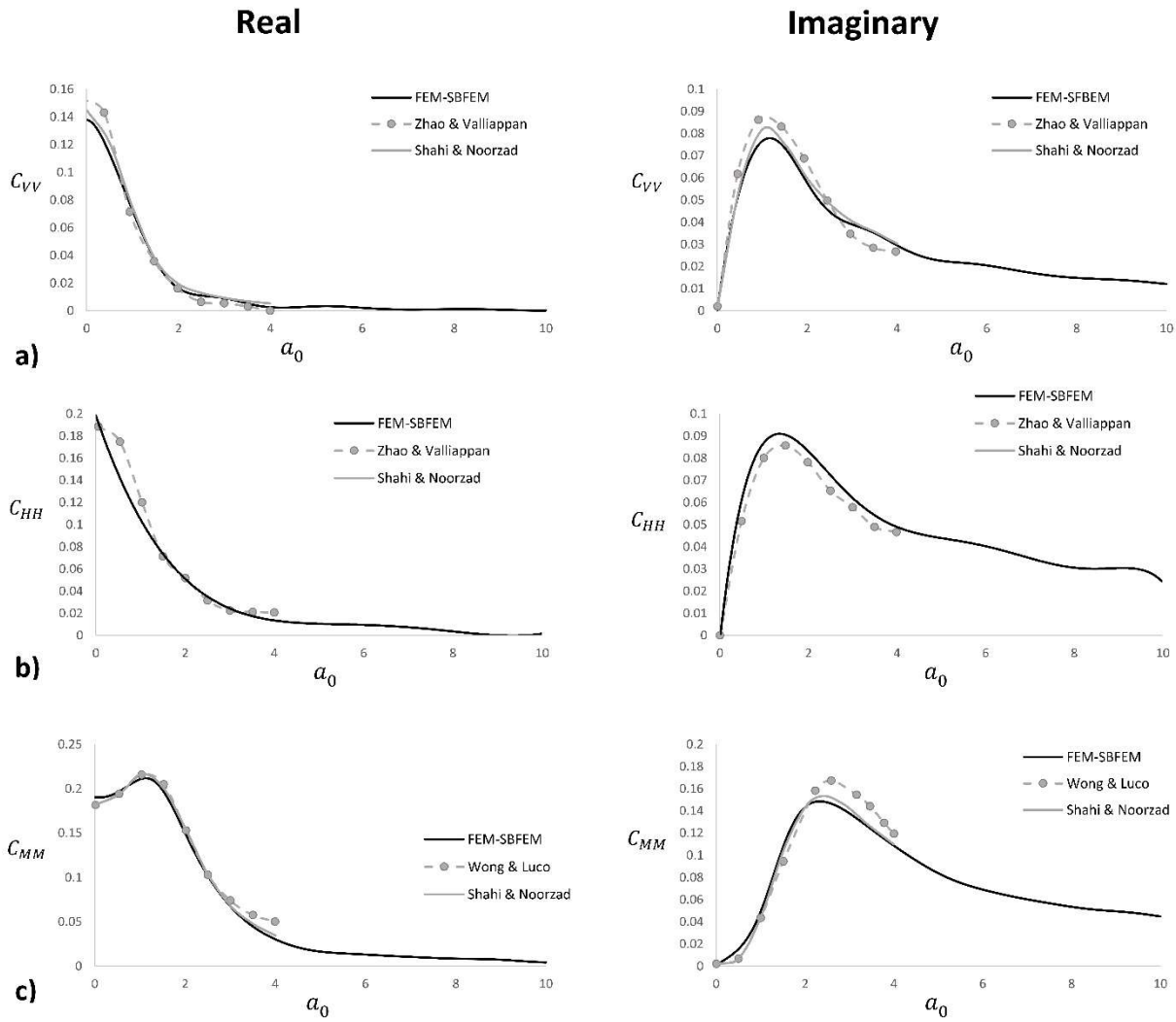

Figure 4-4. (a) Vertical compliance; (b) Horizontal compliance and; (c) Rocking compliance of a rigid square

Several examples were analyzed to consider the effect of nonlinear earth dam behavior in different canyon conditions. Three canyon geometry shapes, including triangular, trapezoidal, and a rectangular canyon with L/H=2.5 and 5, were modeled. The values of the impedance ratio were chosen as α=0.1, 0.3, and 0.5. Material damping was selected as β=10%.

For $\gamma(t)_{eff} > 10^{-6}$, with increasing the effective shear strain, shear modulus, and damping ratio are decreased. For high-intensity excitation, the earth dam shows nonlinear behavior. Against the linear elastic analysis of an earth dam in which the response can be nondimensionalized, for the nonlinear analysis, the actual values of the parameters should be utilized. In the linear analysis, the stiffness matrix is independent of the loading condition, while in the nonlinear analysis, the stiffness matrix changes with the shear strain level.

The earth dam is a homogenous dam with an initial shear wave velocity of $V_e{}^1 = 300m/s$, Poisson ratio of υ=0.25, H=100m, and B=200m. The El Centro record for the 1940 Imperial Valley Earthquake is applied to the canyon domain, and the coefficient C (Equation (4-16)) for the El Centro record is obtained as 0.067. First, the amplification function for the different canyon geometries and material properties is obtained. It should be noted that the nonlinear AF is corresponding with the loading condition.

4.6 The results and discussion

The analysis is begun with the assumption of $\gamma_{eff} < 10^{-6}$. The initial shear wave velocity and dam ratio are chosen. The effective shear strain obtained for each element is obtained, and the shear modulus and damping ratio are updated according to the shear strain level. Figure 4-5 represents a) the effective shear strain, and b) G/G_{max} ratio for the earth dam located in the rectangular canyon with L/H=2.5. Figure 4-6-Figure 4-8 show the AF obtained by FEM-SBFEM. The bullet points indicate the values of the first natural frequencies and $AF_{max.}$ The non-dimensional natural frequency is defined as $a_0=\omega H/V_e{}^1$. The blue and red lines show the nonlinear and linear AF values, respectively.

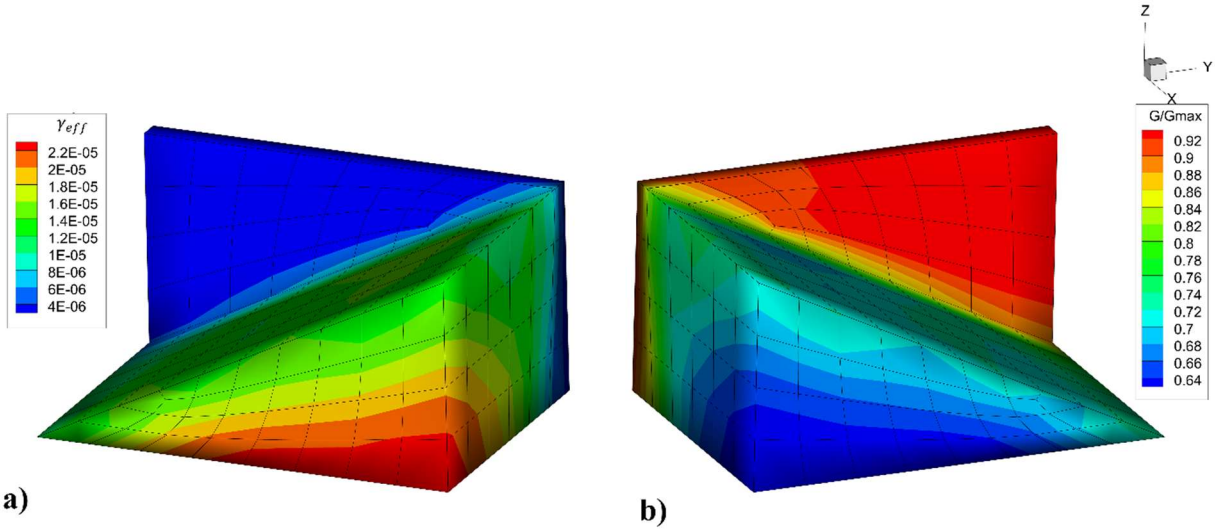

Figure 4-5. a) the effective shear strain, b) G/Gmax ratio for the earth dam located in the rectangular canyon with L/H=2.5

Generally speaking, by increasing the strain levels, the shear modulus decreases and the damping ratio increases. This leads to decreasing the natural periods and increasing the AF_{max} (Figure 4-6-Figure 4-8).

Figure 4-6 compares the linear and nonlinear AF for the earth dam located in the triangular canyon with L/H= 2.5 and 5. The AF_{max} values for the relatively stiff canyon with linear analyses are 10.8 and 11.3 for L/H=2.5 and 5 respectively (Figure 4-6(a), (d)). The corresponding values for the nonlinear analysis are obtained as 28.8 and 33.6, which shows a 167% increase for L/H=2.5 and 197% for L/H=5 (Table 4-1). By increasing the impedance

ratio value (α), the effect of nonlinearity is decreased. Earth dams with relatively stiff canyons show a higher level of nonlinearity. For the earth dam located in a wide triangular canyon(L/H=5) with a relatively flexible material (α=0.5), the AF_{max} are 7.12 and 4.19 for the nonlinear and linear analyses, respectively (Figure 4-6(f)). This shows a 70% increase, which is remarkably lower than the corresponding percentage of the relatively stiff canyon (α=0.1), which is obtained as 197%. Comparing the linear and nonlinear AFs for different canyon conditions (Figure 4-6-Figure 4-8) proves that the presence of the flexible canyon acts as a radiation damping which significantly decreases the dynamic response. Increasing the impedance ratio value, representing the radiation damping, leads to increasing the dissipated energy into infinity. It is observed that this effect is more important in the nonlinear analysis. For example, for the rectangular canyon with L/H=2.5 (Figure 4-8(a), (b)), the linear AF_{max} values are 11.22 and 7.48 for α=0.1 and 0.3, respectively, while corresponding values for the nonlinear AF_{max} values are 28.4 and 16.7 respectively. The nonlinear analysis shows a 70% increase, while the percentage is 40% for the linear analysis.

Natural frequency is the other factor that is affected by the nonlinearity effect. The first peak of the amplification function of the dam crest is defined as the fundamental natural frequency. Table 4-1 quantitively compares the calculated linear and nonlinear normalized natural frequencies, and it is observed that the nonlinear natural periods have lower values in comparison with the corresponding linear values. The nonlinearity effect is more important in relatively stiff canyons (α=0.1). For the earth dam located in a trapezoidal canyon with L/H=5, the natural periods a_0 of linear and nonlinear FEM-SBFEM are obtained as 2.46 and 1.64 respectively (Figure 4-7(d)), which shows a 33% decrease. Similar to the linear natural frequencies, the nonlinear natural frequencies of relatively wide canyons (L/H=5) show lower values than the corresponding values for relatively narrow canyons (L/H=2.5) for the same geometric shapes. By increasing the impedance ratio value, the nonlinear natural frequency value is decreased. The nonlinear natural frequency is also affected by the canyons' shapes. Earth dams located in rectangular canyons have higher nonlinear natural frequency and Earth dams in triangular canyons have a lower nonlinear natural frequency.

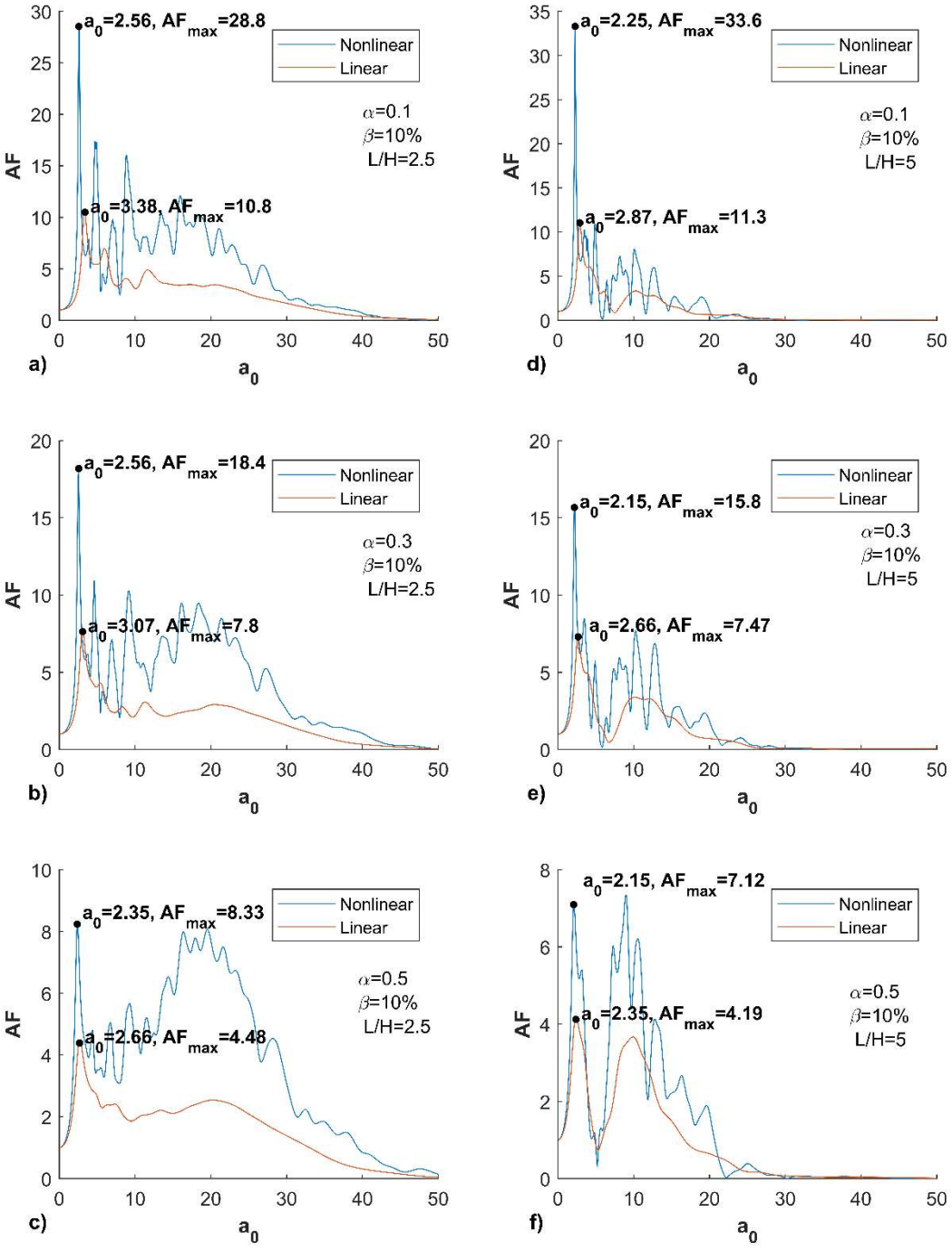

Figure 4-6. Nonlinear and linear amplification functions of earth dams in triangular canyons with different values of α and L/H

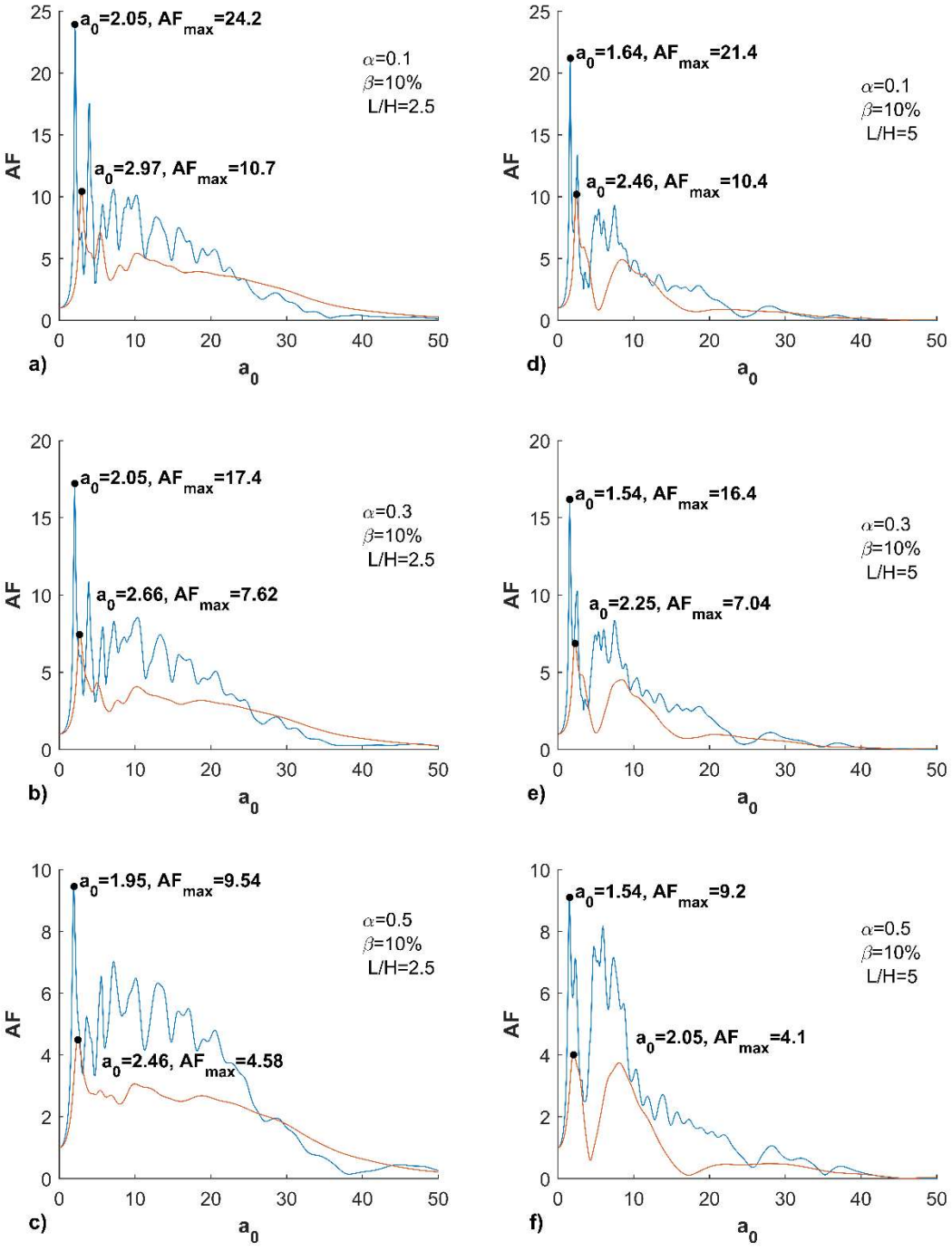

Figure 4-7. Nonlinear and linear amplification functions of the earth dams in trapezoidal canyons with different values of α and L/H

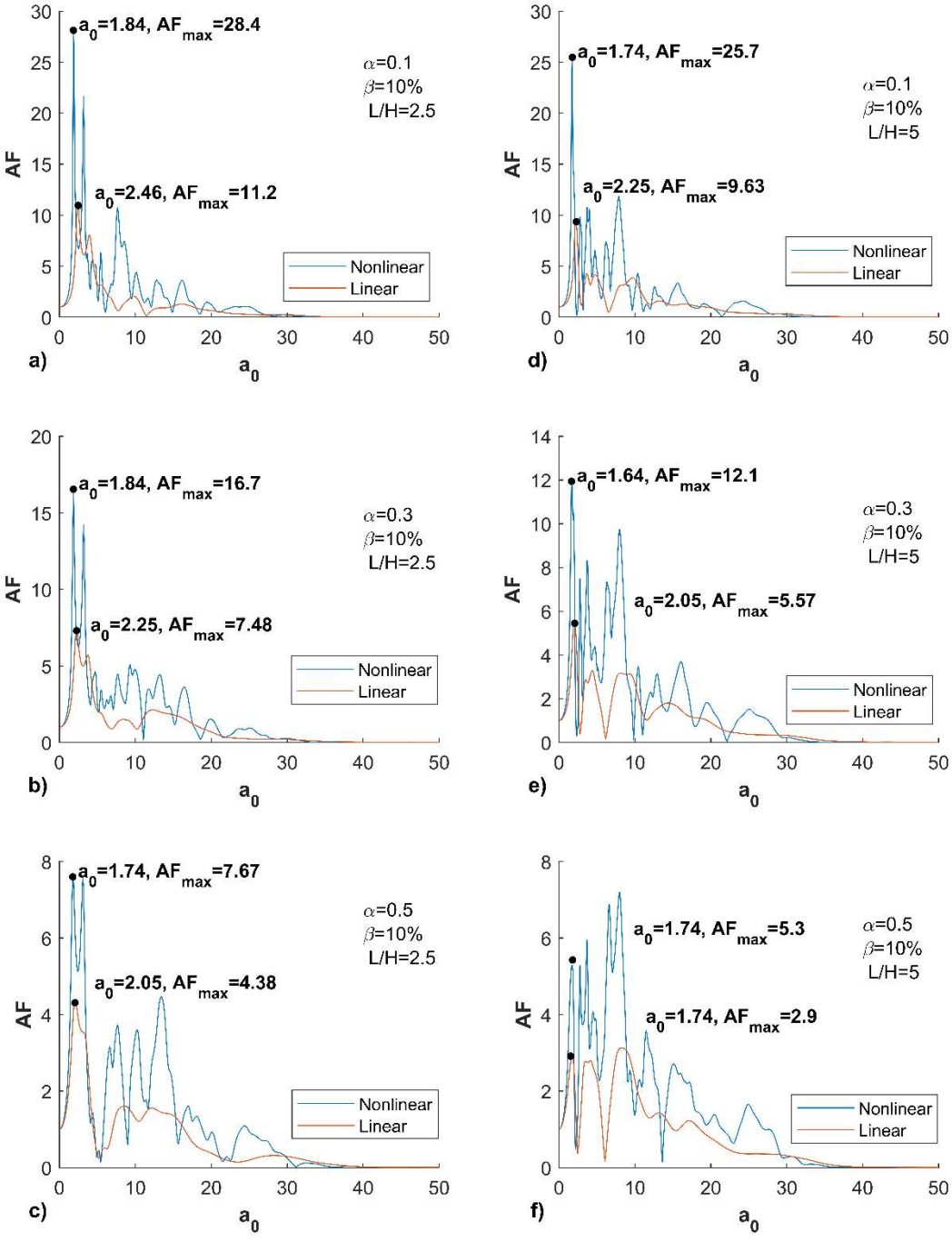

Figure 4-8. Nonlinear and linear amplification functions of the earth dams in rectangular canyons with different values of α and L/H

Table 4-1. The linear and nonlinear natural frequency and AF_{max} calculated by FEM-SBFEM

		L/H=2.5					
		Linear		Nonlinear		% Change	
	α	$a_{0\,max}$	AF_{max}	$a_{0\,max}$	AF_{max}	$a_{0\,max}$	AF_{max}
Rectangular	0.1	2.46	11.2	1.84	28.4	-25	154
	0.3	2.25	7.48	1.84	16.7	-18	123
	0.5	2.05	4.38	1.74	7.67	-15	75
Trapezoidal	0.1	2.97	10.7	2.05	24.2	-31	126
	0.3	2.66	7.62	2.05	17.4	-23	128
	0.5	2.46	4.58	1.95	9.2	-21	101
Triangular	0.1	3.38	10.8	2.56	28.8	-24	167
	0.3	3.07	7.8	2.56	18.4	-17	136
	0.5	2.66	4.48	2.35	8.33	-12	86
		L/H=5					
		Linear		Nonlinear		% Change	
	α	$a_{0\,max}$	AF_{max}	$a_{0\,max}$	AF_{max}	$a_{0\,max}$	AF_{max}
Rectangular	0.1	2.25	9.63	1.74	25.7	-23	167
	0.3	2.05	5.57	1.64	12.1	-20	117
	0.5	1.74	2.9	1.74	5.3	0	83
Trapezoidal	0.1	2.46	10.4	1.64	21.4	-33	106
	0.3	2.25	7.04	1.54	16.4	-32	133
	0.5	2.05	4.1	1.54	9.2	-25	124
Triangular	0.1	2.87	11.3	2.25	33.6	-22	197
	0.3	2.66	7.47	2.15	15.8	-19	112
	0.5	2.35	4.19	2.15	7.12	-9	70

Figure 4-9 illustrates step by step how the calculated amplification functions are utilized to obtain the time domain response of an earth dam under the S90W El-Centro earthquake horizontal ground motion (1940) (Figure 4-9(a)). The input motion is converted to the frequency domain by the fast Fourier transform (Figure 4-9(b)). Figure 4-9(c) represents the calculated crest amplification functions by the linear and nonlinear FEM-SBFEM for the earth dam, with β=10%, located in a rectangular canyon with L/H=5 and α=0.5. Multiplying the crest amplifications (Figure 4-9(c)) and the input Fourier amplitudes (Figure 4-9(b)) results in the crest response under the earthquake in the frequency domain (Figure 4-9(d)). The crest response in the time domain is obtained by converting the frequency domain response (Figure 4-9(d)) to the time domain by utilizing the inverse Fourier transform (Figure 4-9(e)).

The crest response in the time domain is similarly obtained for the earth dams with different impedance ratio values. Figure 4-10 compares the linear and nonlinear crest response of the dam embedded in a rectangular canyon with L/H=5 and α=0.1, 0.3, and 0.5. The nonlinear peak crest accelerations show remarkably higher values in comparison to the corresponding linear values. Similar to the linear response, the nonlinear amplification functions are amplified by decreasing the impedance ratio values. The calculated peak crest acceleration for different canyon conditions, in terms of geometry and material, are compared quantitatively in Table *4-2*. The nonlinear effect reaches to 120% increase in the peak crest acceleration value in comparison with the linear one for an earth dam in the rectangular canyon with L/H=5 and α=0.3.

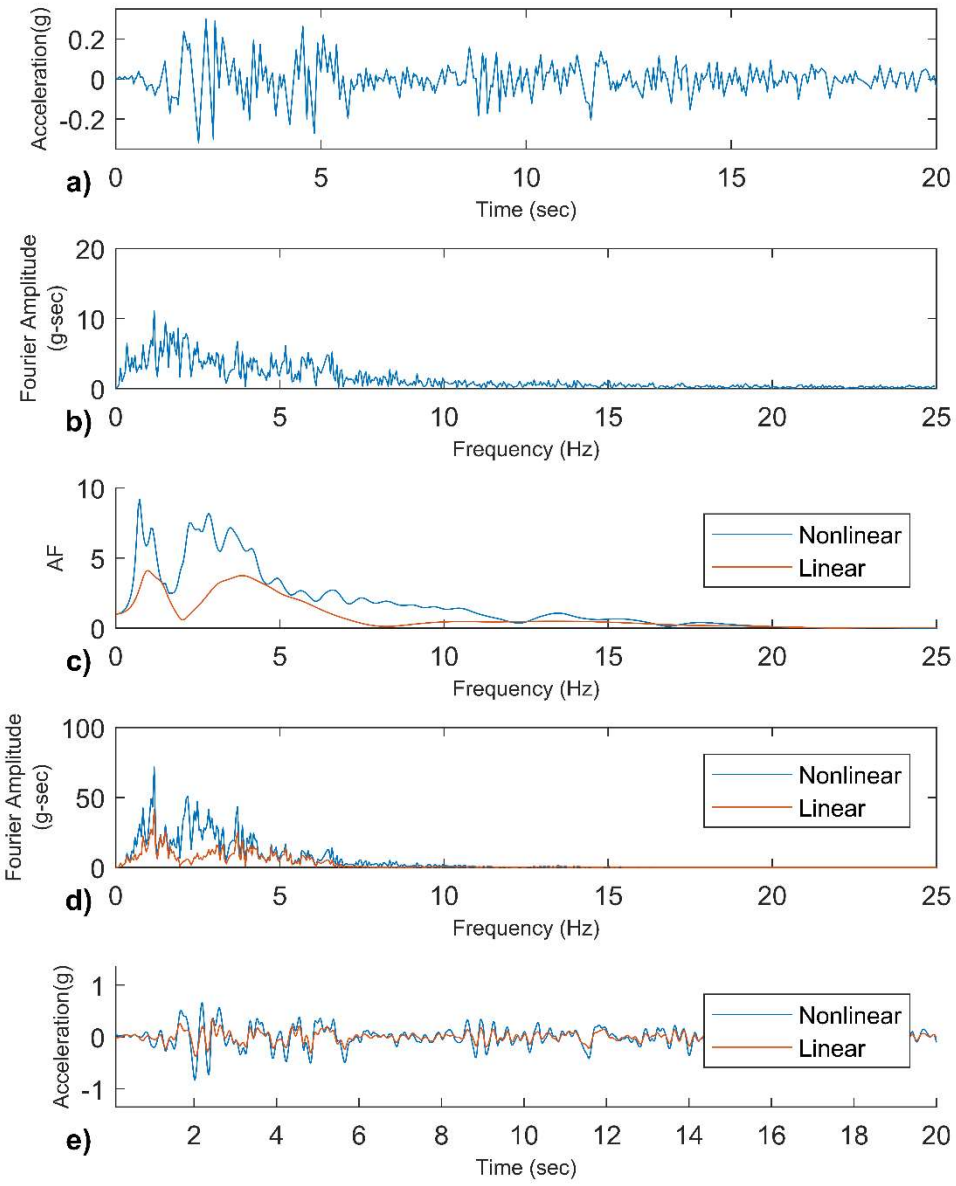

Figure 4-9. a) The S90W El-Centro earthquake horizontal ground motion (1940); b) The input motion in the frequency domain; c) The calculated crest amplification functions by the linear and nonlinear FEM-SBFEM for the earth dam, with β=10%, located in a rectangular canyon with L/H=5 and α=0.5; d) Multiplying the crest amplifications (c) and the input Fourier amplitude (b); e) The crest response in the time domain

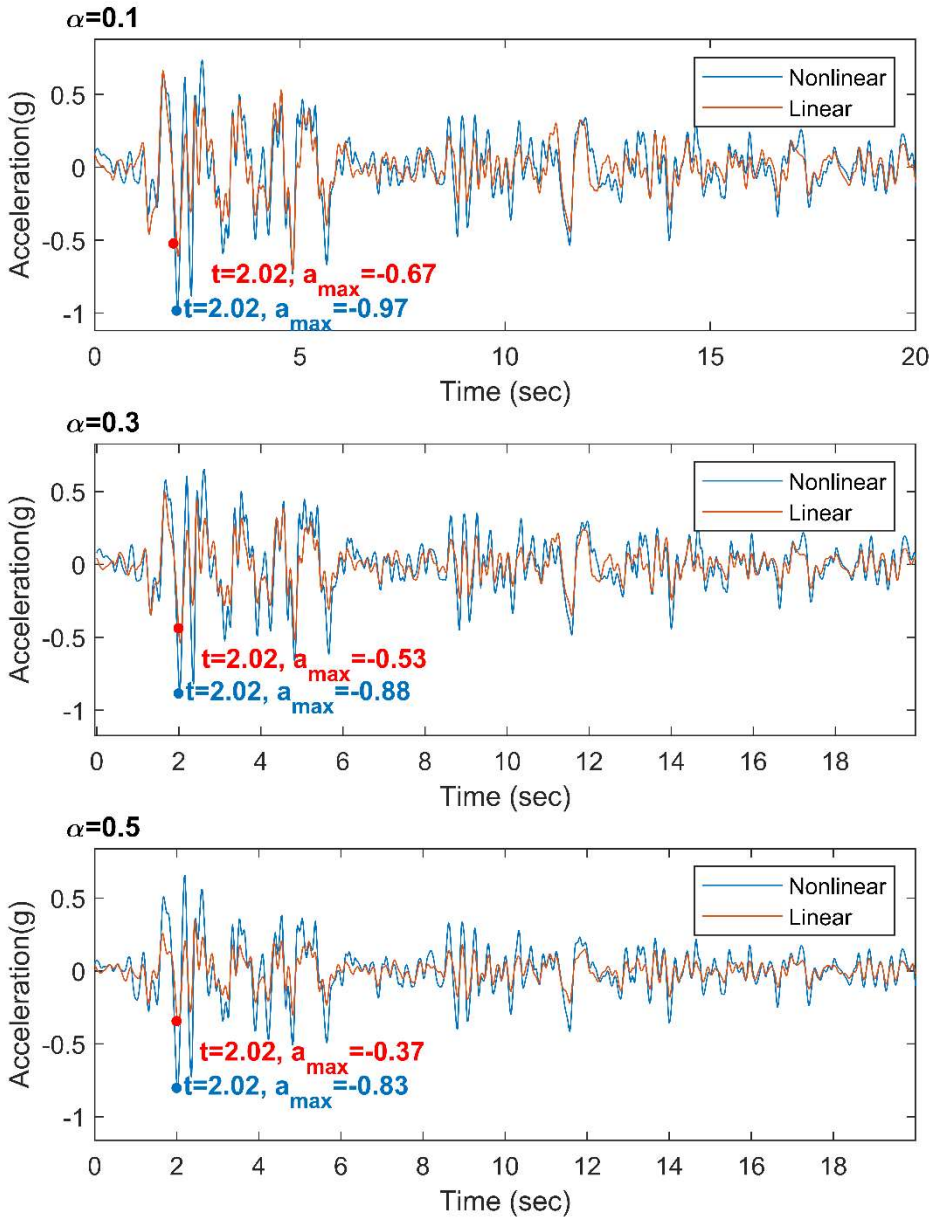

Figure 4-10. Crest acceleration time history, obtained by linear and nonlinear FEM-SBFEM under the El Centro earthquake, for the earth dam with L/H=5 located in a rectangular canyon with different values of the impedance ratio (α),

Table 4-2. Comparison of the crest acceleration obtained by linear and nonlinear FEM-SBFEM

	L/H=2.5				
	α	t	Linear	Nonlinear	Change(%)
Rectangula	0.1	2.02	-0.67	-1.1	64
	0.3	2.02	-0.55	-0.81	47
	0.5	2.02	-0.31	-0.48	55
Trapezoida	0.1	2.02	-0.81	-1.45	79
	0.3	2.02	-0.58	-1.12	93
	0.5	2.02	-0.47	-0.85	81
Triangular	0.1	2.02	-0.91	-1.2	32
	0.3	2.02	-0.64	-0.9	41
	0.5	2.02	-0.45	-0.74	64

	L/H=5				
	α	t	Linear	Nonlinear	Change(%)
Rectangula	0.1	2.02	-0.51	-1.1	116
	0.3	2.02	-0.38	-0.87	129
	0.5	2.02	-0.32	-0.64	100
Trapezoida	0.1	2.02	-0.67	-0.97	45
	0.3	2.02	-0.53	-0.88	66
	0.5	2.02	-0.37	-0.83	124
Triangular	0.1	2.02	-0.64	-1	56
	0.3	2.02	-0.45	-0.75	67
	0.5	2.02	-0.33	-0.52	58

4.6.1 The El Infiernillo dam

The El Infiernillo dam is an earth and rockfill dam located on the Balsas River, Mexico. Figure 4-11 depicts the plan view and the maximum cross-section of the dam. The dam is 148 m in height and 350 m in length. The dam is located in a very active seismic region and has undergone several severe earthquake loadings, including the event on 14/3/79. The material properties of the different parts of the dam are shown in Table 4-3. The foundation and canyon were made with similar materials [118]. The impedance ratio α and damping ratio β for the El Infiernillo dam have been reported in the literature [61] as 0.3 and 8%, respectively.

Table 4-3. Material properties

	Material	Shear Modules (Mpa)	Mass Density (Kg/m3)	v
1)	Compacted Rockfill	682	2100	0.42
2)	Impervious Core	227	2100	0.49
3)	Dumped Rockfill	245	2100	0.38

To accurately model the geometry of the canyon and the earth dam, the elevation contour lines (Figure 4-11(a)) were imported into AUTOCAD to make a 3D model (Figure 4-12(a)). The 3D model was simplified to be exported to Gambit to generate a 3D mesh. The earth dam was discretized with 590 brick 8-node elements, and the canyon with 286 4-node surface elements (Figure 4-12(b)).

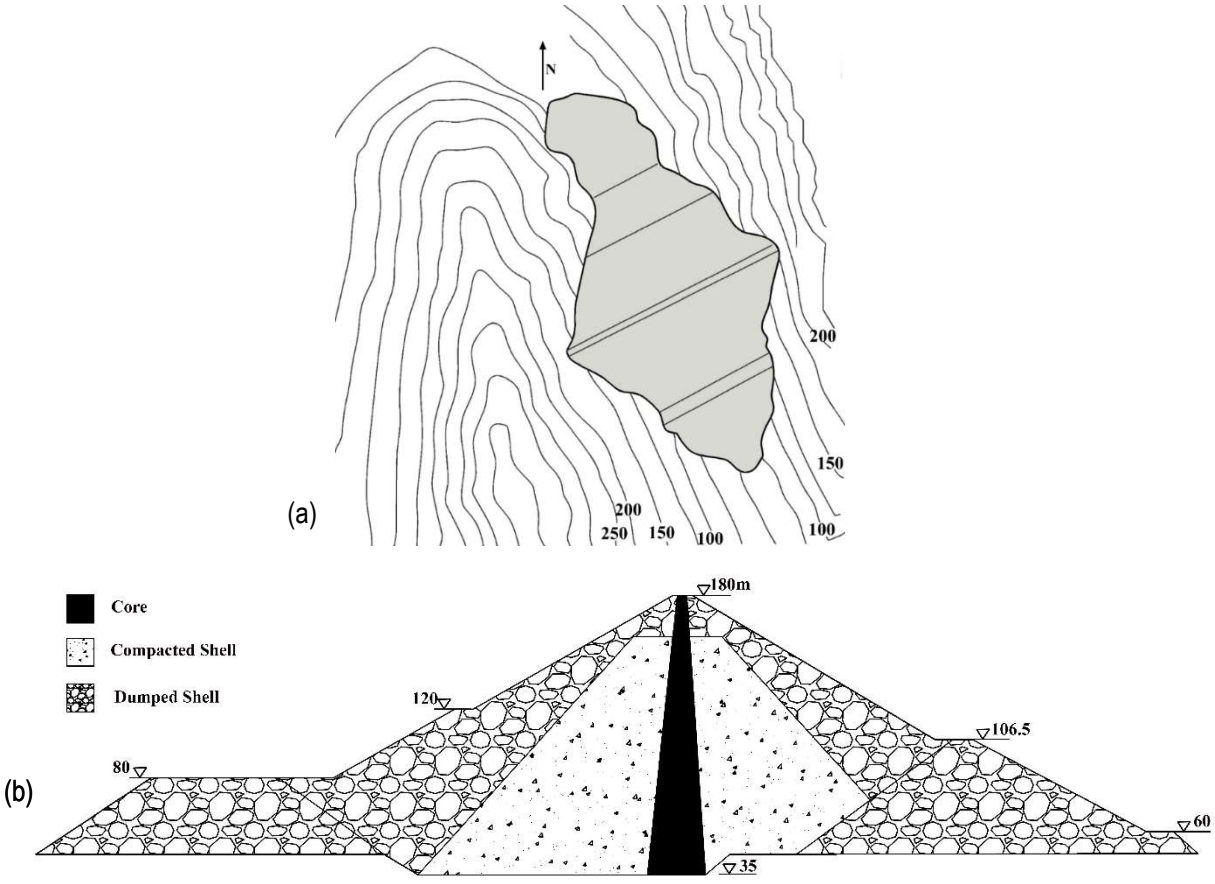

Figure 4-11. a) Plan view of the El Infiernillo Dam; b) Cross-section of the El Infiernillo Dam

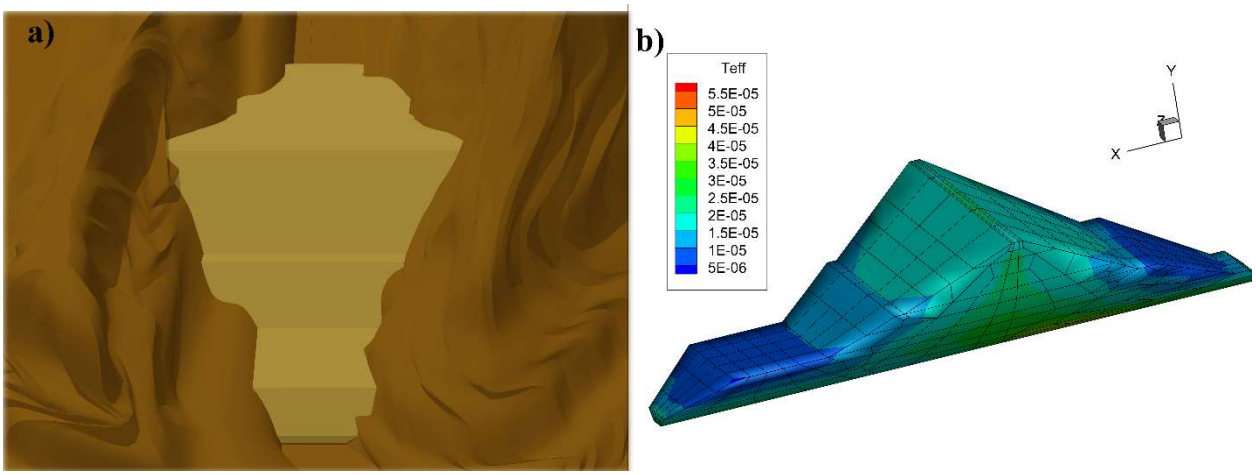

Figure 4-12. a) 3D CAD model of El Infiernillo; b) 3DFEM model of El Infiernillo

Figure 4-13 shows the recorded crest-bedrock amplification spectra of the El Infiernillo dam due to the earthquake on November 15, 1975. The nonlinear AFs of the earth dam-canyon system (with α=0.3 and β=8%) in the upstream-downstream direction were obtained by 3D FEM-SBFEM (red dotted line in Figure 4-13). The first natural frequency obtained by the nonlinear FEM-SBFEM is f1=1.68Hz, and the AF_{max} is calculated as 13. A comparison of the crest amplification function obtained by the proposed method with the recorded data shows the accuracy of the nonlinear FEM-SBFEM. It indicates really good fits for the first nonlinear natural frequency and the maximum amplification function.

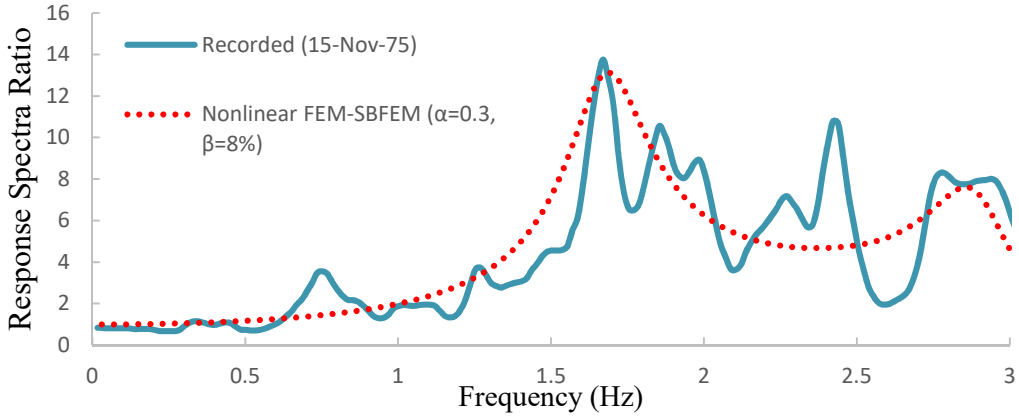

Figure 4-13. a) The AF of the earth dam-canyon system with α=0.3 and β=8% by nonlinear FEM-SBFEM, and the response spectra of the 1975 earthquake

4.7 Conclusion

The FEM-SBFEM was developed for the nonlinear analysis, and the shear modulus and damping ratio are adapted by changing the strain level. The linear natural frequency and amplification function are independent of loading conditions. As the nonlinear natural frequency and amplification function are dependent on the strain level and the intensity of the excitation, it is assumed that the earth dam-flexible canyon system is under the

S90W El-Centro earthquake horizontal ground motion (1940). With this assumption, the nonlinear natural frequency and amplification function for earth dams in different canyon conditions were obtained. The following conclusions are obtained from the results calculated by the nonlinear FEM-SBFEM:

The amplification function:

- By increasing the strain levels, the shear modulus decreases, and the damping ratio increases, which leads to an increasing AF_{max}. Comparison of the linear and nonlinear AF_{max} values for the triangular canyon with L/H=5 shows a 197% increase in comparison with the corresponding linear value.

- By increasing the impedance ratio value (α), the effect of nonlinearity is decreased. For the earth dam located in a wide triangular canyon with an elastic material (α=0.5), the effect of nonlinearity was 70%. This effect for the relatively stiff canyon (α=0.1) was 197%.

- The effects of the impedance ratio and the flexible canyon are more important in the nonlinear analysis in comparison with the linear analysis. For the rectangular canyon with L/H=2.5, the nonlinear AF_{max} for α=0.3 shows a 70% increase in comparison with that of α=0.1, while the corresponding percentage for the linear analysis is 40%.

The natural frequency:

- The nonlinearity effect is more important in relatively stiff canyons (α=0.1). In comparison with the linear natural frequency, the nonlinear natural frequency shows a 33% decrease for the earth dam located in the trapezoidal canyon with L/H=5.

- By increasing the impedance ratio, the nonlinear natural frequency is decreased.

- For the same geometric shapes, the nonlinear natural frequency of relatively wide canyons shows lower values in comparison with the corresponding values for the relatively narrow canyon.

- The nonlinear natural frequency is also affected by the canyon shapes. Earth dams located in rectangular, trapezoidal, and triangular canyons show higher to lower values, respectively, for nonlinear natural frequency.

The crest acceleration response in the time domain:

- The nonlinear peak crest accelerations show remarkably higher values in comparison to the corresponding linear values. The nonlinear effect reaches to 120% increase in the peak crest

acceleration value in comparison with the linear one for the earth dam in the rectangular canyon with L/H=5 and α=0.3.

- Similar to the linear response, the nonlinear amplification functions are amplified by decreasing the impedance ratio values.

The El Infiernillo dam was modeled by the 3D nonlinear FEM-SBFEM method, and nonlinear responses of the dam under the 14/3/79 earthquake scenario were calculated. It shows a reasonable agreement with the recorded data.

4.8 Acknowledgments

This work was supported by the Natural Sciences and Engineering Research Council of Canada (NSERC) through grant no. PCIPJ 395213-3 as well as the Hydro-Québec Industrial Research Chair for lifecycle optimization of embankment dams. The authors also thank their industrial partners: Hydro-Québec, Hatch, SNC-Lavalin, WSP, Qualitas, Golder Associates, Klohn Crippen Berger, and ConeTec. All calculations were carried out on the Niagara High-Performance Computing (HPC) cluster under the administration of Compute Canada.

Conclusion

The objective of this research was to develop the FEM-SBFEM hybrid technique to estimate the natural periods of earth dams, incorporating the effects of 3D geometry and canyon flexibility. The main conclusions are summarized as follows:

- First-order nonlinear ordinary differential SBFEM equations were solved numerically with respect to the frequency ω by using a fourth-order Runge-Kutta method. An asymptotic expansion of the dynamic-stiffness matrix for high frequency was used to start the numerical integration.

- The equilibrium equations and the compatibility conditions were applied at the boundary of the canyon and earth dam to couple the dynamic stiffness obtained by FEM with that of SBFEM.

- As the dynamic-stiffness matrix of the unbounded domain is complex and frequency-dependent, the classical mode-superposition method is not straightforward. Therefore, the dam was excited in the upstream-downstream direction.

- The results of the proposed technique were validated with results available in the literature, and the natural periods of earth dams for different canyon geometries were obtained.

- It was observed that for rigid rectangular canyons, the calculated fundamental natural periods are in agreement with the results of FEM in the literature. However, underestimations from the shear beam method were also observed.

- The roles of flexibility and canyon geometry were also considered. These results suggest that the effect of geometry is of more importance for flexible canyons.

- Some graphs were proposed that may be used by practical engineers for the estimation of the natural periods of earth dams in canyons with different shapes and material properties.

- Relationships were developed to obtain the natural frequencies of earth dams based on the geometry and material properties of their canyons.

- A comparison of the calculated natural periods with actual recorded data demonstrated good agreement. In conclusion, the hybrid FEM-SBEFEM is an accurate approach for modeling earth dams under dynamic loadings.

One hundred and twelve 3D models were created corresponding to 2 different material damping ratios, 2 different canyon lengths, 7 different impedance ratios, and 4 canyon geometries. The conclusions from the results calculated by the FEM-SBFEM are summarized as follows:

- The declining effect of material damping β is more noticeable in wider canyons, and doubling the canyon length leads to a 12% decrease in the maximum amplification function value AF_{max} in rectangular canyons.

- With increases in the α ratio, the AF is significantly reduced, for higher values of α, more flexible canyons, the material damping effect is lower.

- While the amplification function is affected by the canyon shape, The AF_{max} stays constant for different canyon shapes, with the same L/H.

The main practical application of the proposed amplification functions is in the prediction of a dam crest's seismic response parameters, including acceleration, velocity, and displacement. Dam crest acceleration due to an actual earthquake was obtained by using a fast Fourier transform, and the recorded response spectra of the El Infiernillo dam under the two 1966 earthquakes were utilized to compare with a proposed amplification function. A reasonable agreement was seen between the recorded data and the FEM-SBFEM results.

The FEM-SBFEM was developed for the nonlinear analysis, and the shear modulus and damping ratio are adapted by changing the strain level. The linear natural frequency and amplification function are independent of the loading conditions. As the nonlinear natural frequency and amplification function are dependent on the strain level and intensity of the excitation, it is assumed that the earth dam-flexible canyon system is under the S90W El-Centro earthquake horizontal ground motion (1940). With this assumption, the nonlinear natural frequencies and amplification functions for earth dams in different canyon conditions were obtained. The following conclusions are drawn from the results calculated by the nonlinear FEM-SBFEM:

Amplification function:

- By increasing the strain levels, the shear modulus decreases and the damping ratio increases, which leads to increases in the AF_{max}. Comparison of the linear and nonlinear AF_{max} values for the triangular canyon with L/H=5 shows a 197% increase in comparison with the corresponding linear value.

- By increasing the impedance ratio value (α), the effect of nonlinearity is decreased. For the earth dam located in a wide triangular canyon with an elastic material (α=0.5), the effect of nonlinearity was 70%, while this effect for the relatively stiff canyon (α=0.1) was 197%.

- The effects of the impedance ratio and flexible canyon are more important in the nonlinear analysis compared to the linear analysis. For the rectangular canyon with L/H=2.5, the nonlinear AF_{max} for α=0.3 shows a 70% increase in comparison with that of α=0.1, while the corresponding percentage for the linear analysis is 40%.

Natural frequency:

- The nonlinearity effect is more important in relatively stiff canyons (α=0.1). In comparison with the linear natural frequency, the nonlinear natural frequency shows a 33% decrease for the earth dam located in the trapezoidal canyon with L/H=5.

- By increasing the impedance ratio, the nonlinear natural frequency is decreased.

- For the same geometric shapes, the nonlinear natural frequency of relatively wide canyons shows lower values in comparison with the corresponding values for relatively narrow canyons.

- The nonlinear natural frequency is also affected by the canyon shape. Earth dams located in rectangular, trapezoidal, and triangular canyons show higher to lower values, respectively, for the nonlinear natural frequency.

Crest acceleration response in the time domain:

- The nonlinear peak crest accelerations show notably higher values in comparison with the corresponding linear values. The nonlinear effect reaches a 120% increase in the peak crest acceleration value in comparison with the linear one for the earth dam in the rectangular canyon with L/H=5 and α=0.3.

- Similar to the linear response, the nonlinear amplification functions are amplified by decreasing the impedance ratio values.

The El Infiernillo dam was modeled by the 3D nonlinear FEM-SBFEM method, and the nonlinear responses of the dam under the 15 November 1975 earthquake scenario were calculated, showing a reasonable agreement with the recorded data.

Discussion

In this part, it is shown that how the suggested the amplification function can be utilized.

Step 1) the earthquake acceleration or responses are selected.

Step 2) the response of the earthquake in frequency domain using FFT is calculated.

Step 3) the shear wave velocity of earth dam and canyon are obtained, the impedance ratio is calculated.

Step 4) the ratio of length L of canyon per height H of earth dam is determined.

Step 5) Based on the impedance ratio and L/H the amplification function is selected from Figure 3-6 to Figure 3-9.

Step 6) Production the amplification and response of earthquake from step 2 gives crest response in frequency domain.

Step 7) Using IFFT gives the crest response in time domain.

Bibliography

[1] R. W. Clough and A. K. Chopra, “Earthquake stress analysis in earth dams,” *J. Eng. Mech. Div.*, vol. 92, no. 2, pp. 197–212, 1966.

[2] A. K. Chopra, “Hydrodynamic pressures on dams during earthquakes,” *J. Eng. Mech. Div.*, vol. 93, no. 6, pp. 205–224, 1967.

[3] J. Lysmer and R. L. Kuhlemeyer, “Finite dynamic model for infinite media,” *J. Eng. Mech. Div.*, vol. 95, no. 4, pp. 859–878, 1969.

[4] W. D. Smith, “A Nonreflecting Plane Boundary for Wave Propagation Problems,” vol. 503, pp. 492–503, 1974.

[5] D. Givoli, “Non-reflecting boundary conditions,” *J. Comput. Phys.*, vol. 94, no. 1, pp. 1–29, 1991.

[6] A. Majda, “Radiation Boundary Conditions for Acoustic and Elastic Wave Calculations ",” vol. XXXII, pp. 313–357, 1979.

[7] F. Itasca, “Fast Lagrangian Analysis of Continua, Version 7.00, User Manual, Itasca Consulting Group,” *Inc., Minneap.*, 2011.

[8] Y. Parish, M. Sadek, and I. Shahrour, “Review Article: Numerical analysis of the seismic behaviour of earth dam,” *Nat. Hazards Earth Syst. Sci.*, vol. 9, no. 2, pp. 451–458, 2009.

[9] B. Ebrahimian, “Numerical analysis of nonlinear dynamic behavior of earth dams,” *Front. Archit. Civ. Eng. China*, vol. 5, no. 1, pp. 24–40, 2011.

[10] a.H.C. Chan *et al.*, “Fully coupled dynamic analysis of an earth dam,” *Géotechnique*, vol. 61, no. 7, pp. 549–563, 2011.

[11] P. Dakoulas, “Nonlinear seismic response of tall concrete-faced rockfill dams in narrow canyons,” *Soil Dyn. Earthq. Eng.*, vol. 34, no. 1, pp. 11–24, 2012.

[12] S. S. Saini, P. Bettess, and O. C. Zienkiewicz, “Coupled hydrodynamic response of concrete gravity

dams using finite and infinite elements," *Earthq. Eng. Struct. Dyn.*, vol. 6, no. 4, pp. 363–374, 1978.

[13] P. Bettess, *Infinite elements.* Penshaw Press, 1992.

[14] S. Valliappan and C. Zhao, "Dynamic response of concrete gravity dams including dam–water–foundation interaction," *Int. J. Numer. Anal. Methods Geomech.*, vol. 16, no. 2, pp. 79–99, 1992.

[15] R. J. Astley, "Inÿnite elements for wave problems : a review of current formulations and an assessment of accuracy," no. November 1999, pp. 951–976, 2000.

[16] M. A. Hariri-ardebili and H. Mirzabozorg, "A comparative study of seismic stability of coupled arch dam-foundation-reservoir systems using infinite elements and viscous boundary models," *Int. J. Struct. Stab. Dyn.*, vol. 13, no. 06, p. 1350032, May 2013.

[17] J. Berenger, "A Perfectly Matched Layer for the Absorption of Electromagnetic Waves," vol. 200, pp. 185–200, 1994.

[18] I. Harari, M. Slavutin, and E. L. I. Turkel, "Analytical and numerical studies of a finite element pml for the helmholtz equation," vol. 8, no. 1, pp. 121–137, 2000.

[19] Q. Qi and T. L. Geers, "Evaluation of the perfectly matched layer for computational acoustics," *J. Comput. Phys.*, vol. 139, no. 1, pp. 166–183, 1998.

[20] U. Basu and A. K. Chopra, "Perfectly matched layers for time-harmonic elastodynamics of unbounded domains : theory and finite-element implementation," *Comput. Methods Appl. Mech. Engrg.*, vol. 192, pp. 1337–1375, 2003.

[21] U. Basu, *Perfectly Matched Layers for Acoustic and Elastic Waves: Theory, Finite-element Implementation and Application to Earthquake Analysis of Dam-water-foundation Rock Systems*. University of California, Berkeley, 2004.

[22] U. Basu, "Explicit finite element perfectly matched layer for transient three-dimensional elastic waves," no. July 2008, pp. 151–176, 2009.

[23] U. Basu and A. K. Chopra, "Perfectly matched layers for transient elastodynamics of unbounded domains," vol. 1074, no. May 2003, pp. 1039–1074, 2004.

[24] J. Lysmer and G. Waas, "Shear waves in plane infinite structures," *J. Eng. Mech.*, 1972.

[25] E. Kausel and J. M. Roesset, “Semianalytic hyperelement for layered strata,” *J. Eng. Mech. Div.*, vol. 103, no. 4, pp. 569–588, 1977.

[26] S. Bougacha, J. L. Tassoulas, and J. M. Roësset, “Analysis of foundations on fluid-filled poroelastic stratum,” *J. Eng. Mech.*, vol. 119, no. 8, pp. 1632–1648, 1993.

[27] E. Kausel, “Thin-Layer Method: Formulation in the Time Domain,” *Int. J. Numer. Methods Eng.*, vol. 37, no. April 1993, pp. 927–941, 1994.

[28] S. Park and J. L. Tassoulas, “Layered Strata with Zigzag Boundaries 1,” vol. 128, no. 3, pp. 359–368, 2002.

[29] S. Bougacha and J. L. Tassoulas, “Seismic analysis of gravity dams. I: Modeling of sediments,” *J. Eng. Mech.*, vol. 117, no. 8, pp. 1826–1837, 1991.

[30] D. Givoli and J. B. Keller, “Non-reflecting boundary conditions for elastic waves,” *Wave motion*, vol. 12, no. 3, pp. 261–279, 1990.

[31] J. B. Keller and M. J. Grote, “Exact nonreflecting boundary condition for elastic waves,” *SIAM J. Appl. Math.*, vol. 60, no. 3, pp. 803–819, 2000.

[32] M. J. Grote, “Nonreflecting boundary conditions for elastodynamic scattering,” *J. Comput. Phys.*, vol. 161, no. 1, pp. 331–353, 2000.

[33] I. L. Sofronov, “Artificial boundary conditions of absolute transparency for two- and three-dimensional external time-dependent scattering problems,” vol. 000, 1998.

[34] H. Abouseeda and P. Dakoulas, “Non-linear dynamic earth dam -foundation interaction using a BE-FE method,” vol. 936, no. June 1996, pp. 917–936, 1998.

[35] M. Yazdchi, N. Khalili, and S. Valliappan, “Dynamic soil-structure interaction analysis via coupled finite-element-boundary-element method,” *Soil Dyn. Earthq. Eng.*, vol. 18, no. 7, pp. 499–517, 1999.

[36] J. P. Wolf and C. Song, *Finite-element modelling of unbounded media*. Wiley Chichester, 1996.

[37] M. H. Bazyar and C. Song, “Transient analysis of wave propagation in non-homogeneous elastic unbounded domains by using the scaled boundary finite-element method,” *Earthq. Eng. Struct. Dyn.*, vol. 35, no. 14, pp. 1787–1806, 2006.

[38] M. H. Bazyar and C. Song, “Time-harmonic response of non-homogeneous elastic unbounded domains using the scaled boundary finite-element method,” *Earthq. Eng. Struct. Dyn.*, vol. 35, no. 3, pp. 357–383, 2006.

[39] C. Song, “Dynamic analysis of unbounded domains by a reduced set of base functions,” *Comput. Methods Appl. Mech. Eng.*, vol. 195, no. 33–36, pp. 4075–4094, 2006.

[40] C. Song and M. H. Bazyar, “Development of a fundamental-solution-less boundary element method for exterior wave problems,” *Commun. Numer. Methods Eng.*, vol. 24, no. 4, pp. 257–279, Nov. 2006.

[41] C. Song and M. H. Bazyar, “A boundary condition in Padé series for frequency-domain solution of wave propagation in unbounded domains,” *Int. J. Numer. Methods Eng.*, vol. 69, no. 11, pp. 2330–2358, 2007.

[42] T. Ekevid and N. Wiberg, “Wave propagation related to high-speed train,” *Computer Methods in Applied Mechanics and Engineering*, vol. 191, no. 36. pp. 3947–3964, 2002.

[43] T. Ekevid, H. Lane, and N. E. Wiberg, “Adaptive solid wave propagation - Influences of boundary conditions in high-speed train applications,” *Comput. Methods Appl. Mech. Eng.*, vol. 195, no. 4–6, pp. 236–250, 2006.

[44] N. M. Syed and B. K. Maheshwari, “Improvement in the computational efficiency of the coupled FEM – SBFEM approach for 3D seismic SSI analysis in the time domain,” *Comput. Geotech.*, vol. 67, pp. 204–212, 2015.

[45] N. M. Syed and B. K. Maheshwari, “Non-linear SSI analysis in time domain using coupled FEM–SBFEM for a soil–pile system,” *Géotechnique*, vol. 67, no. 7, pp. 572–580, Jul. 2017.

[46] H. Xu, D. Zou, X. Kong, and Z. Hu, “Study on the effects of hydrodynamic pressure on the dynamic stresses in slabs of high CFRD based on the scaled boundary finite-element method,” *Soil Dyn. Earthq. Eng.*, vol. 88, pp. 223–236, 2016.

[47] A. Seiphoori, S. Mohsen Haeri, and M. Karimi, “Three-dimensional nonlinear seismic analysis of concrete faced rockfill dams subjected to scattered P, SV, and SH waves considering the dam-foundation interaction effects,” *Soil Dyn. Earthq. Eng.*, vol. 31, no. 5–6, pp. 792–804, 2011.

[48] K. Chen, D. Zou, X. Kong, and X. Yu, “An efficient nonlinear octree SBFEM and its application to complicated geotechnical structures,” *Comput. Geotech.*, vol. 96, no. October 2018, pp. 226–245,

2018.

[49] G. Lin, Y. Wang, and Z. Hu, “An efficient approach for frequency-domain and time-domain hydrodynamic analysis of dam-reservoir systems,” *Earthq. Eng. Struct. Dyn.*, vol. 41, no. 13, pp. 1725–1749, Oct. 2012.

[50] M. Zhao, X. Wang, P. Wang, X. Du, and J. Liu, “Seismic water-structure interaction analysis using a modified SBFEM and FEM coupling in a frequency domain,” *Ocean Eng.*, vol. 189, p. 106374, 2019.

[51] A. Yaseri, M. H. Bazyar, and N. Hataf, “3D coupled scaled boundary finite-element/finite-element analysis of ground vibrations induced by underground train movement,” *Comput. Geotech.*, vol. 60, pp. 1–8, Jul. 2014.

[52] J. P. Wolf, *The Scaled Boundary Finite Element Method*. John Wiley & Sons, 2003.

[53] I. M. Smith, D. V. Griffiths, and L. Margetts, *Programming the finite element method*. John Wiley & Sons, 2013.

[54] S. L. Kramer, “Geotechnical Earthquake Engineering,” *Prentice-Hall, Inc.*, vol. 6. p. 653, 1996.

[55] N. Ambraseys, “On the shear response of a two-dimensional truncated wedge subjected to an arbitrary disturbance,” *Bull. Seismol. Soc. Am.*, vol. 50, no. 1, pp. 45–56, 1960.

[56] P. Dakoulas and H. Hashmi, “Response of Earth Dams in Canyons Subjected to Asynchronous Base Excitation,” 1991.

[57] P. Dakoulas and G. Gazetas, “SEISMIC SHEAR VIBRATION OF EMBANKMENT DAMS IN SEMI-CY LINDRICAL VALLEYS,” vol. 14, no. April 1985, pp. 19–40, 1986.

[58] P. Dakoulas and C. Hsu, “Lateral response of dams in semi-elliptical rigid canyons,” *Soil Dyn. Earthq. Eng.*, vol. 12, no. 8, pp. 497–507, 1993.

[59] N. N. Ambraseys, “On the shear response of a two-dimensional truncated wedge subjected to an arbitrary disturbance,” *Bull. Seismol. Soc. Am.*, vol. 50, no. 1, pp. 45–56, 1960.

[60] A. K. Chopra, “Earthquake response of earth dams,” *J. Soil Mech. Found. Div.*, vol. 93, no. 2, pp. 65–81, 1967.

[61] G. Gazetas, “Seismic response of earth dams: some recent developments,” *Soil Dyn. Earthq. Eng.*,

vol. 6, no. 1, pp. 2–47, 1987.

[62] M. Hatanaka, “Three dimensional consideration on the vibration of earth dams,” *J. Japanese Soc. Civ. Eng.*, vol. 37, no. 10, pp. 302–305, 1952.

[63] B. Martinez and J. Bielak, “On the three-dimensional seismic response of earth structures.” Proc. 7th World Conf. Earthq. Engrg., Instanbul, 1980, 8, 523-528.

[64] L. H. Mejia and H. B. Seed, “Comparison of 2-D and 3-D dynamic analyses of earth dams,” *J. Geotech. Eng.*, vol. 109, no. 11, pp. 1383–1398, 1983.

[65] P. Dakoulas and G. Gazetas, “Vibration characteristics of dams in narrow canyons,” *J. Geotech. Eng.*, vol. 113, no. 8, pp. 899–904, 1987.

[66] A. Papalou and J. Bielak, “Seismic elastic response of earth dams with canyon interaction,” *J. Geotech. Geoenvironmental Eng.*, vol. 127, no. 5, pp. 446–453, 2001.

[67] A. Papalou and J. Bielak, “Nonlinear Seismic Response of Earth Dams with Canyon Interaction,” *J. Geotech. Geoenvironmental Eng.*, vol. 130, no. 1, pp. 103–110, Jan. 2004.

[68] A. K. Chopra and P. R. Perumalswami, “Dynamics of earth dams with foundation interaction,” *J. Eng. Mech.*, 1971.

[69] S. Rampello, E. Cascone, and N. Grosso, “Evaluation of the seismic response of a homogeneous earth dam,” *Soil Dyn. Earthq. Eng.*, vol. 29, no. 5, pp. 782–798, 2009.

[70] P. N. Psarropoulos and Y. Tsompanakis, “Stability of tailings dams under static and seismic loading,” *Can. Geotech. J.*, vol. 45, no. 5, pp. 663–675, 2008.

[71] H. B. Seed and I. M. Idriss, “Soil moduli and damping factors for dynamic response analysis. Rep. No. EERC 70-10,” *Earthq. Eng. Res. Centre, Berkeley, CA*, 1970.

[72] S. H. Schnabel PB, Lysmer J, “SHAKE: A computer program for earthquake response analysis of horizontally layered sites,” *EERC Rep. 72-12, Univ. California, Berkeley.*, 1972.

[73] J. Lysmer, T. Udaka, C. Tsai, and H. B. Seed, “FLUSH-A computer program for approximate 3-D analysis of soil-structure interaction problems,” California Univ., 1975.

[74] R. F. J. Ghaffar, A M; Scott, “Shear moduli and damping factors of earth dam: Abdel- Geotech Engng

Div ASCE, V105, NGT12, Dec 1979, P1405–1426," *Int. J. Rock Mech. Min. Sci. Geomech. Abstr.*, vol. 17, no. 5, pp. 92–93, 1980.

[75] D. Choudhury and P. Savoikar, "Equivalent-linear seismic analyses of MSW landfills using DEEPSOIL," *Eng. Geol.*, vol. 107, no. 3–4, pp. 98–108, 2009.

[76] L. H. Mejia, H. B. Seed, and J. Lysmer, "Dynamic analysis of earth dams in three dimensions," *J. Geotech. Eng. Div.*, vol. 108, no. 12, pp. 1586–1604, 1982.

[77] E. Cascone and S. Rampello, "Decoupled seismic analysis of an earth dam," *Soil Dyn. Earthq. Eng.*, vol. 23, no. 5, pp. 349–365, 2003.

[78] T. Touhei and T. Ohmachi, "A FE-BE method for dynamic analysis of {Dam-Foundation-Reservoir systems in the time domain," *Earthqu. Eng. Struct. Dyn.*, vol. 22, no. July 1992, pp. 195–209, 1993.

[79] A. M. Abdel-Ghaffar and A.-S. Koh, "Three-dimensional dynamic analysis of nonhomogeneous earth dams," *Int. J. Soil Dyn. Earthq. Eng.*, vol. 1, no. 3, pp. 136–144, 1982.

[80] P. Dakoulas and C. H. Hsu, "Response of Dams in Semielliptic Canyons To Oblique Sh-Waves," *J. Eng. Mech.*, vol. 121, no. 3, pp. 379–391, 1995.

[81] M. A. Hariri-Ardebili and L. K. Nuss, "Seismic risk prioritization of a large portfolio of dams: Revisited," *Adv. Mech. Eng.*, vol. 10, no. 9, pp. 1–20, 2018.

[82] C. Song and J. P. Wolf, "The scaled boundary finite-element method—alias consistent infinitesimal finite-element cell method—for elastodynamics," *Comput. Methods Appl. Mech. Eng.*, vol. 147, no. 3–4, pp. 329–355, 1997.

[83] M. H. Bazyar and A. Talebi, "Transient seepage analysis in zoned anisotropic soils based on the scaled boundary finite-element method," *Int. J. Numer. Anal. Methods Geomech.*, vol. 39, no. 1, pp. 1–22, Jan. 2015.

[84] M. H. Bazyar and C. Song, "A continued-fraction-based high-order transmitting boundary for wave propagation in unbounded domains of arbitrary geometry," *Int. J. Numer. Methods Eng.*, vol. 74, no. 2, pp. 209–237, 2008.

[85] M. C. Genes and S. Kocak, "Dynamic soil–structure interaction analysis of layered unbounded media via a coupled finite element/boundary element/scaled boundary finite element model," *Int. J. Numer.*

Methods Eng., vol. 62, no. 6, pp. 798–823, Feb. 2005.

[86] J. Yan, C. Zhang, and F. Jin, "A coupling procedure of FE and SBFE for soil-structure interaction in the time domain," *Int. J. Numer. Methods Eng.*, vol. 59, no. 11, pp. 1453–1471, 2004.

[87] S. R. Chidgzey, J. Trevelyan, and A. J. Deeks, "Coupling of the boundary element method and the scaled boundary finite element method for computations in fracture mechanics," *Comput. Struct.*, vol. 86, no. 11–12, pp. 1198–1203, 2008.

[88] G. E. Bird, J. Trevelyan, and C. E. Augarde, "A coupled BEM/scaled boundary FEM formulation for accurate computations in linear elastic fracture mechanics," *Eng. Anal. Bound. Elem.*, vol. 34, no. 6, pp. 599–610, 2010.

[89] Z. J. Yang, X. F. Wang, D. S. Yin, and C. Zhang, "A non-matching finite element-scaled boundary finite element coupled method for linear elastic crack propagation modelling," *Comput. Struct.*, vol. 153, pp. 126–136, 2015.

[90] A. J. Deeks and C. E. Augarde, "A hybrid meshless local Petrov-Galerkin method for unbounded domains," *Comput. Methods Appl. Mech. Eng.*, vol. 196, no. 4–6, pp. 843–852, 2007.

[91] A. Yaseri, M. H. Bazyar, and S. Javady, "2.5D coupled FEM-SBFEM analysis of ground vibrations induced by train movement," *Soil Dyn. Earthq. Eng.*, vol. 104, no. October 2017, pp. 307–318, 2018.

[92] R. Shahi and A. Noorzad, "Dynamic Response of Rigid Foundations of Arbitrary Shape Using Half-Space Green's Function," *Int. J. Geomech.*, vol. 11, no. 5, pp. 391–398, 2010.

[93] H. L. Wong and J. E. Luco, "Dynamic response of rigid foundations of arbitrary shape," *Earthq. Eng. Struct. Dyn.*, vol. 4, no. 6, pp. 579–587, 1976.

[94] A. Ghaemi and J.-M. Konrad, "A semi-empirical relationship for predicting earthquake-induced crest settlement of concrete faced rockfill dams," *Soil Dyn. Earthq. Eng.*, p. 105990, 2020.

[95] T. Touhei and T. bi. Ohmachi, "MODAL ANALYSIS OF A DAM-FOUNDATION SYSTEM BASED ON AN FE-BE METHOD IN THE TIME DOMAIN," *10.1002/eqe.4290230102*, no. October 1992, 1994.

[96] R. W. Boulanger, J. D. Bray, S. M. Merry, and L. H. Mejia, "Three-dimensional dynamic response analyses of Cogswell Dam," *Can. Geotech. J.*, vol. 32, no. 3, pp. 452–464, 1995.

[97] J. F. Hall and A. K. Chopra, "Hydrodynamic effects in the dynamic response of concrete gravity dams,"

J. Geotech. Geoenvironmental Eng., vol. 108, no. GT4, 1982.

[98] J. Dominguez and J. M. Roesset, "Dynamic stiffness of rectangular foundations," *STIN*, vol. 79, p. 16152, 1978.

[99] A. C. Eringen and E. S. Suhubi, "Elastodynamics. Volume 2- Linear theory(Book)," *New York, Acad. Press. Inc., 1975. 671 p*, 1975.

[100] A. K. Chopra and P. Chakrabarti, "Earthquake analysis of concrete gravity dams including dam-water-foundation rock interaction," *Earthq. Eng. Struct. Dyn.*, vol. 9, no. 4, pp. 363–383, 1981.

[101] K. Fok and A. K. Chopra, "Earthquake analysis of arch dams including dam–water interaction, reservoir boundary absorption and foundation flexibility," *Earthq. Eng. Struct. Dyn.*, vol. 14, no. 2, pp. 155–184, 1986.

[102] C. Zienkiewicz, D. W. Kelly, and P. Bettess, "Marriage a la mode: The best of both worlds- Finite elements and boundary integrals," *Int. Symp. Innov. Numer. Anal. Appl. Eng. Sci. Versailles, Fr.*, pp. 19–26, 1977.

[103] T. Touhei and T. Ohmachi, "Modal analysis of a DAM–Foundation system based on an FE–BE method in the time domain," *Earthq. Eng. Struct. Dyn.*, vol. 23, no. 1, pp. 1–15, 1994.

[104] F. Guan and I. D. Moore, "New techniques for modelling reservoir-dam and foundation-dam interaction," *Soil Dyn. Earthq. Eng.*, vol. 16, no. 96, pp. 285–293, 1997.

[105] P. Dakoulas and H. Abouseeda, "Response of earth dams to Rayleigh waves using coupled FE-BE method," *J. Eng. Mech.*, vol. 123, no. 12, pp. 1311–1321, 1997.

[106] J. Wolf and C. Song, "The scaled boundary finite element method," *Appl. Mech. Rev.*, vol. 57, no. 3, p. B14, 2004.

[107] M. H. Bazyar and A. Graili, "A practical and efficient numerical scheme for the analysis of steady state unconfined seepage flows," *Int. J. Numer. Anal. Methods Geomech.*, vol. 36, no. 16, pp. 1793–1812, 2012.

[108] M. H. BAZYAR and A. GRAILI, "Scaled Boundary Finite-Element solution to confined seepage problems," 2011.

[109] M. H. Bazyar and A. Talebi, "Transient seepage analysis in zoned anisotropic soils based on the

scaled boundary finite-element method," *Int. J. Numer. Anal. Methods Geomech.*, vol. 39, no. 1, pp. 1–22, 2015.

[110] M. R. Jabbari Lak and M. H. Bazyar, "A Non-linear Scaled Boundary Finite-Element Analysis Applied to Geotechnical Problems," *Geotech. Geol. Eng.*, vol. 37, no. 1, pp. 501–515, 2019.

[111] K. Chen, D. Zou, X. Kong, A. Chan, and Z. Hu, "A novel nonlinear solution for the polygon scaled boundary finite element method and its application to geotechnical structures," *Comput. Geotech.*, vol. 82, pp. 201–210, 2017.

[112] H. Rahnema, S. Mohasseb, and B. JavidSharifi, "2-D soil-structure interaction in time domain by the SBFEM and two non-linear soil models," *Soil Dyn. Earthq. Eng.*, vol. 88, pp. 152–175, 2016.

[113] N. M. Syed and B. K. Maheshwari, "Modeling Using Coupled FEM-SBFEM for Three-Dimensional Seismic SSI in Time Domain," no. February, pp. 118–129, 2014.

[114] A. Yaseri and J. Konrad, "Estimation of Natural periods of Earth Dam-Flexible canyon systems with 3D coupled FEM-SBFEM," *Comput. Geotech.*, vol. 123, no. March, p. 103546, 2020.

[115] C. Song and J. Wolf, "Consistent infinitesimal finite element cell method: three-dimensional scalar wave equation," *J. Appl. Mech.*, vol. 63, no. 3, p. 650, 1996.

[116] P. Dakoulas, "Earth Dam-Canyon Interaction Effects for Obliquely Incident SH Waves," *J. Geotech. Eng.*, vol. 119, no. 11, pp. 1696–1716, Nov. 1993.

[117] A. M. Elgamal and R. V Gunturi, "Dynamic behaviour and seismic response of El Infiernillo dam," *Earthq. Eng. Struct. Dyn.*, vol. 22, no. 8, pp. 665–684, Aug. 1993.

[118] S. Sica, L. Pagano, and A. Modaressi, "Influence of past loading history on the seismic response of earth dams," *Comput. Geotech.*, vol. 35, no. 1, pp. 61–85, 2008.

[119] L. Pelecanos, "Seismic response and analysis of earth dams." Imperial College London London, United Kingdom, 2013.

[120] L. H. Mejia and H. B. Seed, "Comparison of 2-D and 3-D Dynamic Analyses of Earth Dams," *J. Geotech. Eng.*, vol. 109, no. 11, pp. 1383–1398, 2008.

[121] H. Abouseeda and P. Dakoulas, "Non-linear dynamic earth dam–foundation interaction using a BE–FE method," *Earthq. Eng. Struct. Dyn.*, vol. 27, no. 9, pp. 917–936, Sep. 1998.

[122] Y. Wang, G. Lin, and Z. Hu, “Novel Nonreflecting Boundary Condition for an Infinite Reservoir Based on the Scaled Boundary Finite-Element Method,” *J. Eng. Mech.*, vol. 141, no. 5, pp. 1–9, 2015.

[123] Y. Wang, G. Lin, and Z. Hu, “A Novel Non-Reflecting Boundary Condition for the Scaled Boundary Finite Element Analysis of Infinite Reservoir,” *J. Eng. Mech.*, vol. 3, no. 5, p. 130113202711003, 2013.

[124] S. M. Li, “Diagonalization procedure for scaled boundary finite element method in modeling semi-infinite reservoir with uniform cross-section,” *Int. J. Numer. Methods Eng.*, vol. 80, no. 5, pp. 596–608, Oct. 2009.

[125] G. Lin, J. Du, and Z. Hu, “Dynamic dam-reservoir interaction analysis including effect of reservoir boundary absorption,” *Sci. China, Ser. E Technol. Sci.*, vol. 50, no. SUPPL. 1, pp. 1–10, 2007.

[126] J. P. Wolf and C. Song, “The scaled boundary finite-element method - A fundamental solution-less boundary-element method,” *Comput. Methods Appl. Mech. Eng.*, vol. 190, no. 42, pp. 5551–5568, 2001.